VERIFICATION OF HEATED WATER JET NUMERICAL MODEL

by James G. Weil

SMHI Rapporter

HYDROLOGI OCH OCEANOGRAFI

Nr RHO 1 (1974)

SVERIGES METEOROLOGISKA OCH HYDROLOGISKA INSTITUT

VERIFICATION OF HEATED WATER JET NUMERICAL MODEL

by James G. Weil

SMHI Rapporter

HYDROLOGI OCH OCEANOGRAFI

Nr RHO 1 (1974)

SVERIGES METEOROLOGISKA OCH HYDROLOGISKA INSTITUT

Stockholm 1974

ABSTRACT

Reported are diverse efforts to verify, or test the accuracy of, a numerical model for thermal pollution predictions. The model, developed by Prych (1972) at S.M.H.I., is an integral analysis of a buoyant, turbulent surface jet. The program is slightly revised, and effects of the changes are presented.

Numerical model results are compared directly with ten prototype situations: eight sets of data from a Swedish power station on the coast of the Baltic Sea, and data from two power plants on Lake Michigan in the United States. A few direct comparisons are made with a laboratory model of the Swedish plant and with laboratory data for momentumless surface jets. To minimize coastal effects, a scheme is presented for interfacing the numerical model with undistorted laboratory model results.

The discharge situation is described nondimensionally, and numerical experiments are made to determine the sensitivities of jet temperatures to input variables. Results are compared with phenomenological and analytical models. In addition to the main verification effort, investigations are made concerning methods of field data collection.

Conclusions are presented for direct application and for relative or comparative use of the numerical model.

ACKNOWLEDGMENTS

All work herein was performed at the Swedish Meteorological and Hydrological Institute (S.M.H.I.), Hydrological Bureau, Oceanographic Section. Financial support came from the Swedish State Power Board Environmental Foundation. The author thanks Dr. Edmund A. Prych for his discussions of the details of the numerical model. Appreciation is extended to Mr. Jörgen Nässén and Ms. Gunilla Berg for their help in preparation of the report.

CONTENTS

LIST OF FIGURES

LIST OF FIGURES (cont.)

LIST OF TABLES

CHAPTER 1. INTRODUCTION

1.1 Thermal pollution prediction methods

It is convenient to consider mixing of heated surface jets in terms of four overlapping mixing zones. These zones represent regions where certain mechanisms dominate dilution of temperature:

1. momentum zone, where jet excess velocity determines mixing
2. buoyancy zone, producing lateral spreading and vertical stability
3. turbulence zone, where ambient turbulence induces vertical and horizontal mixing
4. heat loss zone, where temperature is lost by atmospheric heat transfer.

Many prototype situations exhibit all of these, in complicated overlapping regions.

Presently prediction of prototype temperatures can follow several directions, and these will be discussed with reference to the above mixing zones. The first prediction scheme is the phenomenological model. Dimensional analysis is generally used to present thermal plume dependent variables (e.g. axial temperature, plume surface width, centerline layer thickness, heated surface area) as functions of outlet and hydrological variables. The functional forms are then approximated by comparison with laboratory and prototype data. Phenomenological models are of course aided by hydraulic analysis, but do not actually depend on theoretical analyses. They rather blindly include all four mixing zones. A defect is that they cannot confidently be extrapolated beyond existing power plant sizes, and many plants now being designed are much larger than operating plants.

The second prediction scheme involves use of laboratory and prototype data, patching together results for special situations and producing a complete plume prediction. The method is especially useful where the mixing zones are easily separated, or where one or more mechanisms can be ignored. For example, the region nearest a power plant outlet might be considered as a momentum jet in a cross flow, for which results are available. Plume spreading might be included as independent of ambient current, for which laboratory results are also available. At some point one would then assume that momentum is no longer important, and further prediction could be based on interaction of buoyancy and turbulence. Results are also available for this regime. In this way the plume is completely described. However, errors propagate from stage to stage. Recent analytical work has attempted to include more of the mixing mechanisms simultaneously.

The third predictive method is use of hydraulic, or laboratory, models. Many of these models are distorted, and all are subject to theoretical objections concerning the turbulent mixing zone, although the momentum and buoyancy mechanisms can be scaled

reasonably well. Hydraulic models can provide pictorial details of plume behavior due to nearshore geography, but cannot be relied upon for quantitative predictions except in a comparative sense. Proper scaling of atmospheric losses depends on correct matching of complicated meteorological parameters in prototype and in the laboratory.

The last predictive scheme is of immediate concern, that of numerical modeling. The Prych (1972) computer model includes temperature dilution due to all four mechanisms. Expressions for the individual mixing rates are written using fundamental hydraulics equations and empirical relationships. It is hoped that all mechanisms interface properly and that accurate predictions can be made for the entire plume region. However, effects of coastal boundaries cannot be included (although bottom slope is included by Stolzenbach and Harleman; 1971), and effects of individual mechanisms are difficult to separate due to numerical complexity. If the final predictions are inaccurate it is difficult to determine the source of the error.

Although all these methods have been used to make temperature predictions, there exists very little literature comparing predictions and prototype data. In a few cases hydraulic model results are compared with real power plants (Hindley, Miner, and Cayot; 1971), sometimes determining empirical adjustments to allow predictions for other plants nearby. Correlation for numerical models has been limited to comparison with hydraulic model results (Stolzenbach and Harleman; 1971) and one field study (Doret, Harleman, Ippen, and Pearce; 1973). It is the goal of this report to compare predictions using the Prych (1972) numerical model with selected prototype results. The term verification herein shall mean a check or test of the exactness or accuracy of the numerical model, not necessarily a confirmation or substantiation of the model's predictive accuracy.

1.2 Program revisions

For the details of the numerical scheme the reader is referred to the original report (Prych; 1972). The numerical model is an integral analysis of a turbulent, buoyant surface jet into uniform density, uniform current, unbounded receiving water. Small integration steps are taken along the jet axis outward from the source. A Runge-Kutta numerical technique solves seven simultaneous equations for each slice of the plume. Entrainment is due to jet momentum and ambient turbulence, buoyancy suppresses vertical mixing and causes lateral spreading due to wave front motion, plume trajectory is altered by ambient flow momentum and form and shear drag, and heat is lost to the atmosphere.

A few revisions have been made to the original program. An errata sheet (dated October 1973, S.M.H.I.) has been distributed to direct recipients of the original report, and it is not included here. Aside from typographical errors, changes were made in choosing some empirical constants and in correcting some algebraic mistakes. The differential equation for non-buoyant horizontal spreading originally contained two terms with the quantity $\Delta\rho$, plant density difference. Because non-buoyant

spreading should be independent of $\Delta\rho$, these terms were somewhat arbitrarily deleted. The effects of all the changes are shown in Figures 1.1 and 1.2. Using S.M.H.I. terminology the original computer program was labeled version EAP-1W, and the revised version is labeled JW-7. The data for the figures were chosen for a restricted discharge condition at Oskarshamnsverket, a Swedish power station. It is seen that the revisions reduce plume widths slightly, but have little effect on axis temperatures.

Because prototype plumes are usually asymmetric (increased lateral spreading on the downstream side), an attempt was made to alter lateral spreading rates by correction of layer depth due to axis curvature. Results showed plume asymmetry much less than is seen in prototype, so the revision was abandoned. The original report shows acceptable initial angle (between ambient current and discharge velocity vectors) limits of 0° to 180°, but the indeterminate nature of mixing of directly opposed currents limits practical use of the program to an approximate range of 0° to 100°.

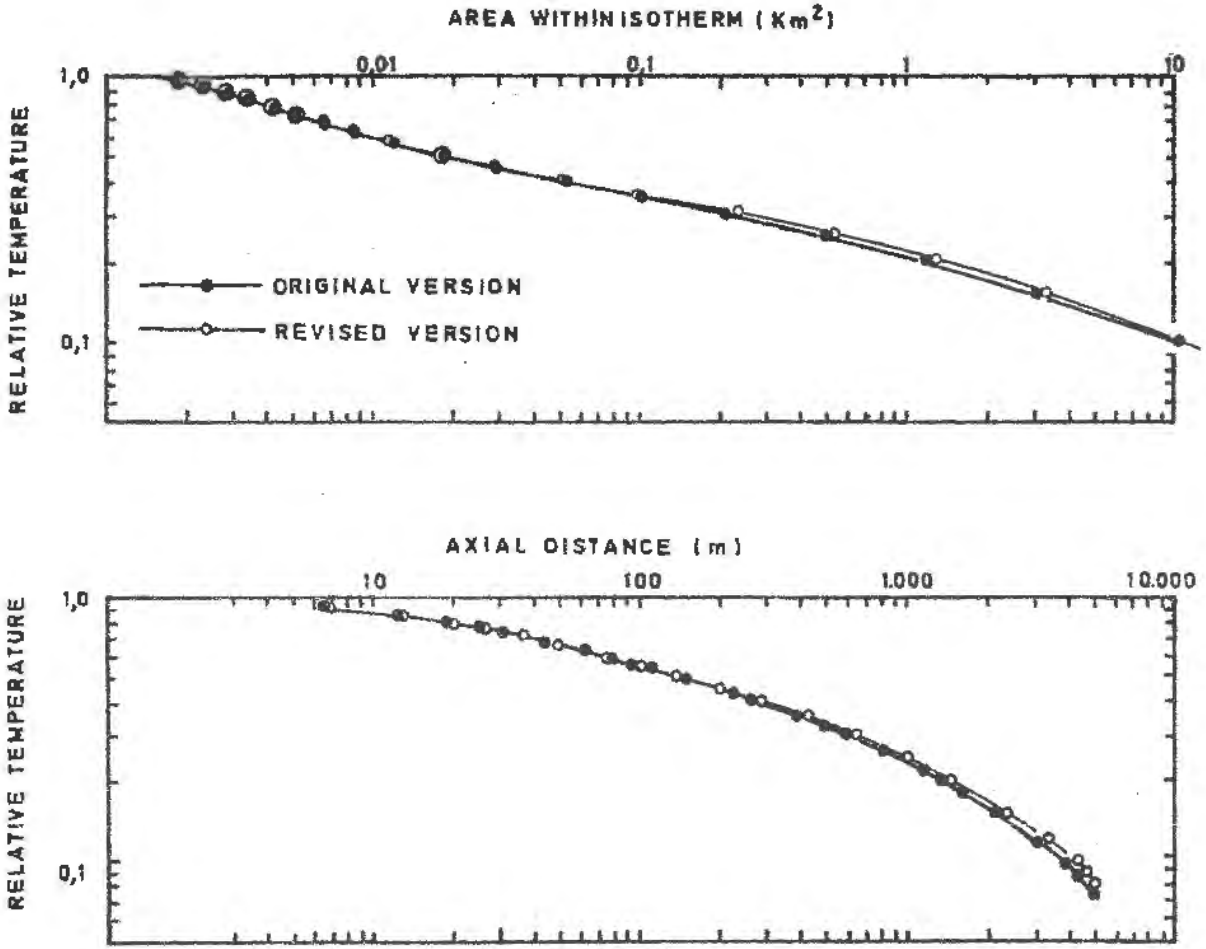

Figure 1.1 Effects of program revisions. Data for Oskarshamnsverket, restricted outlet, Q_o = 22 m³/s

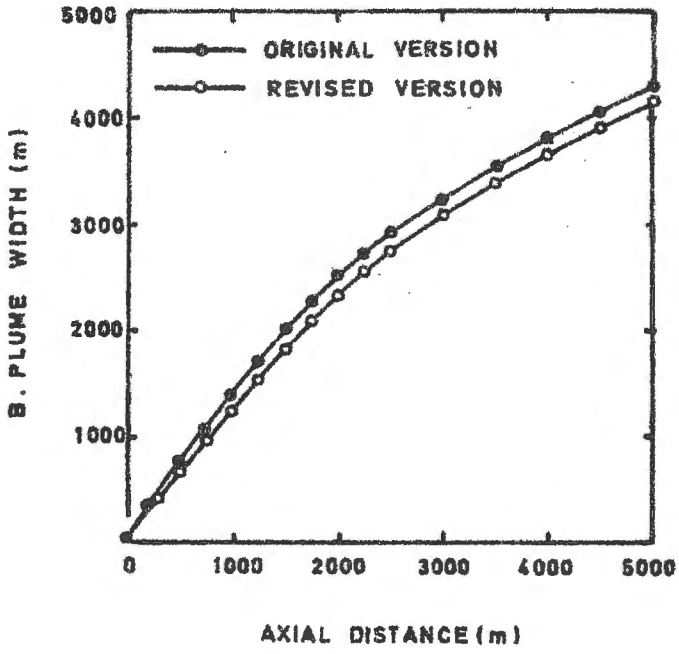

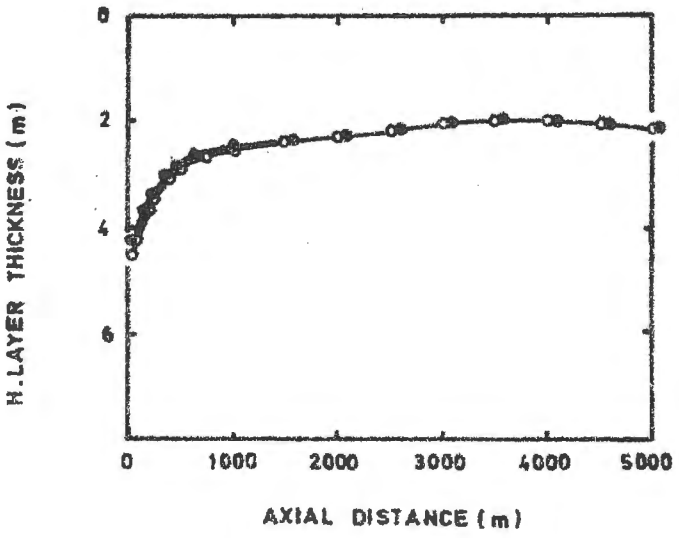

Figure 1.2 Effects of program revisions. Data for Oskarshamnsverket, restricted outlet, Q_o = 22 m^3/s

CHAPTER 2. DIRECT DATA COMPARISONS

2.1 Power plant site descriptions

To completely compare numerical model results with prototype situations, data are needed from many power plants encompassing ranges of all important independent variables. Unfortunately this is not possible. The numerical model can be used only for surface discharges. Often discharge sites are in areas of complicated nearby geography, and many situations show inhibited vertical mixing due to shallow water depth. Published data for some locations are incomplete, reporting isotherms and flow rate without discharge structure dimensions.

The principal power plant used for verification is Oskarshamnsverket, on the southeast coast of Sweden. It is chosen because it has a surface discharge, receiving waters are relatively deep, geographic obstructions are few, and there exists a large body of temperature data taken during normal plant operation. Qualifications to model application are that the heated water plumes sometimes interfere with the natural coastline, ambient currents sometimes vary during data collection periods, and the discharge conditions are not precisely known. Oskarshamnsverket operates at a maximum power level of 460 MWE, constant flow rate of 22 m^3/s, and temperature increase of approximately 10°C. The plant discharge is into an inlet called Hamnefjärden, approximately 1200 m by 100 m, with a 3 m sill located 200 m from the sea. The receiving water is the Baltic Sea, which nearby has a depth of 6-18 m once clear of the shoreline by more than 200 m. The Baltic Sea exhibits typical salinities of 7-8 o/oo and ambient temperatures of 0-20°C. There exists a weak thermal stratification near the surface during the warmest summer months, but the upper layer is considered to be of uniform density for modeling purposes. Prevailing winds are from the southwest. Prevailing currents are up to 10 cm/s and usually parallel to the coastline, which runs northeast-southwest (33° compass heading). All temperature data are taken from monthly surveys during 1972 by S.M.H.I. During the summer months the plant was not in operation, and midwinter data is not reported because the heated plumes had negative buoyancy. Eight situations are compared. Prototype conditions are shown in Table 2.1.

In addition to Oskarshamnsverket, data are compared at two power plants on the western shore of Lake Michigan in the United States. One situation is at Point Beach Power Plant, Wisconsin on 20 July 1971. Data are from Frigo and Frye (1972, p. 66). Point Beach Power Plant operates at 480 MWE, 25.0 m^3/s, through a discharge channel 10.7 m wide by 4.21 m deep. The second situation is at Waukegan Power Plant, Illinois on 12 August 1970. Data are from Tokar (1971, p. 64). Waukegan Power Plant operates at 970 MWE, 49 m^3/s, through a natural channel. Prototype conditions for these two plants are also shown in Table 2.1.

Special discharge conditions at Oskarshamnsverket and Waukegan Power Plant dictated numerical model input values different from operating values. These will be explained below.

Case	Location	Date	Time	Currents (m/s)		Ambient temperature (°C)
A	Oskarshamn	3 May 1972	09.00-13.00	0.091	SW	6.5
B	"	3 October 1972	08.30-13.00	0.033	NE	11.5
C	"	3 October 1972	15.30-16.40	0.105	NE	11.5
D	"	4 October 1972	08.20-11.30	0.07	NE	11.5
E	"	4 October 1972	12.25-17.10	0.07	NE	11.5
F	"	5 October 1972	07.25-11.00	0.03	NE	11.5
G	"	14 November 1972	10.00-14.30	0.075	SE	7.0
H	"	20 December 1972	08.45-13.00	0.04	SSE	4.5
I	Point Beach	20 July 1971	16.32-18.05	0.0915	N	12.7
J	Waukegan	12 August 1970	12.00-13.57	0.18	S	23.5

Table 2.1. Prototype data situations

2.2 Data presentation

The numerical model input data for all ten cases (labeled A-J) are shown in Table 2.2. The symbols used are the same as those used by Prych (1972) wherever possible. Receiving water conditions are described by ambient current magnitude V, wind speed W, angle between discharge and ambient velocities θ, water density ρ, and temperature T_a. Discharge dimensions are total width $2B_o$ and depth H_o. Power plant operation is described by heated water flow Q_o, outlet velocity u_o, outlet temperature rise ΔT, outlet density decrease $\Delta\rho$, and initial Froude number $F_o = u_o/(H_o\, g\, \Delta\rho/\rho)^{1/2}$. Temperatures are reported as axis temperature T_s, relative temperature $T = (T_s - T_a)/\Delta T$, and axial distance s. Trajectory is reported as axis location y vs. x, distance in the direction of the ambient current (y perpendicular to x).

In addition to discharge quantities, several other coefficients are required for the numerical model. A value of k = 0.00001 m/s is used for atmospheric cooling, and the suggested values of 0.1, 0.2, 0.5, 1.0, and 1.0 are used for entrainment, form drag, shear drag, horizontal mixing, and vertical mixing coefficients.

The numerical model input parameters have been adjusted to reflect mixing inside Hamnefjärden. Actual plant outlet dimensions are unimportant because much of the discharge jet energy is dissipated in the inlet. For computational purposes the origin of the heated water jet is taken as the point where the inlet opens onto the Baltic Sea. From topographic charts the discharge velocity is directed at an angle of 104° from north. Thus for north-flowing currents parallel to the coast the initial discharge angle is $\theta = 71°$. From detailed measurements of flow in the inlet (Chapter 4) it is assumed that in every case the bulk or overall mixing at the mouth of the inlet is constant, and that the constant value of inlet dilution is 0.66. Thus for every situation the computer input density difference $\Delta\rho$ is 0.66 times the plant density difference, and the input flow is 1/0.66 times the plant flow, or $Q_o = 33.4\ m^3/s$. Data for inlet velocities were not taken during every field situation, but the evidence is that the overall dilution of 0.66 was more consistently reproduced than the dilution of surface temperature. For this reason the initial tempera-

Input parameter	Case									
	A	B	C	D	E	F	G	H	I	J
Month	May	Oct	Oct	Oct	Oct	Oct	Nov	Dec	July	Aug
V direction	SW	NE	NE	NE	NE	NE	SE	SSE	N	S
V (m/s)	0.091	0.033	0.105	0.07	0.07	0.03	0.075	0.04	0.092	0.18
V/u_o	0.52	0.19	0.59	0.4	0.4	0.17	0.42	0.24	0.16	0.12
W direction	NE	SSE	S	SSW	WSW	SW	NW	WSW	S	E
W (m/s)	4	2	4-5	8	5-6	4-6	5-7	5-6	6.5	3
V/W (%)	2.3	1.7	2.3	0.9	1.3	0.6	1.3	0.7	1.4	5.8
Power (MWE)	415	450	450	450	450	450	460	460	480	970
Q_o (m^3/s)	33.4	33.4	33.4	33.4	33.4	33.4	33.4	33.4	25.0	53.2
u_o (m/s)	0.18	0.18	0.18	0.18	0.18	0.18	0.18	0.18	0.56	1.47
$2B_o$ (m)	63.0	63.0	63.0	63.0	63.0	63.0	63.0	63.0	10.7	25.0
H_o (m)	3.0	3.0	3.0	3.0	3.0	3.0	3.0	3.0	4.2	1.45
θ (°)	109[1]	71	71	71	71	71	39	56	79	90
ΔT (°C)	11.5	5.5	4.5	6.0	5.5	4.0	4.0	5.0	8.8	7.0
$\Delta\rho$ (kg/m^3)	0.76	1.0	1.0	0.96	0.97	1.02	0.61	0.47	1.53	1.92
F_o	1.18	1.03	1.03	1.05	1.05	1.02	1.32	1.51	2.22	8.9
Correlation	Goodness of fit [2]									
T vs. distance	-,0	0	-	+	0,+	-	-	0,+	-	-
T vs. area	-,0	0	-	0,+	0,+	-	-	0,+	-	-
Trajectory	0	-	+	-,+	+	+	0	-	+	+
Overall	good	good	poor	fair	fair	fair	fair	good	fair	poor

1) Adjusted to 90° for numerical model.

2) Plus (+) values indicate numerical model temperatures exceeding field values, minus (-) values the opposite. When two values are given, the plotted results cross. Plus trajectory values indicate model plumes becoming parallel to ambient current more rapidly than in the field.

Table 2.2. Correlation of results with oceanographic parameters

ture differences in the numerical model were taken as the measured temperature differences from the field data. This implies that the temperature distribution at the inlet mouth was inconsistent from case to case, which was seen in the data. Details of the inlet velocity and temperature distributions show a constant initial depth of 3.0 m, which matches the sill depth. Data taken by Chalmers Tekniska Högskola indicate significant mixing between the sill and the inlet mouth. With the flow Q_o and depth H_o fixed, a continuity calculation was used to fix the effective initial width at $2B_o = 63.0$ m. The difficulty with such calculations is that they somewhat arbitrarily determine the initial Froude number. If Q_o, $2B_o$, and H_o are constant, then velocity u_o is constant, and Froude number changes only through variation of $\Delta\rho$. Physically it is more likely that the inlet geography determines the Froude number, and overall mixing rate adjusts itself to maintain that Froude number. Numerical experiments were made to determine model sensitivity to initial conditions, and results will be reported later.

Outlet conditions at Point Beach Power Plant are well defined, as reported in Table 2.2. At Waukegan Power Plant the outlet temperature was lower than the plant discharge temperature, apparently because of mixing in the outlet channel. For this reason the initial flow is adjusted from $Q_o = 49.0$ m^3/s to $Q_o = 53.2$ m^3/s. By approximate measurement $2B_o = 25.0$ m. From conservation of initial momentum the flow depth is $H_o = 1,45$ m.

For all ten cases the direct comparisons between numerical model results and field data are shown in Figures 2.1-2.20. The first figure for each case compares measured and modeled isotherms. Occasionally changing conditions would contort field trajectories. Numerical model isotherms can overlap the shoreline because the model receiving water is unbounded. For each case the second figure compares relative temperature vs. area enclosed within that isotherm and relative temperature vs. distance along the plume axis. Note that relative temperature refers to temperatures in excess of values at the inlet mouth, not the plant outlet. These values of field data should not be used to study the Oskarshamnsverket situation without adjustment for inlet mixing. For this reason values of ΔT in Table 2.2 are lower than actual plant temperature differences.

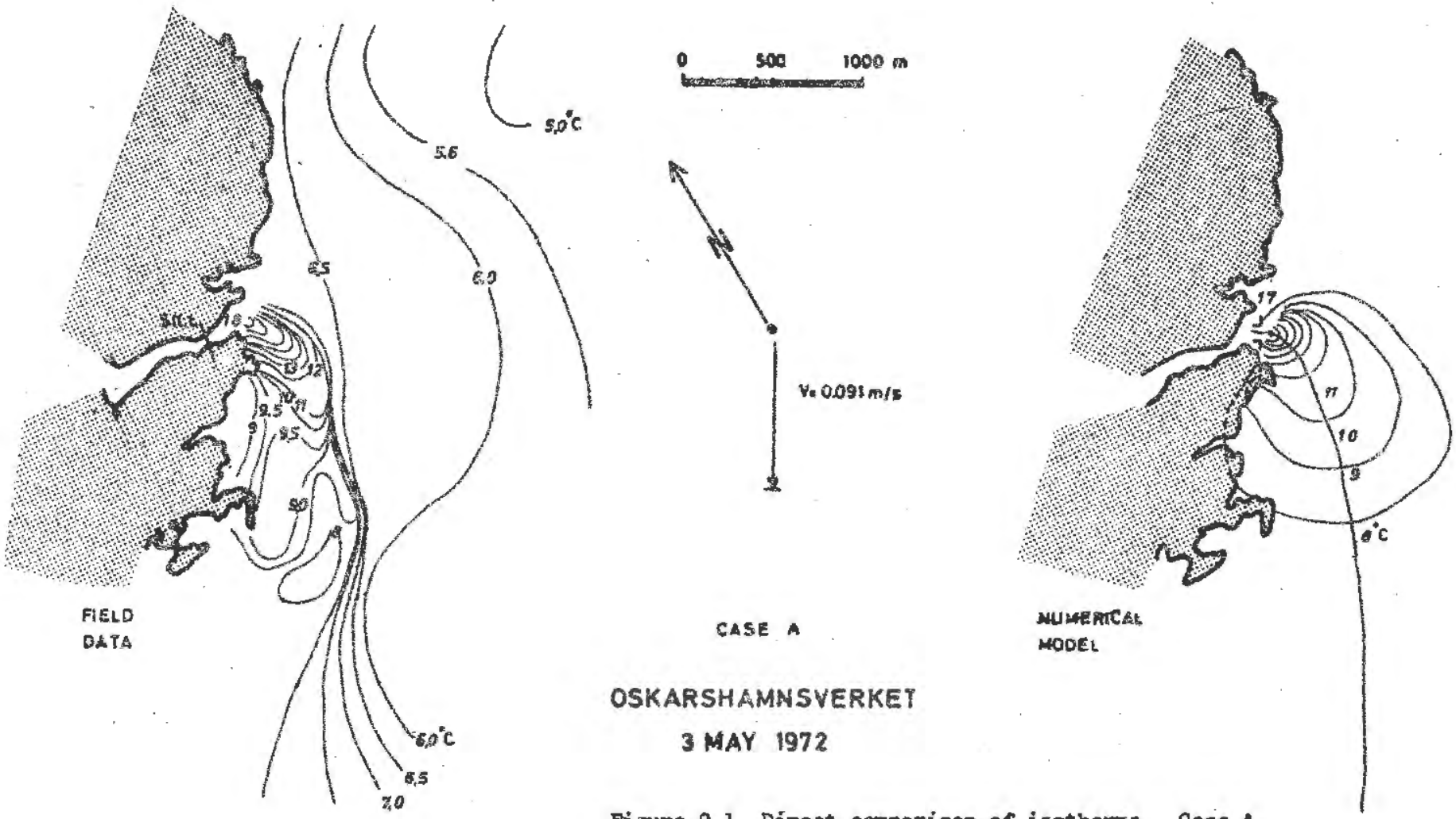

Figure 2.1 Direct comparison of isotherms, Case A

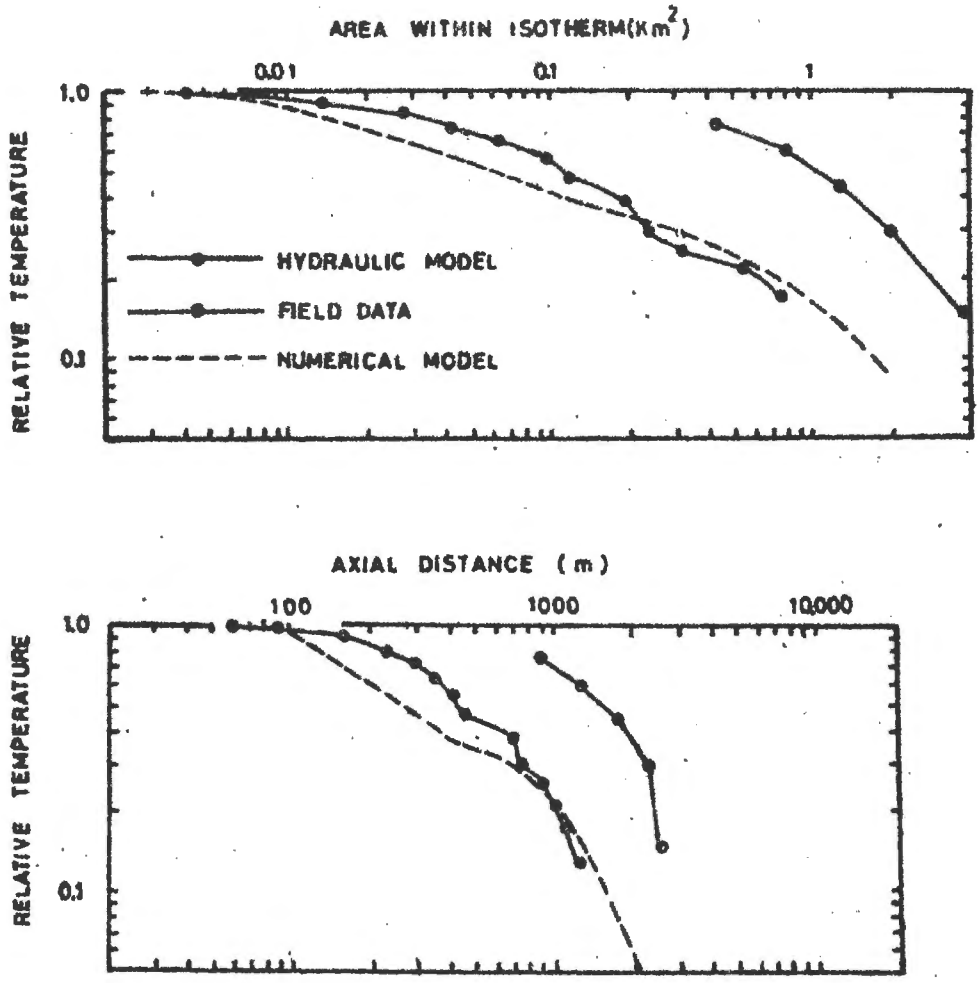

Figure 2.2 Relative temperature vs. enclosed area and distance, Case A

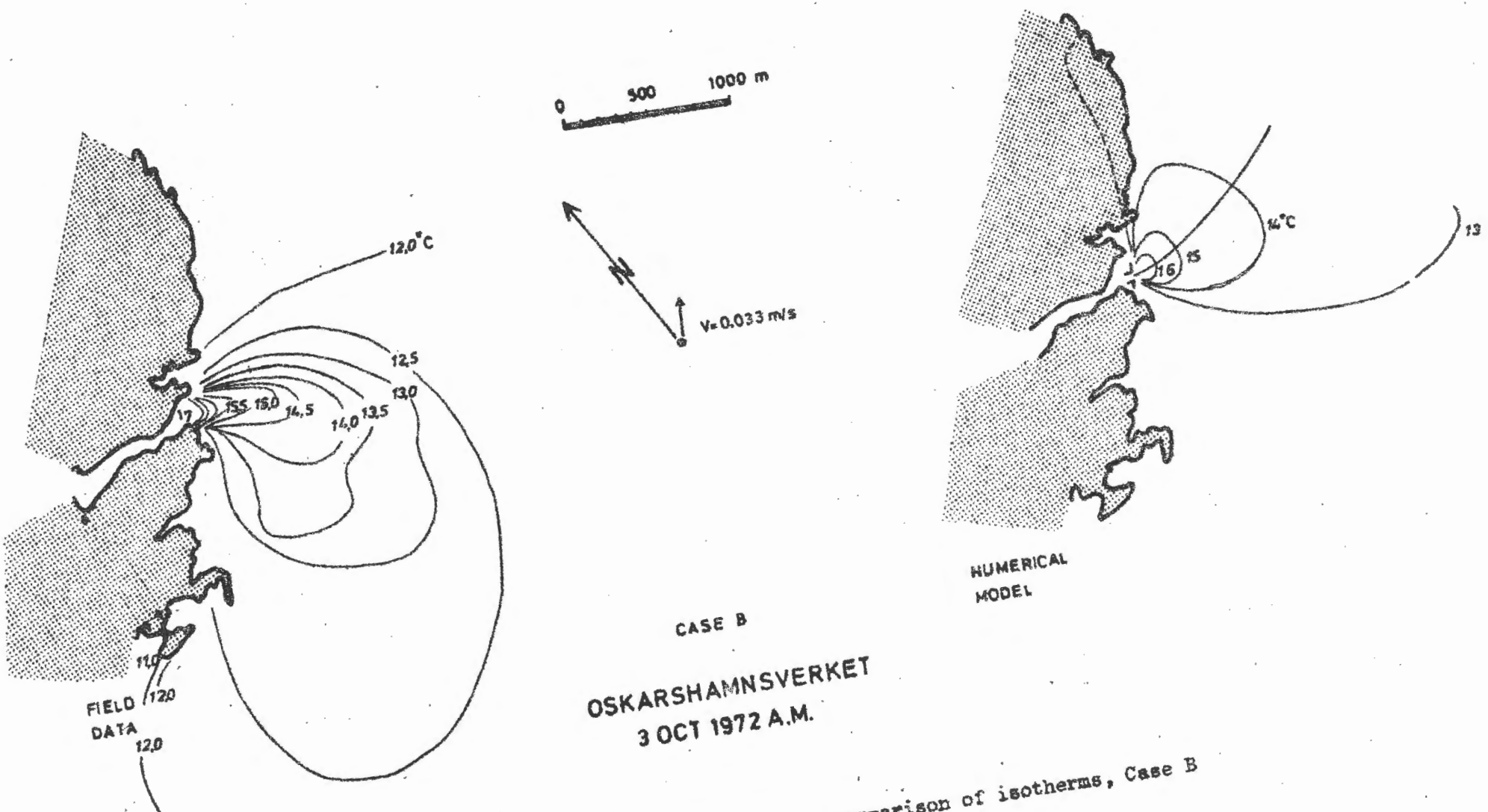

Figure 2.3 Direct comparison of isotherms, Case B

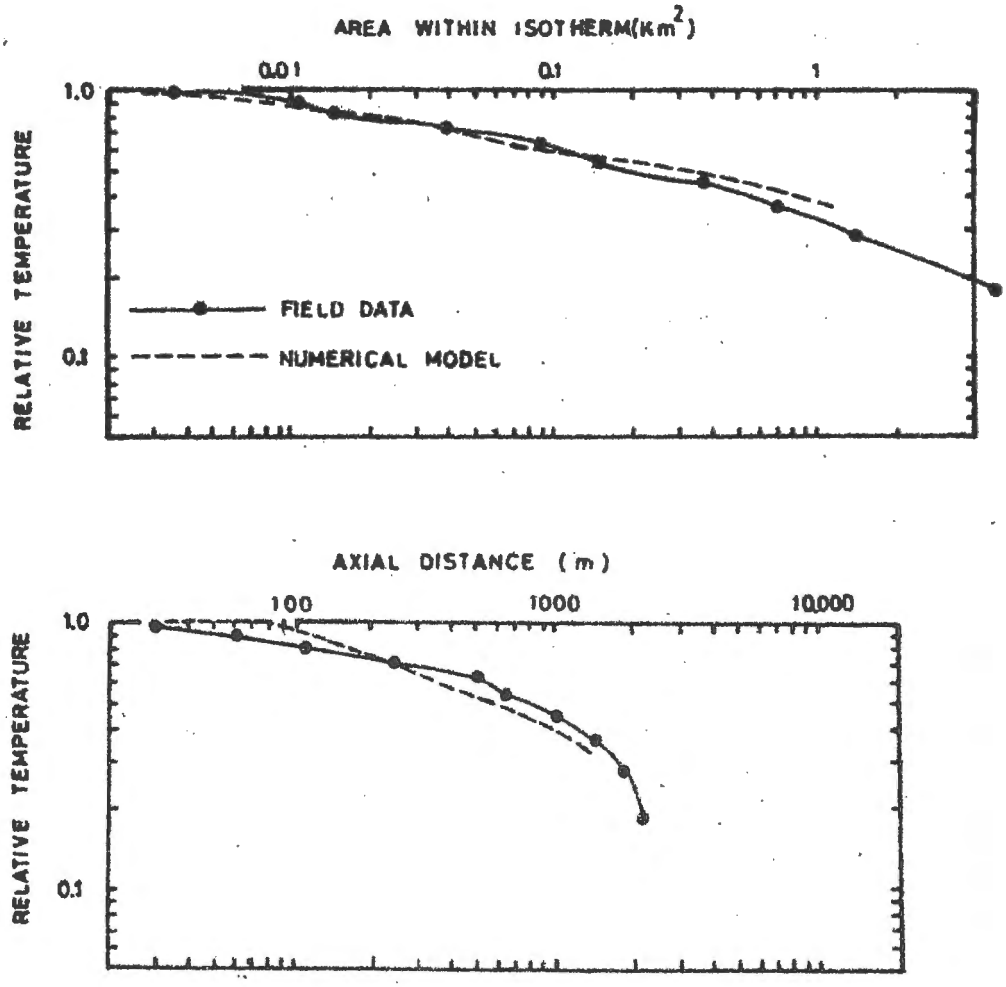

Figure 2.4 Relative temperature vs. enclosed area and distance, Case B

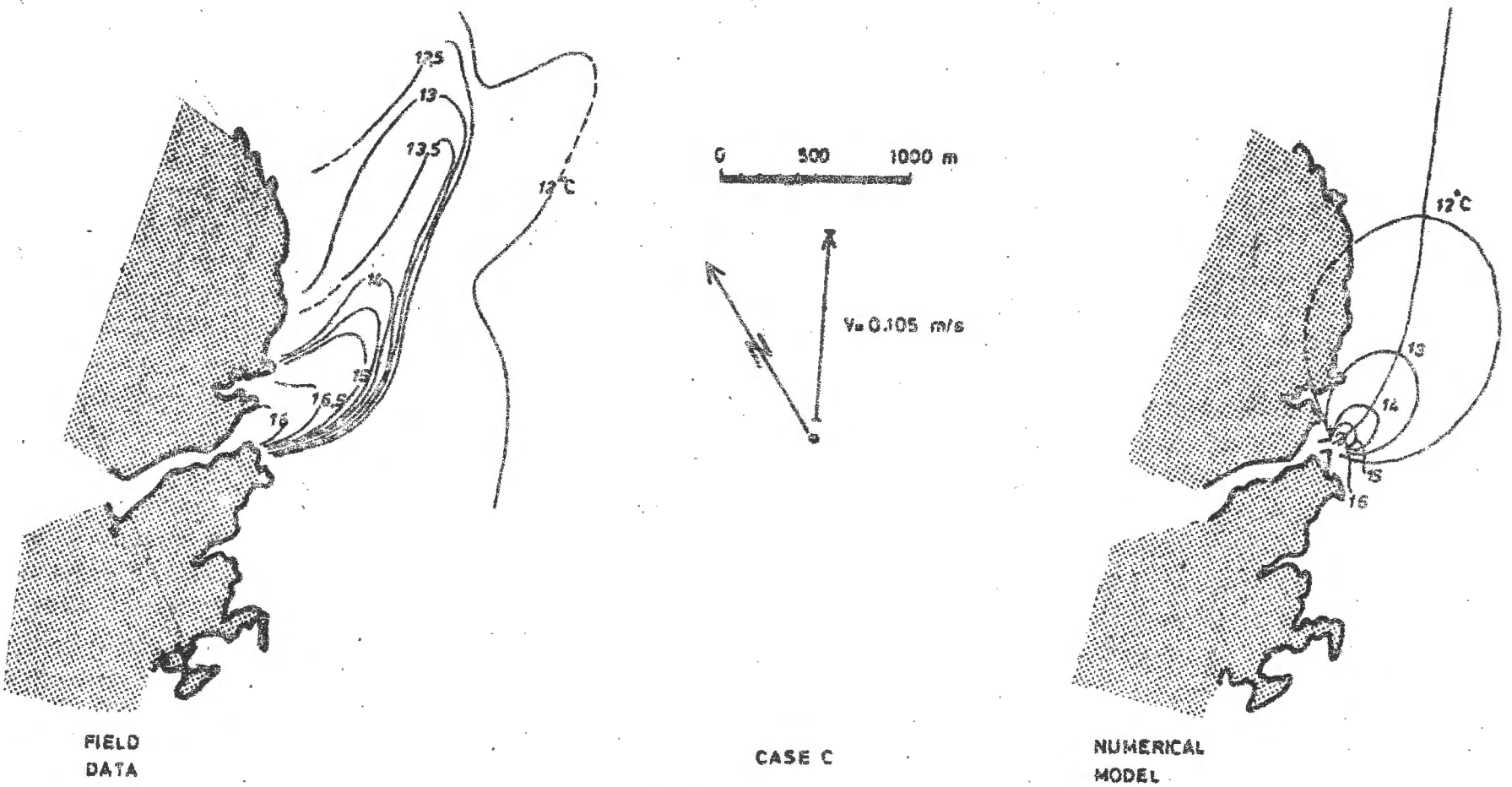

Figure 2.5 Direct comparison of isotherms, Case C

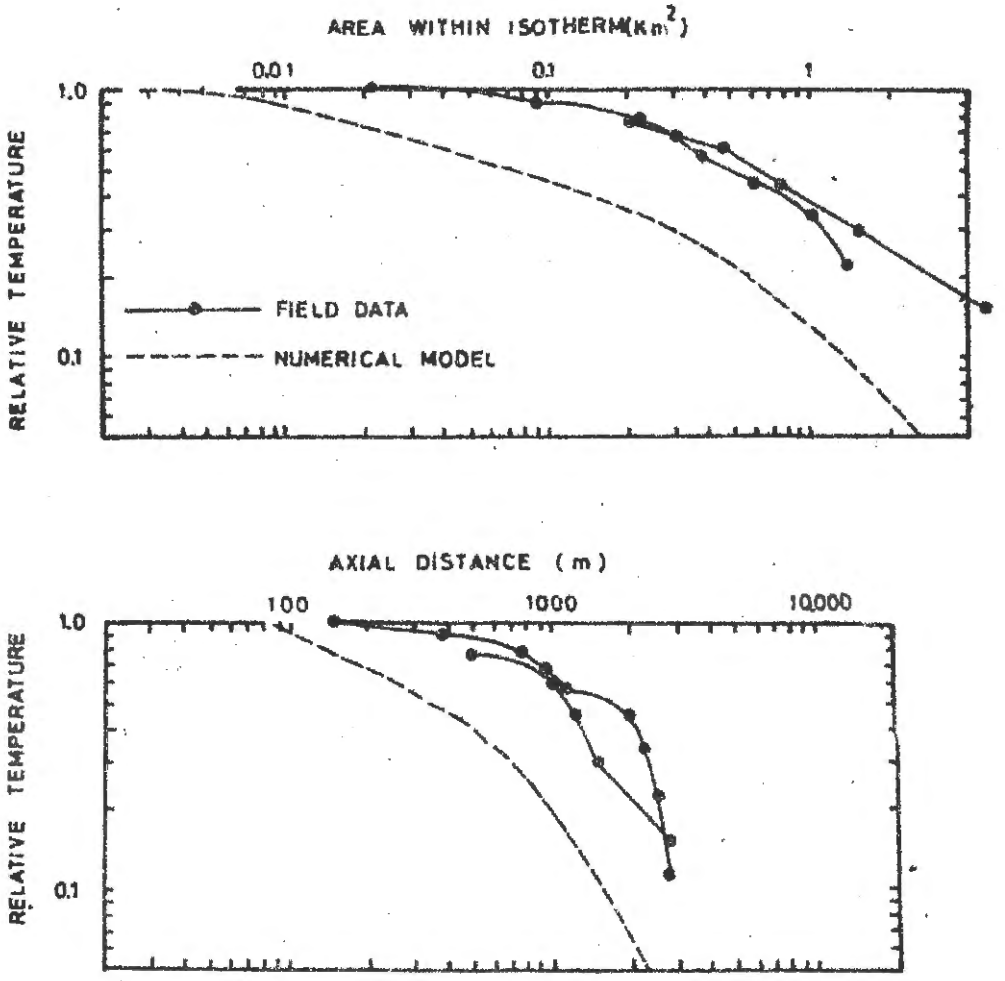

CASE C

OSKARSHAMNSVERKET 3 OCT 1972 P.M.

Figure 2.6 Relative temperature vs. enclosed area and distance, Case C

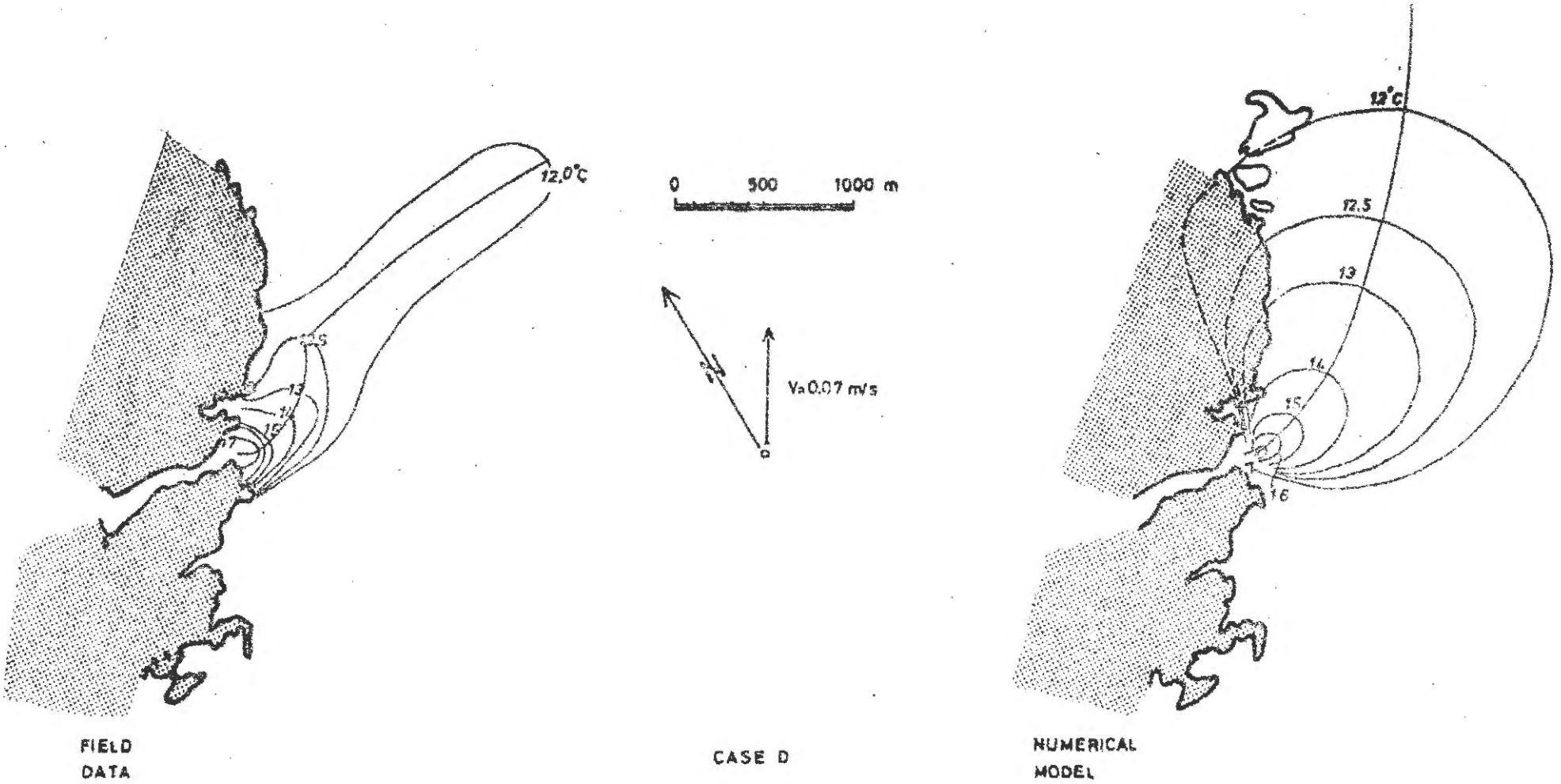

Figure 2.7 Direct comparison of isotherms, Case D

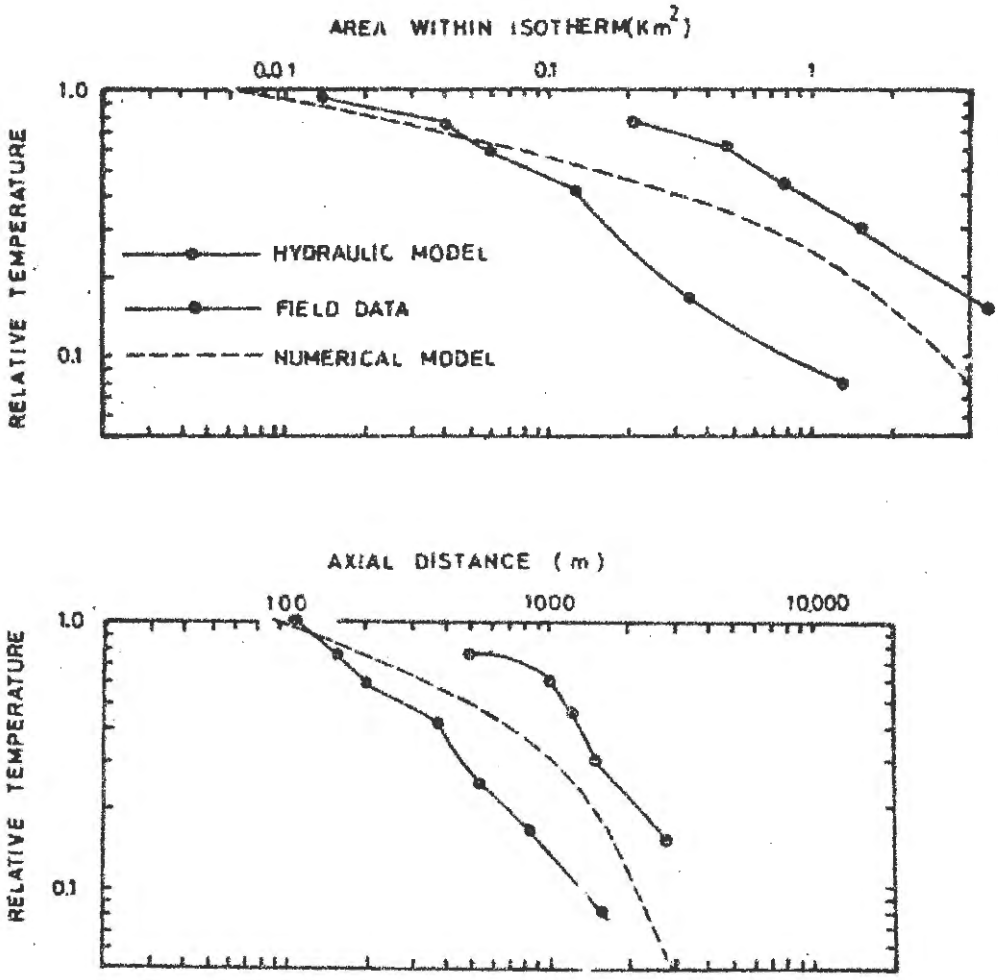

Figure 2.8 Relative temperature vs. enclosed area and distance, Case D

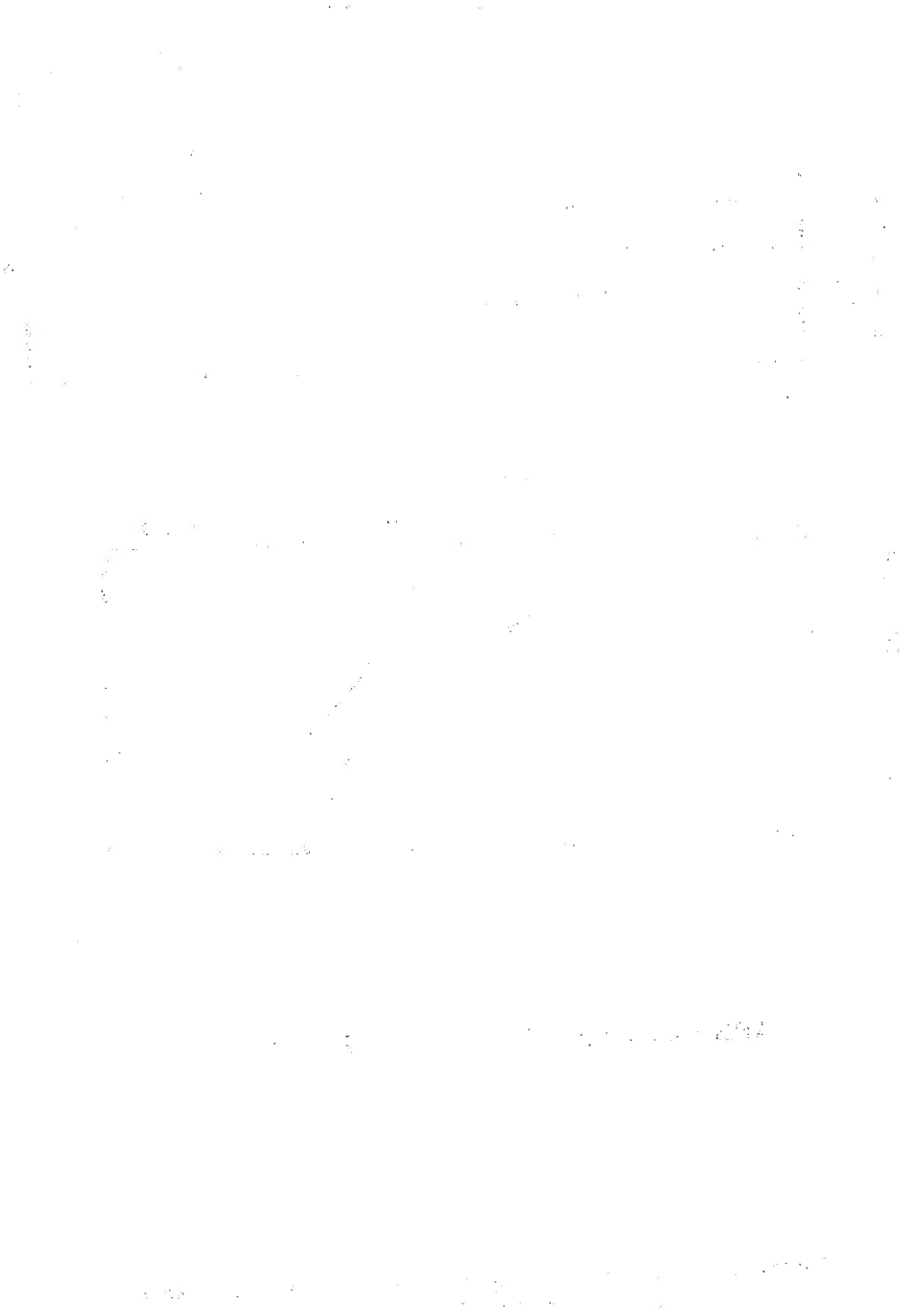

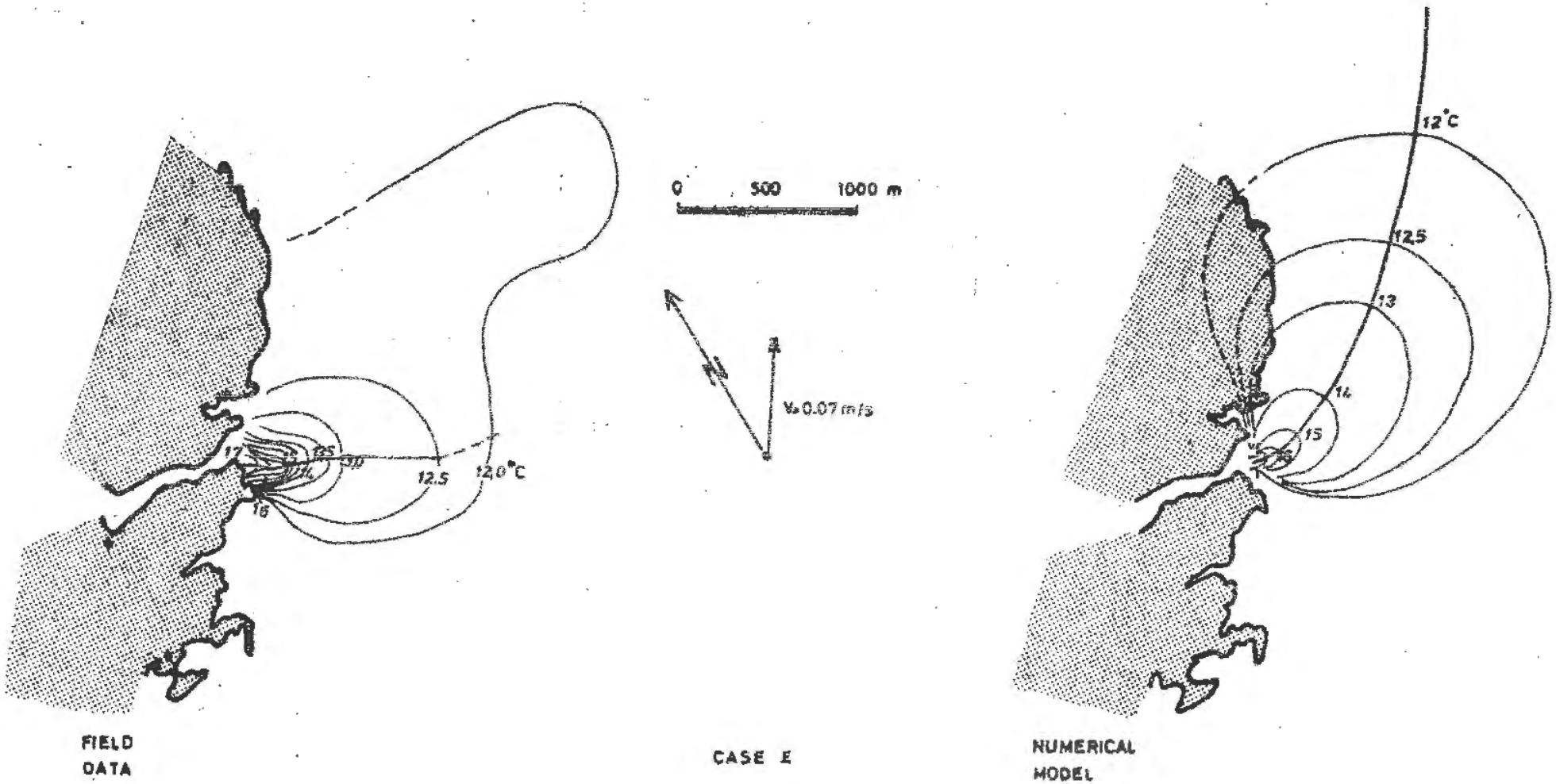

OSKARSHAMNSVERKET
4 OCT 1972 P.M.

Figure 2.9 Direct comparison of isotherms, Case E

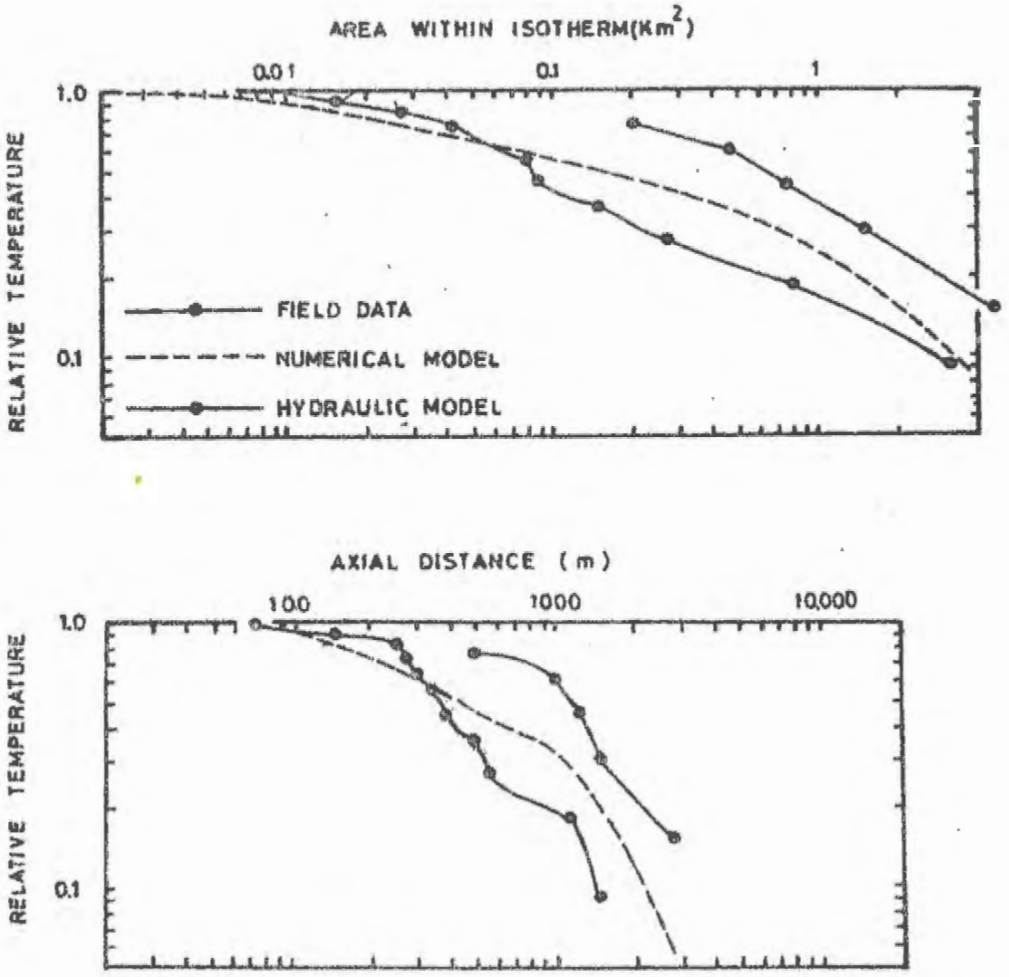

CASE E

OSKARSHAMNSVERKET 4 OCT 1972 P.M.

Figure 2.10 Relative temperature vs. enclosed area and distance, Case E

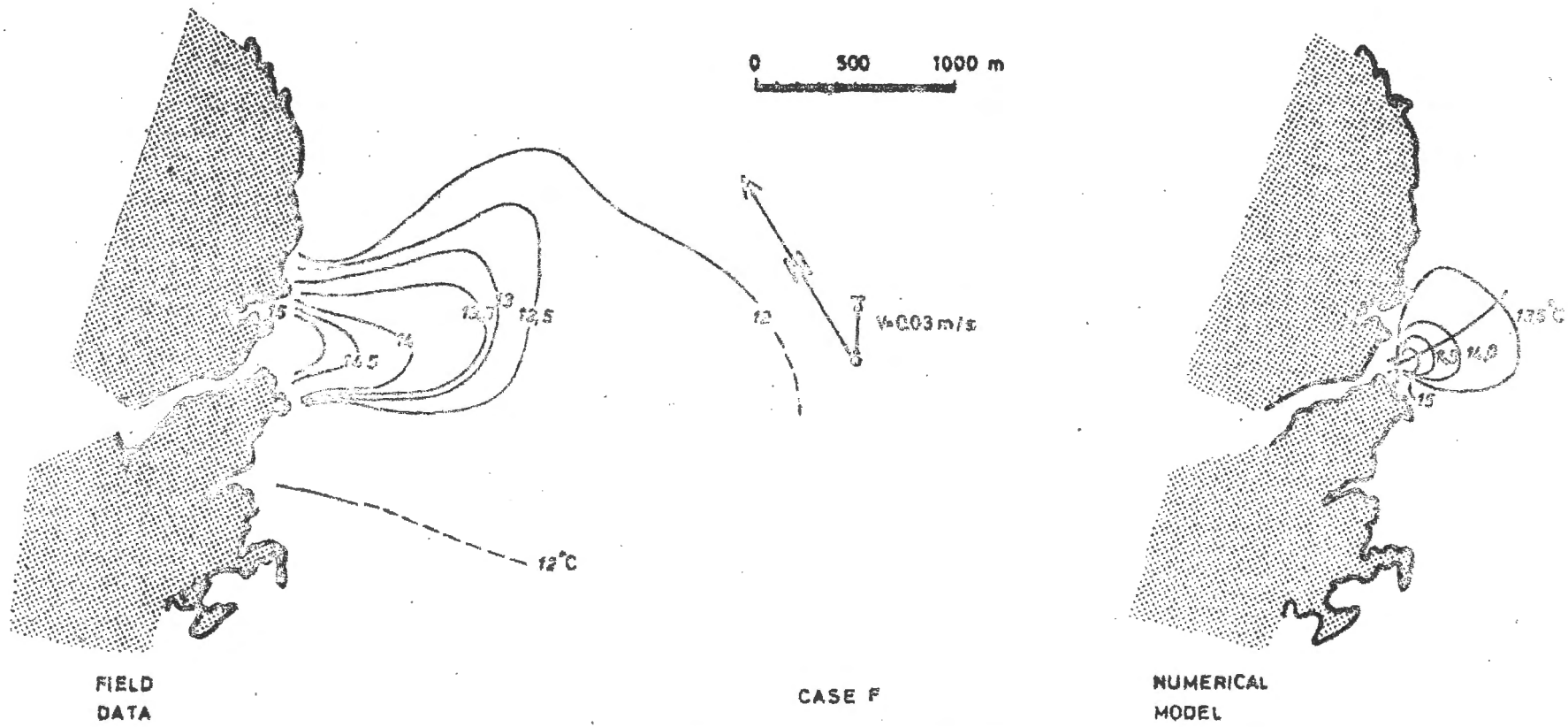

OSKARSHAMNSVERKET
5 OCT 1972

Figure 2.11 Direct comparison of isotherms, Case F

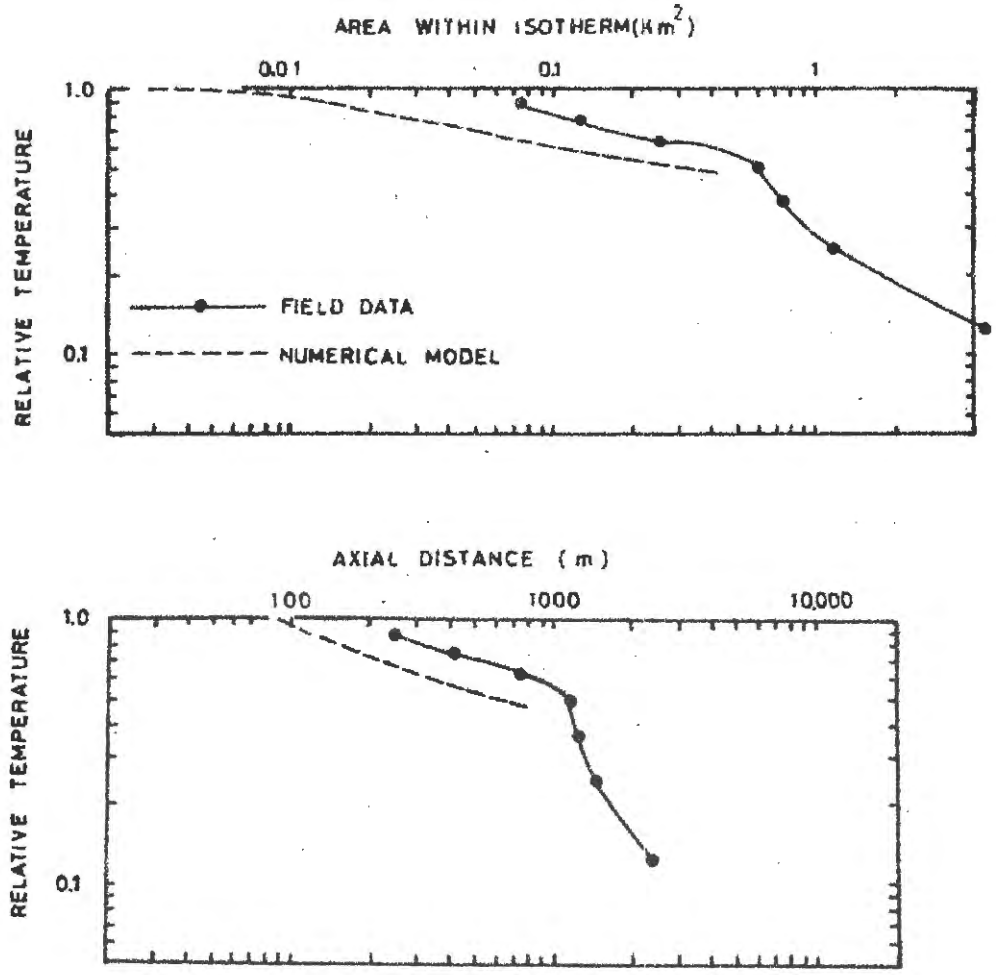

CASE F

OSKARSHAMNSVERKET 5OCT 1972

Figure 2.12 Relative temperature vs. enclosed area and distance, Case F

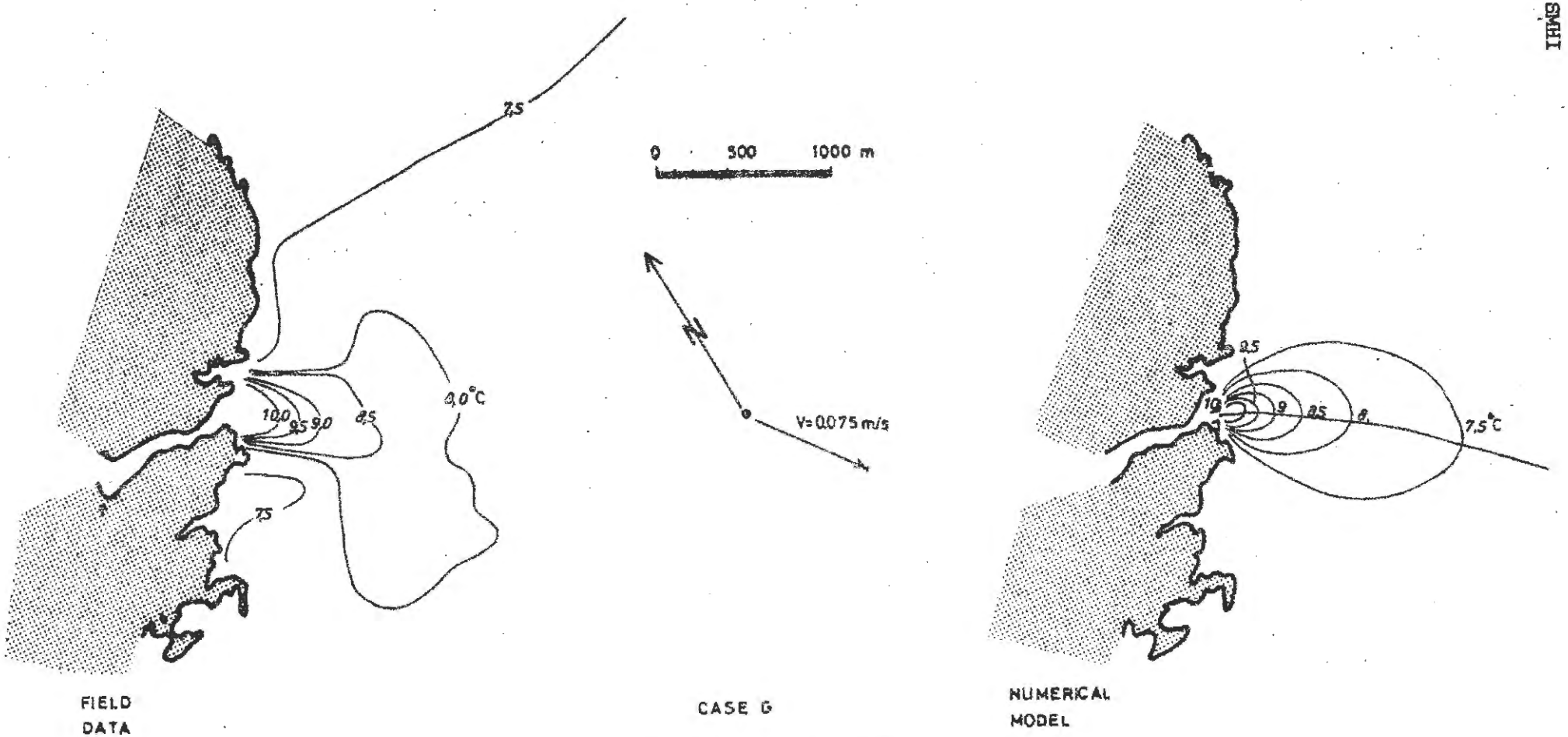

OSKARSHAMNSVERKET
14 NOV 1972

Figure 2.13 Direct comparison of isotherms, Case G

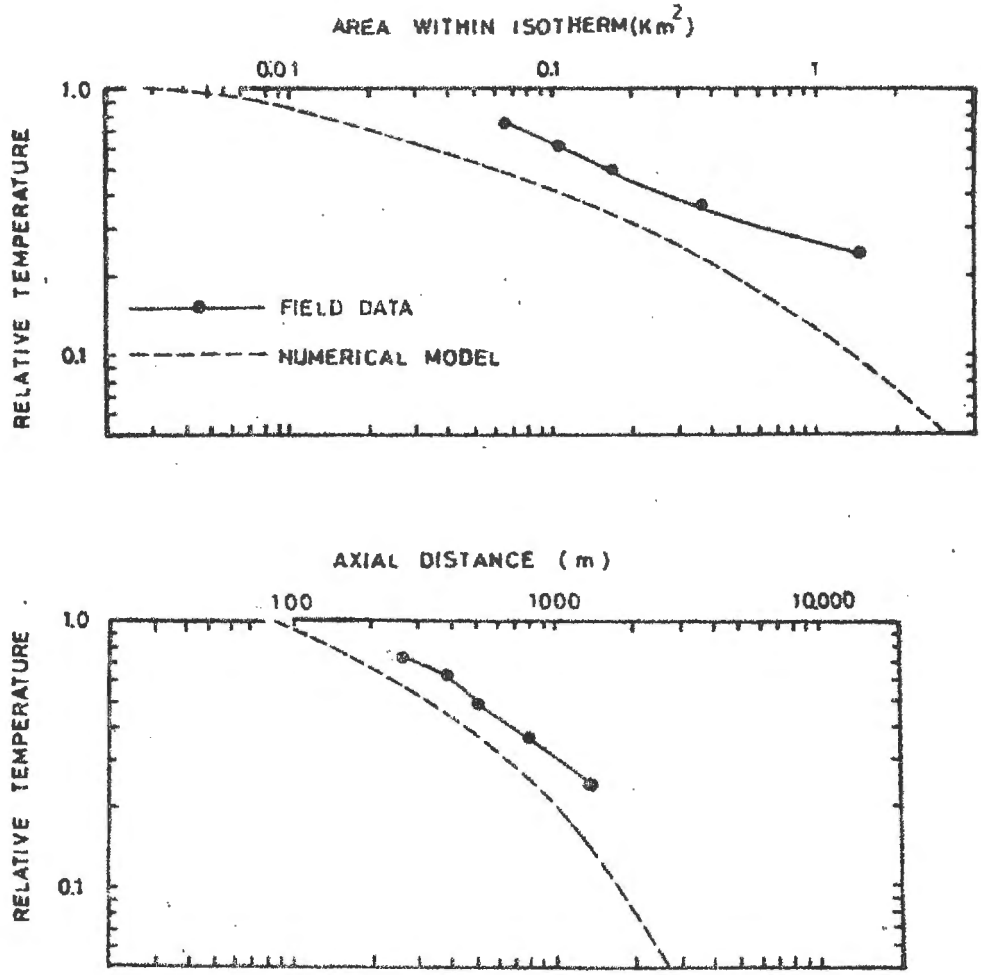

CASE G

OSKARSHAMNSVERKET 14 NOV 1972

Figure 2.14 Relative temperature vs. enclosed area and distance, Case G

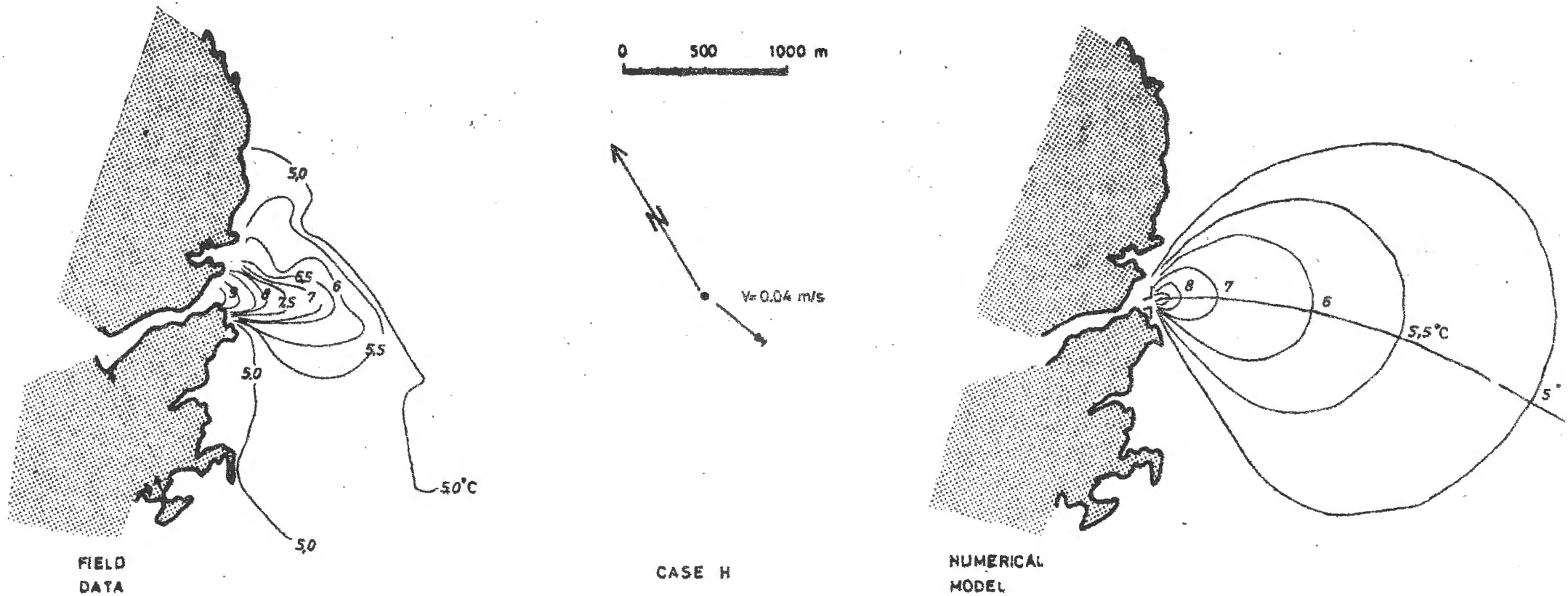

Figure 2.15 Direct comparison of isotherms, Case H

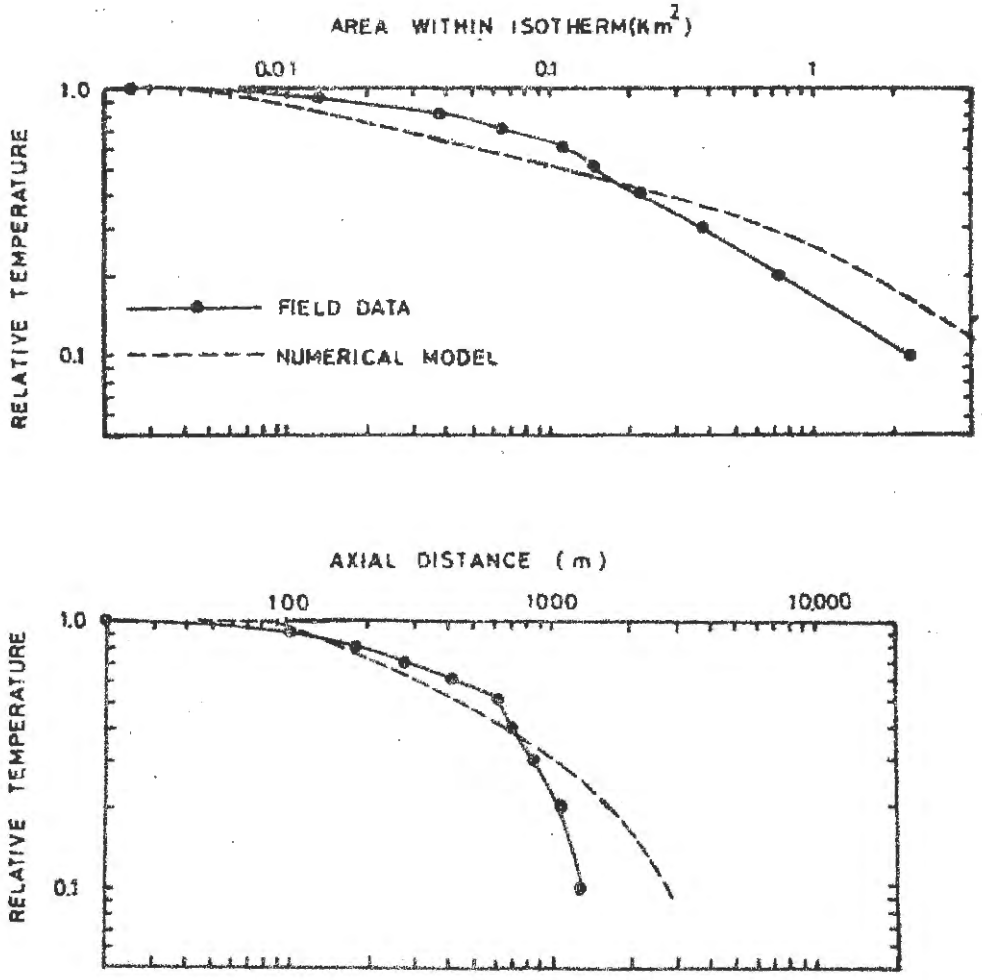

Figure 2.16 Relative temperature vs. enclosed area and distance, Case H

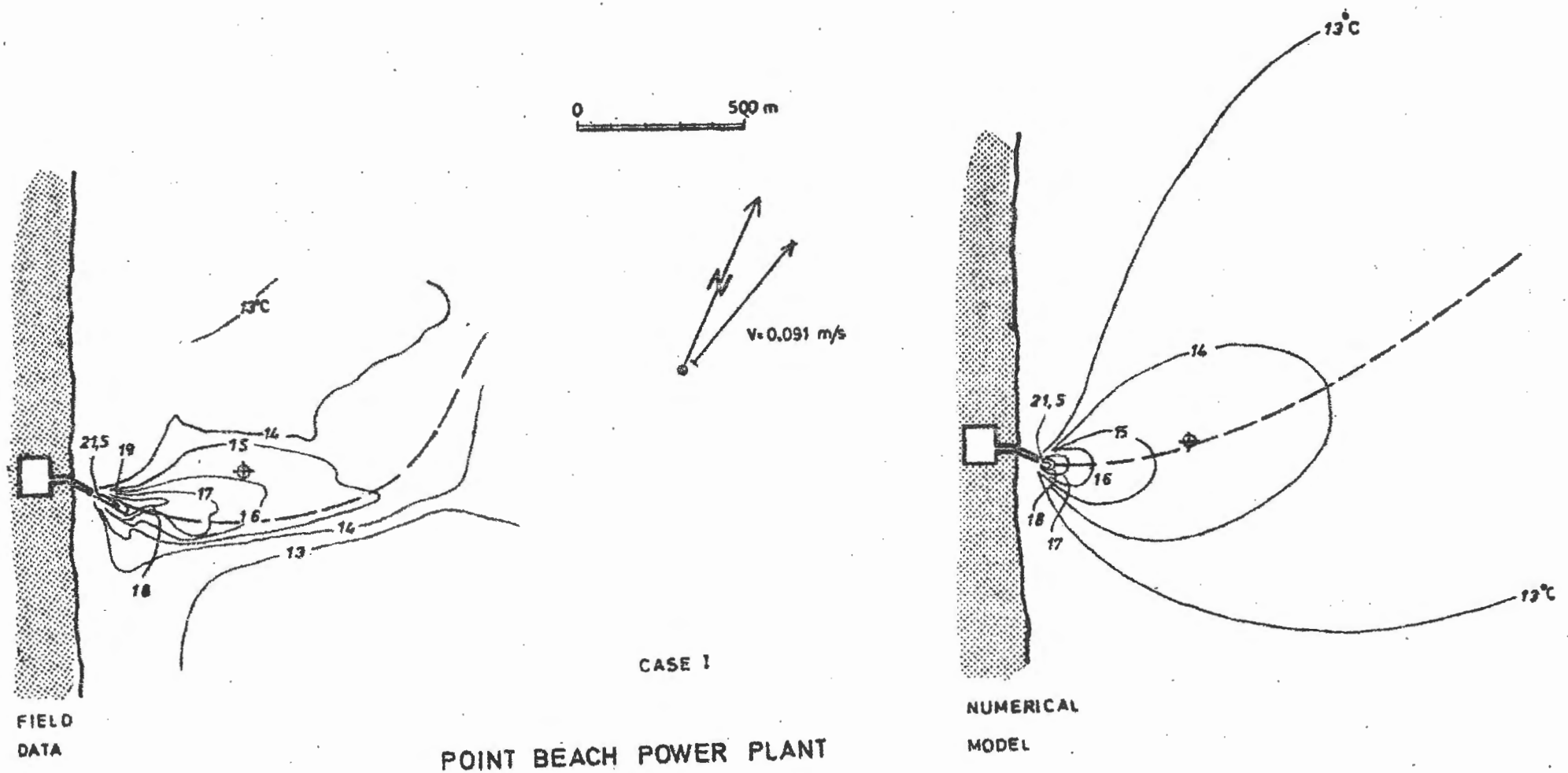

Figure 2.17 Direct comparison of isotherms, Case I

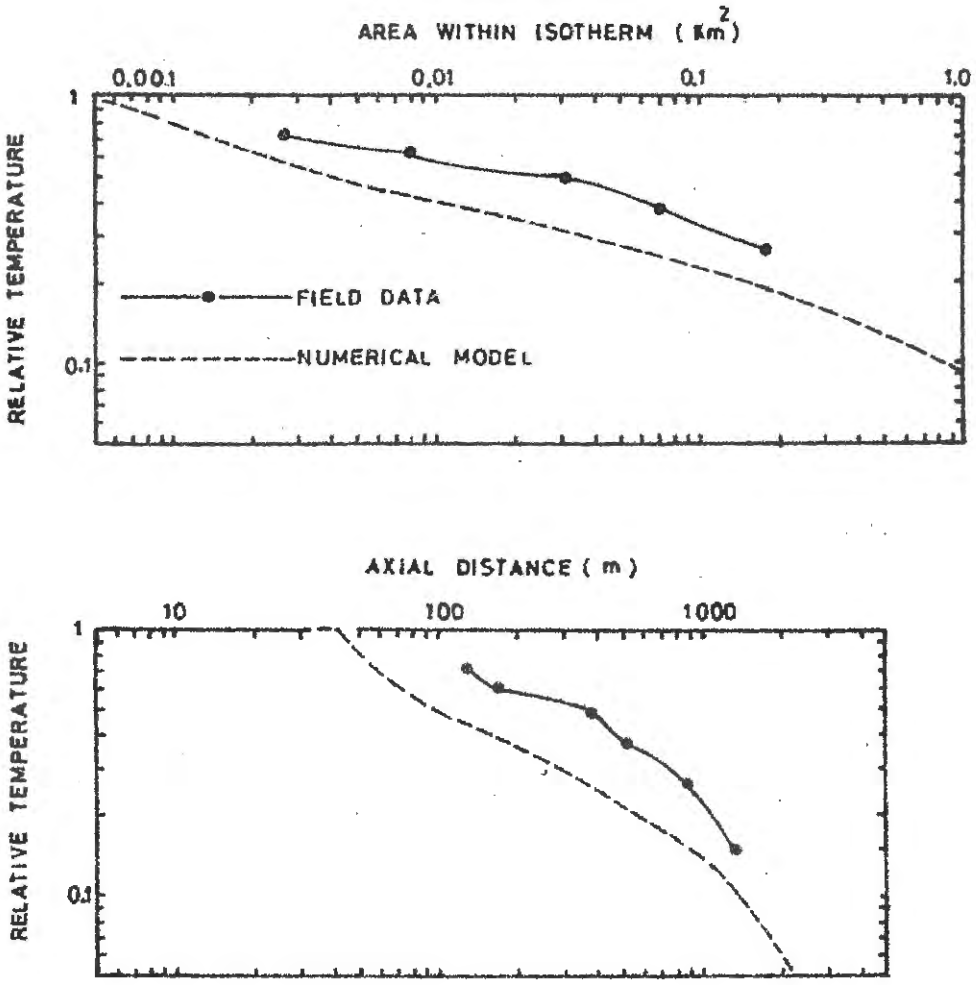

Figure 2.18 Relative temperature vs. enclosed area and distance, Case I

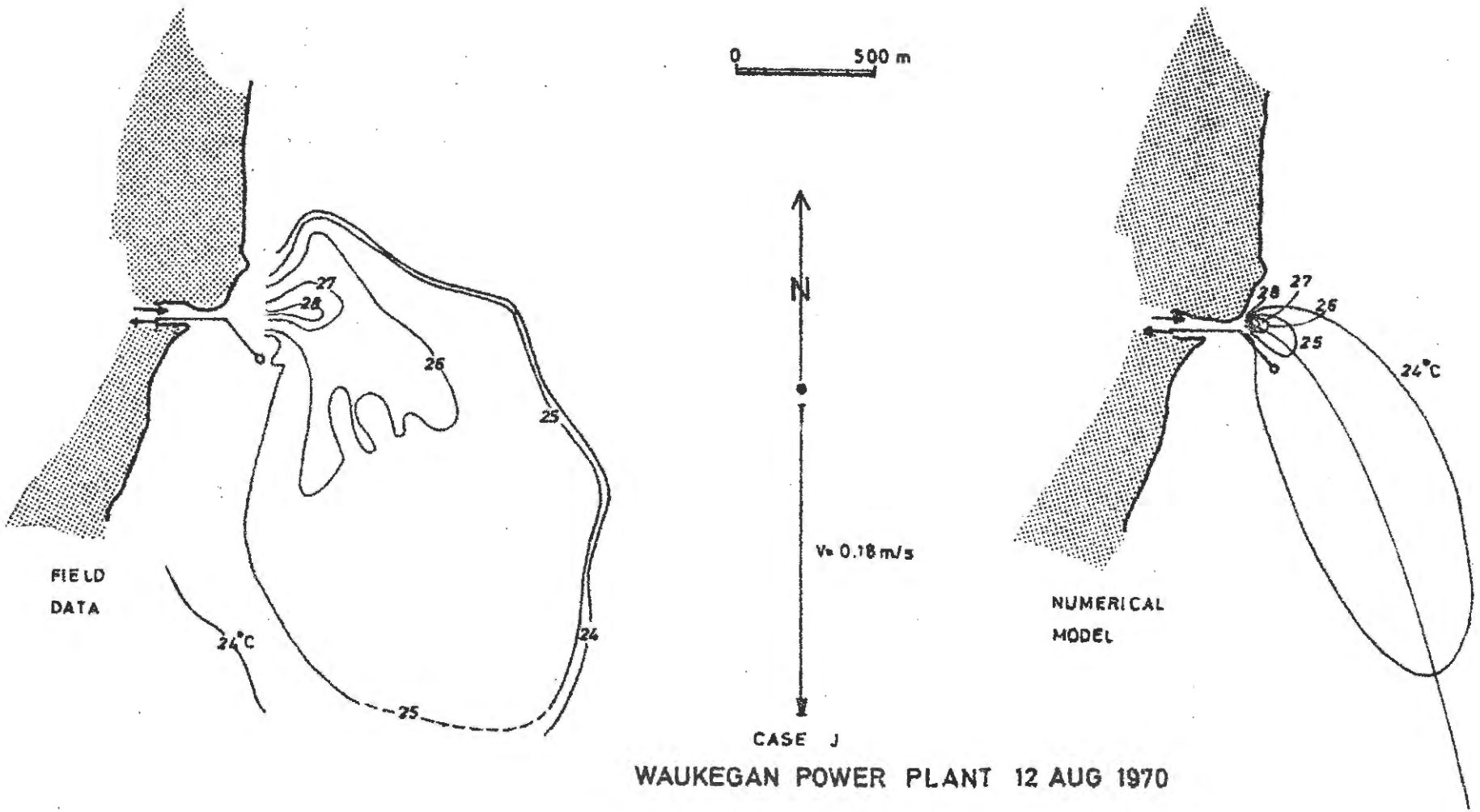

Figure 2.19 Direct comparison of isotherms, Case J

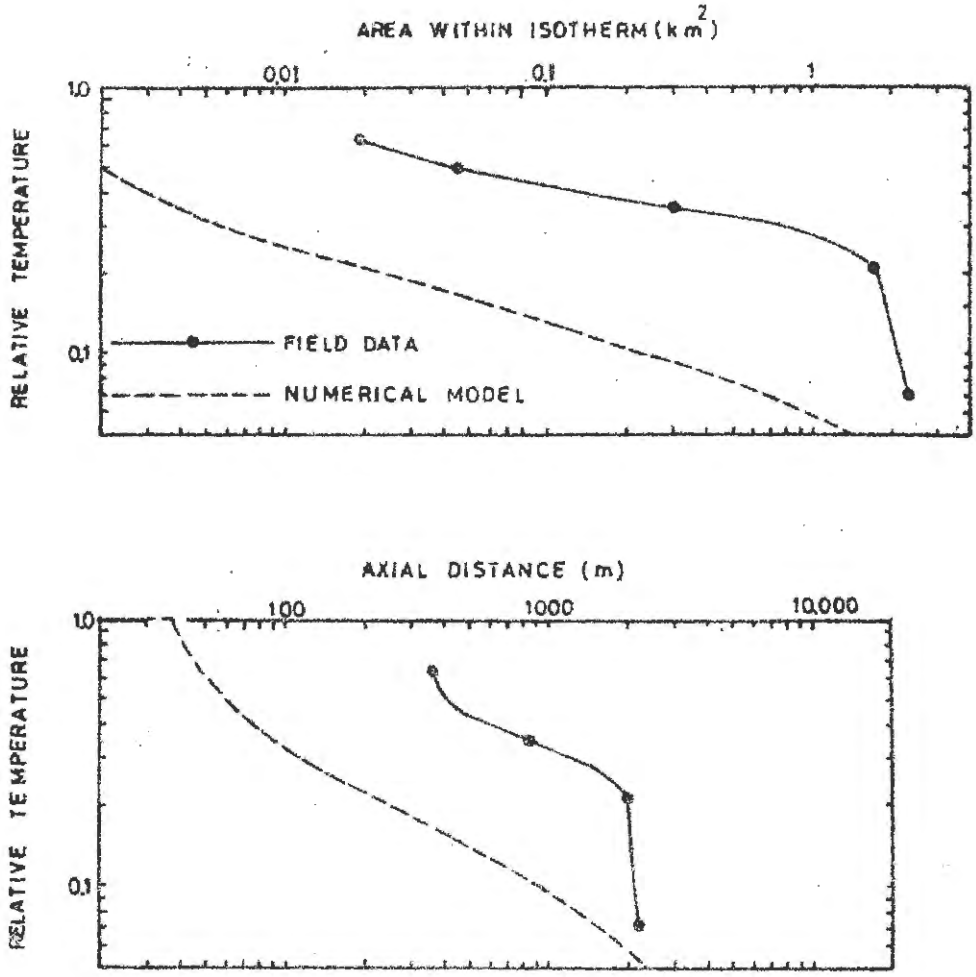

Figure 2.20 Relative temperature vs. enclosed area and distance, Case J

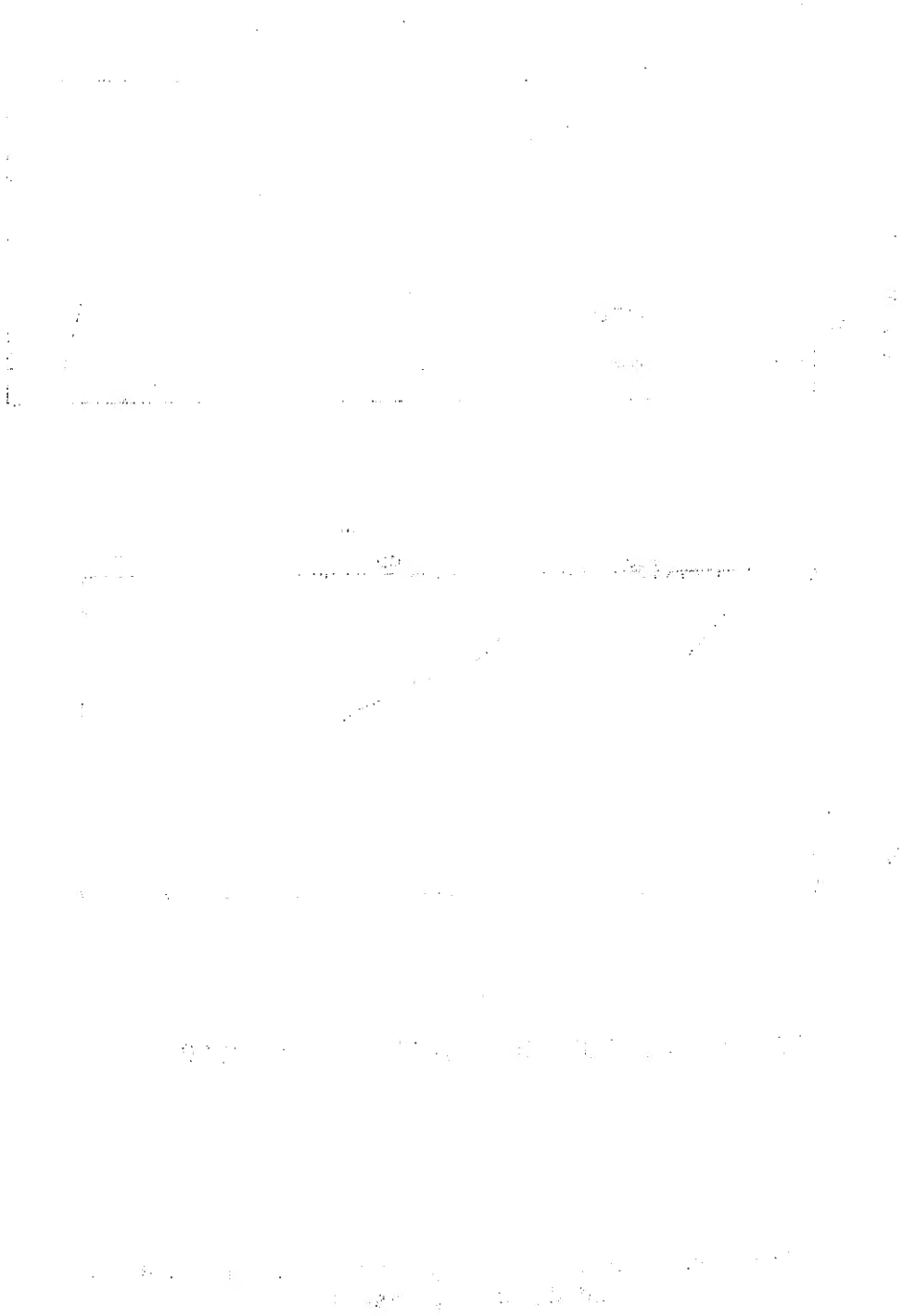

2.3 Correlation with input parameters

It is seen that the accuracy of the numerical model ranges from very good (Case B) to poor (Case C). In Cases I and J it is suspected that the prototype plumes are attached to the bottom. Numerical model layer depth predictions ($\sqrt{2}$ H vs. s) show that layer thickness exceeds lake depth in both cases. Thus prototype vertical mixing is inhibited, and temperature predictions are too low. This is especially true for Case J, where high initial Froude number produces greater layer thickness. The model's utility is somewhat limited at high Froude number if nearshore waters are not deep. Inhibited vertical mixing eliminates the only two situations not at Oskarshamnsverket, and the ranges of correlation variables, especially Froude number, are much reduced.

In order to investigate the effects of oceanographic parameters on prediction trends, correlations are listed at the bottom of Table 2.2. The accuracy of numerical prediction is subjectively evaluated for each case, judging results for relative temperature vs. enclosed area, relative temperature vs. distance, trajectory, and overall fit. The trends of predictive error (-,0, or + in the table) are then compared to each of the entries in the top part of the table. For example, does the model consistently underestimate temperature vs. distance for high or low ambient current, or for offshore winds, or at higher Froude number? Every possible such pairing was observed, with no significant correlation found. Thus predictive inaccuracy cannot be reliably correlated with any of the listed oceanographic or input parameters, within the ranges available. Admittedly, the range of Froude number is limited, as is expected for a single power plant, but temperature predictions are both too high and too low. Apparently model use at low Froude number does not induce systematic errors. Good data are not available for high Froude numbers.

One correlation to be found in Table 2.2 is between temperature error vs. distance and temperature error vs. area, but this is obvious because the two are interdependent. Another correlation is found between temperature error and trajectory error. When numerical model temperatures are too low, predicted plumes tend to become parallel to the ambient current too quickly. This is due to increased momentum in the ambient current direction due to increased entrainment for mixing. Indication that predicted plumes overlap coastal boundaries cannot be correlated with temperature error.

All such correlations were made subjectively, reasoning that for only ten situations the trends sought could be seen by direct comparison. Rather than statistically correlate all the predictive errors with input parameters, the comparative results are presented directly, leaving to the reader's judgment the determination of "accuracy" according to his own intuition. Predictions are presented without limits or error bands because the ranges of input variables are too small to allow use of such confidence intervals in other situations.

Predictive inaccuracies for the cases presented are apparently due to effects not included in simple hydrological description

of the ten situations. The question then arises as to whether errors are due to true model inaccuracy or imprecise description of input variables. This is especially important at Oskarshamnsverket, where the input conditions are not well known. In order to test the sensitivity of temperature errors to chosen values of input variables, some numerical experiments were made. For Case A the model input was adjusted for three different values of H_c (2.5, 3.0, and 4.0 m). Discharge velocity, Froude number, and heat output were kept constant, adjusting Q_o and $\Delta\rho$ for different degrees of mixing in Hamnefjärden. Model results for the three cases are shown in Figure 2.21, along with field data. Two other variations were tested, one by changing H_o and F_o for constant dilution in the inlet, and the other by changing only $\Delta\rho$. Model temperature sensitivities to these changes are even less than that shown in Figure 2.21. One concludes that model temperature errors are due principally to hydrological factors, not imprecise description of input variables at the mouth of the inlet. Two such hydrological factors could be time-varying ambient flow conditions and inconsistency of the forms of vertical temperature and velocity distributions.

2.4 Hydraulic model data

Although it is not intended to verify hydraulic (laboratory) model results with prototype temperatures, a few such results are available for comparison. A distorted hydraulic model of the Oskarshamnsverket area has been built and operated at Chalmers Tekniska Högskola, Göteborg, horizontal scale 1:400 and vertical scale 1:50. Results presented are by private communication from Chalmers.

The model situations applicable to prototype comparison are for discharge flow of 22 m^3/s, ambient currents parallel to the coastline (north and south) at 5-10 cm/s. Different values of $\Delta\rho$ were tested. Model surface temperatures for south-flowing current, $\Delta\rho$ = 1.0 kg/m^3 are compared to Case A, as shown on Figure 2.2. See Chapter 4 for a discussion of measurement of temperature at the surface and at 0.5 m depth. Temperatures were normalized with temperatures at the mouth of Hamnefjärden. Thus in Figure 2.2 the highest relative temperature is 0.76, although the data were taken from areas and distances to the 0.5 isotherm relative to the plant discharge temperature.

Model results for north-flowing current, 5-10 cm/s, surface temperatures are shown in Figures 2.6, 2.8, and 2.10 for Cases C, D, and E. Model results are adjusted in two ways. First, temperatures are normalized with temperatures at the mouth of the inlet. Second, results are averaged between results for $\Delta\rho$ = 1.0 kg/m^3 and $\Delta\rho$ = 2.0 kg/m^3 at the plant outlet. The resulting effective density difference is $\Delta\rho = ((1.0+2.0)/2) \times 0.66 = 0.99$ kg/m^3. This best matches prototype values of 1.0, 0.96, and 0.97 kg/m^3. Hydraulic model correlation is not generally as good as numerical model correlation, partly because hydraulic model conditions do not exactly match prototype conditions.

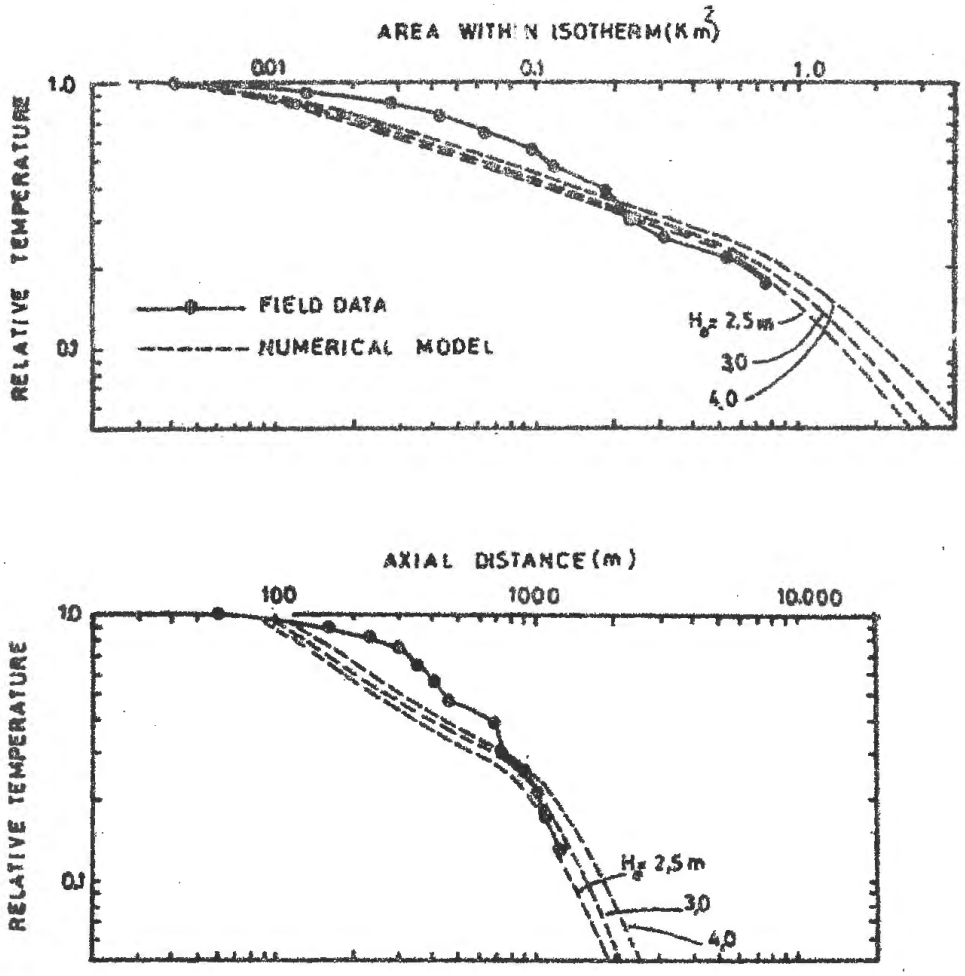

Figure 2.21 Sensitivity of numerical model to input variables, Oskarshamnsverket

2.5 Open channel mixing data

One feature contained in the Prych (1972) model that is not included in the Stolzenbach and Harleman (1971) model is mixing due to ambient turbulence, or turbulent diffusion. In order to verify the model for diffusion, results are compared with experimental results of Weil (1972) for mixing of a heated water jet in open channel flow. In the laboratory situation heated water is injected through a semi-circular nozzle at the surface of a channel flow. The jet velocity is parallel and equal to the local channel velocity. Downstream mixing is due to interaction between jet buoyancy and ambient turbulence. Weil's results for two laboratory runs are shown in Figure 2.22. The flow conditions for Runs 23 och 48 in the figure are density difference $\Delta\rho = 1.9$ kg/m^3, velocity $u_o = V = 30.5$ cm/s, depth of flow d = = 12.7 cm, equivalent jet diameter = 1.35 cm, and Darcy-Weisbach friction factors = 0.022 and 0.070. The numerical model was run for the same conditions, assuming a model scale of 1:100 for numerical purposes. The undistorted scaling does not affect the results. The semi-circular nozzle is scaled as a rectangle with the same width and outlet area. The numerical model has no difficulties in running when the discharge and ambient velocities are equal.

A measured value of horizontal diffusion coefficient is used in the model, calculated from $\varepsilon_H = 0.027\, u_* d$, in which ε_H = horizontal diffusion coefficient and u_* = channel shear velocity. The vertical diffusion coefficient ε_V is taken as one fourth of ε_H, as calculation of ε_V using a Karman similarity profile yields a coefficient that seems unreasonably large. Even the factor 0.027 in the expression above is lower than for most channel flow data, but it was determined by measurement, if only approximate.

The results of the model runs, in terms of axis temperature vs. downstream distance, are shown in Figure 2.22. The model slightly overestimates the relative importance of friction factor, but the overall correlation is good.

The same laboratory experiments show independence of relative temperature and initial density difference. This conclusion is confirmed by the numerical model, as shown in the second graph of Figure 2.22. The computer model was run three times for identical input conditions except density difference $\Delta\rho$. The temperature results for the various values of $\Delta\rho$ are indistinguishable.

2.6 Interfacing with undistorted hydraulic models

In principle the numerical model includes the effects of all four mixing zones described in Chapter 1.1. However, Prych (1972) cautions that the biggest shortcoming of the model is exclusion of the effects of coastal boundaries. It is proposed that the numerical model can be used in conjunction with results from undistorted hydraulic models, dividing the total flow field into two regions that together cover all the important mixing zones. Tsai (in Policastro and Tokar; 1972, pp. 303-328) presents a

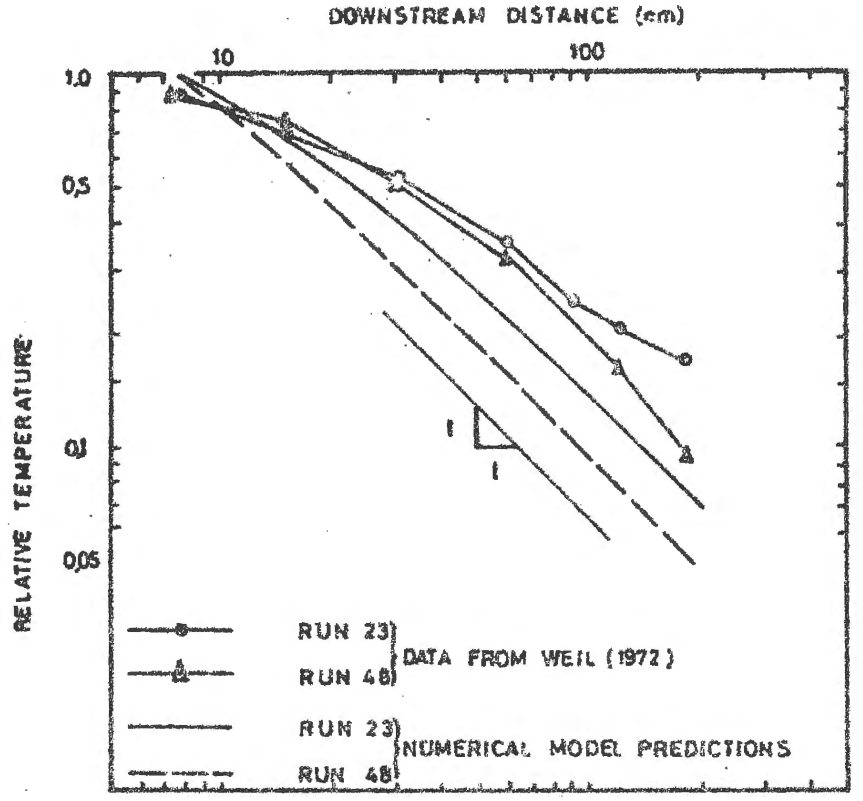

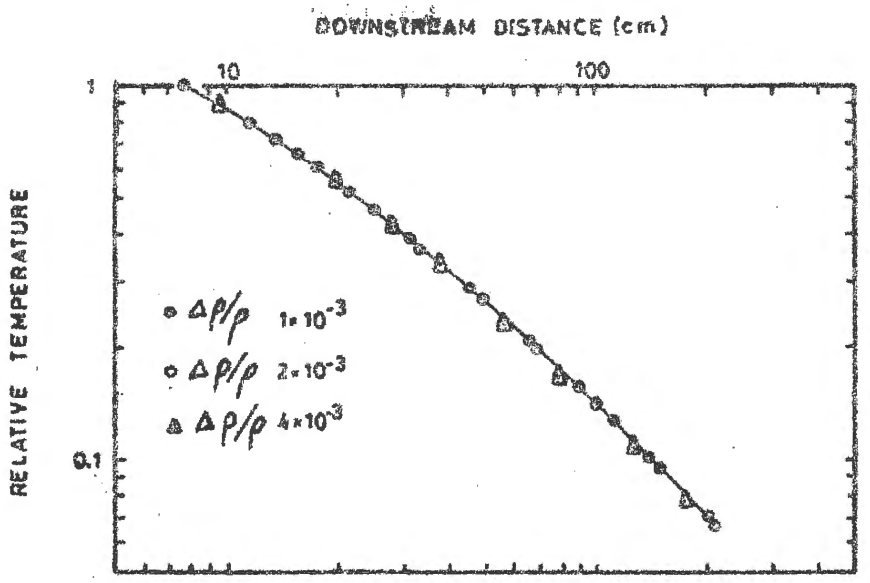

Figure 2.22 Comparison of numerical model and open channel mixing data

scheme for interfacing distorted model results with analytical methods, but does not include all mixing mechanisms.

An undistorted hydraulic model correctly scales the effects of jet momentum and buoyancy, including their interaction with nearby coastal features (in terms of constraint and separation, if not boundary friction). The hydraulic model does not properly reproduce turbulent mixing, and can scale atmospheric heat loss only by careful manipulation of laboratory air conditions. It is proposed that undistorted model results can be used out to a point where the plume is entirely separated from the shoreline and sea bed, but the functional forms of plume temperature and velocity are still reasonably well defined. Measurements at that point, herein called the interface, can be used as input to the numerical model. The numerical model retains what momentum and buoyancy are left, then properly includes turbulence and atmospheric losses into the far field.

It is difficult to verify this concept because few undistorted models are large enough to extend into the far field, and hydraulic models are themselves unverified with respect to prototype temperature data. However, the approach was applied to a special situation at a 1:75 model of the proposed Forsmark Power Plant on the northeast coast of Sweden. The situation chosen is Experiment Nr 19G in a report of model results by Statens Vattenfallsverk (1972), in which 200 m^3/s of 10°C temperature rise cooling water is discharged through an open channel into Öregrundsgrepen, a wide channel in the Baltic Sea. The discharge channel depth is 2.3 m, with discharge velocity of 2.0 m/s. There is an ambient current of 10 cm/s nearly perpendicular to the outlet. Model temperatures for 0.5 m depth are shown in Figure 2.23.

The 6°C isotherm on the plume axis is chosen as the interface, a location 240 m from the outlet. At that section the characteristic width of the plume is (using Prych's terminology) $2B = 188$ m, and the characteristic layer depth is $H = 5.15$ m. The trajectory angle is $\theta = 120°$. Model velocities were not measured, but total flow Q can be calculated from the isotherm value. Using equation (10) from Prych (1972) and assuming no atmospheric losses near the plant, $Q = 2Q_o/T = (2)(200)/0.6 = 667$ m^3/s. This is now enough information to run the numerical model for the continuing hydraulic model situation. For a laboratory model it is suggested that diffusion coefficients be set at zero, but measured values could be used for prototype predictions.

Results from the numerical model are shown in Figures 2.24 and 2.25, starting both at the outlet and at the interface. The improvement by starting at the 6°C isotherm is obvious and not unexpected. It appears that the major source of numerical model error comes in the early stages of mixing. Actually, for the case considered, much the same results could be obtained by merely moving the numerical results for outlet conditions so that the 6°C point coincides with the field data. This type of curve-fitting should be avoided, but the example shows that beyond the interface mixing proceeds nearly independent of the dilution at that point. The hydraulic model results do not extend far enough to adequately describe the far field, stopping at the 3°C iso-

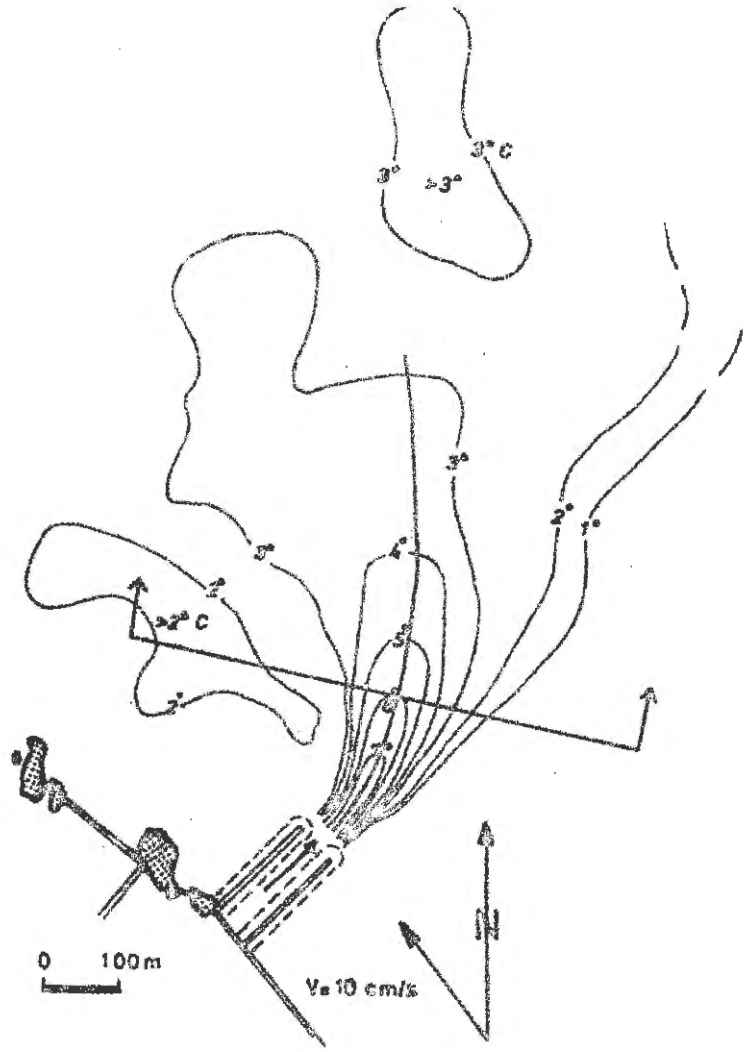

Figure 2.23 Forsmark Power Plant model temperatures

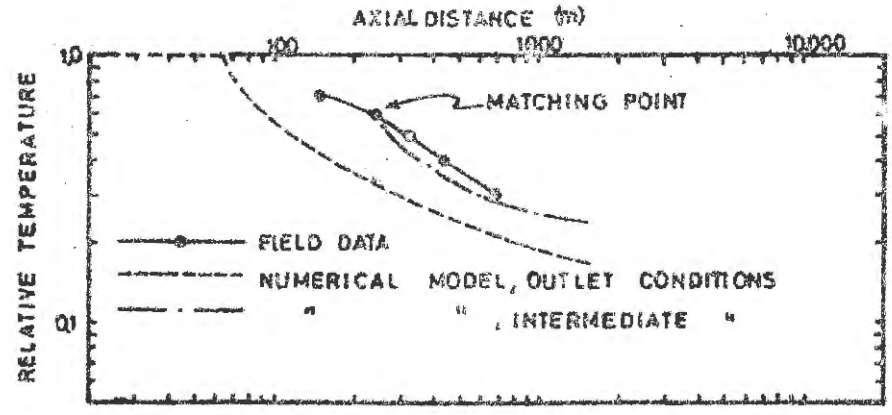

Figure 2.24 Comparison of temperature vs. distance, Forsmark undistorted model

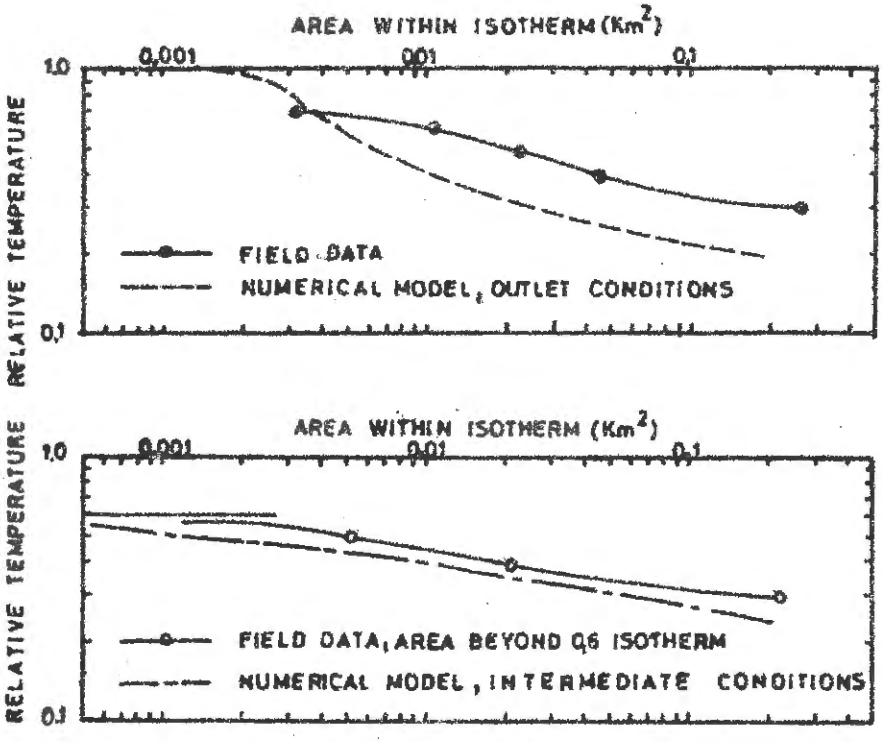

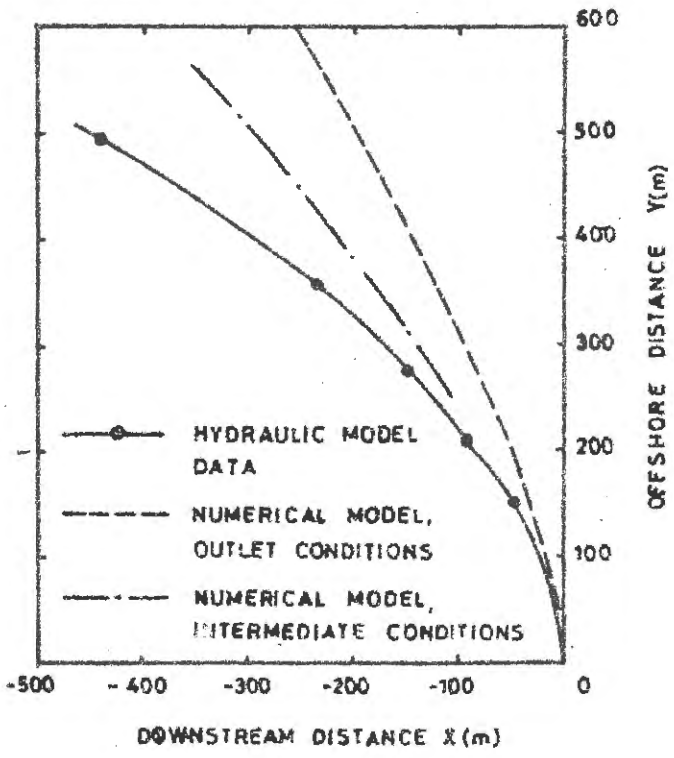

Figure 2.25 Comparison of enclosed areas and trajectory, Forsmark undistorted model

therm. Results for plume trajectory show less marked improvement by starting at the interface. Because axis curvature is still less than in the hydraulic model, perhaps the numerical model would tend to underestimate far field mixing nearer the 2°C and 1°C isotherms. The same effect would be noticed if hydraulic model mixing due to ambient turbulence were significant. Alternately, trajectory errors could be due to hydraulic model imprecision of current direction or persistent coastal effects on ambient current.

CHAPTER 3. COMPARISON WITH OTHER MODELS

3.1 Dimensional analysis

In this chapter numerical model results are compared with results from phenomenological and selected analytical models. In order to account for all important input variables, the discharge situation is described nondimensionally. As seen in Figure 3.1, the four thermal plume dependent variables are: relative temperature $T = (T_s-T_a)/(T_h-T_a)$, plume width B, layer depth H, and axis position Y. In the numerical model the horizontal and vertical temperature distributions are Gaussian, and B and H are defined as $\sqrt{2}$ times the standard deviations of those distributions. The independent variables are:

$$(s, V, Q_o, \Theta, B_o, H_o, \rho, \Delta\rho, \nu, g, \varepsilon_H, k),$$

where s = distance along the plume axis (m), V = ambient current velocity (m/s), Q_o = discharge flow (m^3/s), Θ = discharge angle (^{o}), $2B_o$ = outlet width (m), H_o = outlet depth (m), ρ = ambient water density (kg/m^3), $\Delta\rho$ = discharge density decrease (kg/m^3), ν = ambient water kinematic viscosity (m^2/s), g = acceleration of gravity (m/s^2), ε_H = horizontal diffusion coefficient (m^2/s), and k = atmospheric heat loss coefficient (m/s). There are generally three components to diffusion coefficient, but if they are proportional a single variable suffices. In presentation of data the shoreline-parallel coordinate x is substituted for s as is convenient. Dependent variables T, B and H are best described as functions of s, but trajectory Y is most conveniently given as a function of x.

The twelve independent variables contain three physical dimensions, so we find nine independent dimensionless variables. Substituting outlet velocity $u_o = Q_o/2B_oH_o$ for the flow variable, the nine dimensionless quantities are:

$$\left(\frac{s}{H_o}, \frac{\Delta\rho}{\rho}, \frac{u_oH_o}{\nu}, \frac{V}{u_o}, \Theta, \frac{2B_o}{H_o}, \frac{u_o}{(\frac{\Delta\rho}{\rho} g H_o)^{1/2}}, \frac{\varepsilon_H}{u_oH_o}, \frac{k}{u_o}\right).$$

Assume that $\Delta\rho/\rho$ has no effect, by the Boussinesq approximation. The third term is recognized as a Reynolds number, and experimental evidence shows that it is unimportant if the flow is strongly turbulent. The fourth dimensionless number is a current ratio $R \equiv V/u_o$. The sixth term is the aspect ratio of the outlet $A \equiv 2B_o/H_o$. The seventh term is a jet Froude number, written as $F_o \equiv u_o/((\Delta\rho/\rho)\, g\, H_o)^{1/2}$. The next term is a diffusion ratio $E \equiv \varepsilon_H/u_oH_o$. The diffusion ratio represents the ratio at the outlet of plume entrainment velocities due to ambient diffusion and due to jet velocity. Prych (1973) discusses diffusive entrainment velocity. Thus we write the functional dependencies of the plume variables as:

$$(T, B/H_o, H/H_o, Y/H_o) = f(s/H_o, R, \Theta, A, F_o, E, k/u_o).$$

The choice of H_o as the distance scaling variable is somewhat arbitrary, but is valid if aspect ratio A is retained.

The effect of heat loss coefficient k/u_o on plume variables is discussed by Prych (1972), and prototype data are not available for comparison, so it is not considered in the following sections.

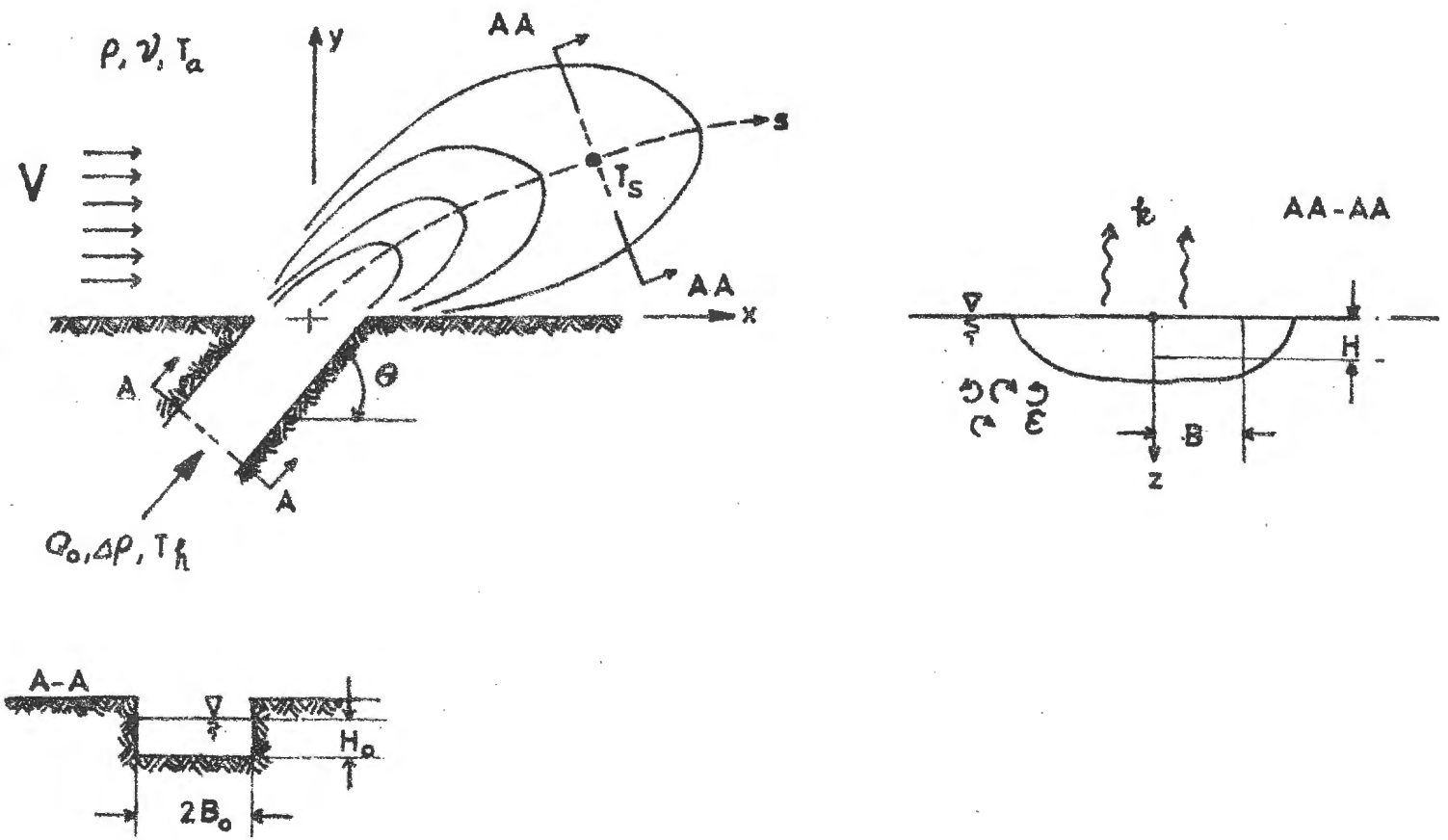

Figure 3.1 Situation for dimensional analysis

3.2 Power law model

The simplest descriptions of thermal discharge plumes are phenomenological models. One such model has been presented by Shirazi (1973). Shirazi writes dimensionless plume parameters as power law functions of the dimensionless independent variables (x/H_o, R, θ, A, F_o). A computer is then used to correlate much laboratory and field data with temperature results. Calculated are the various power law coefficients giving best fit to the data. It is emphasized that the model is not intended to be predictive, but can be used to check the input variable sensitivities of predictive schemes such as the numerical model presently considered. The Shirazi model should not be applied to specific design situations.

Shirazi (1973) presents different power laws for flow into stagnant receiving water, flow over a sloping bed, and flow into a moving current. Results shown here are only for the last case. Using a plume width variable $B_{1/2}$, plume half width to the point where temperature equals half of the axis value, the following best fit relationships are found:

$$T/F_o^{-0.360} A^{0.234} \text{ vs. } (x/H_o)R^{0.370} \theta^{-0.352},$$

$$(B_{1/2}/H_o)/F_o^{-0.372} A^{-0.255} \text{ vs. } (x/H_o)R^{-0.104},$$

$$(Y/H_o)/R^{-0.707} \theta^{0.796} \text{ vs. } x/H_o \text{ for laboratory data,}$$

$$(Y/H_o)/F_o^{-1.013} A^{0.0666} R^{-0.2454} \theta^{0.7084} \text{ vs. } x/H_o \text{ for field data}$$

Plume depth H/H_o cannot be correlated, and diffusion ratio is not considered. Shirazi presents the four functions graphically as hand-drawn curves best representing the many data. Scatter is large, as is expected for such diverse test conditions, but trends are well described. The placements of the dimensionless variables on left or right sides of the functions are not explained, but are probably chosen for best correlation. For this reason, data for the numerical model will be presented in the same way.

It is desired to perform a series of numerical experiments on the model to be verified, developing relationships similar to those above and calculating power law coefficients to compare with the laboratory and field data. Testing of every field condition is impossible. A standard test situation has been designed, and effects of the dimensionless input parameters are tested singly around the standard values. The standard situation is an imaginary power plant called SMHIverket. SMHIverket has a discharge flow Q_o = 113 m^3/s, outlet dimensions $2B_o$ = 21.0 m and H_o = 7.0 m, density difference $\Delta\rho$ = 1.5 kg/m^3, and discharge angle $\theta = 90^o$. For scaling purposes the initial temperature excess is 1.0. Ambient conditions are current V = 0.077 m/s, heat loss coefficient k = 0.00001 m/s, and horizontal diffusion coefficient ε_H = 1.0 m^2/s. In every case the vertical diffusion coefficient $\varepsilon_V = 0.001\ \varepsilon_H$. Other values internal to the numerical model are, as recommended by Prych (1972), entrainment coefficient E_o = 0.1, drag coefficient C_D = 0.2, shear coefficient C_F = 0.5, maximum step size Δs = 50.0 m, and initial zone

size s_o = 77.4 m. Using the above parameters the par values of the five variables to be tested are R = 0.1, $\theta = 90^{\circ}$, A = 3, F_o = 2.4, and E = 0.186.

For standard conditions the behavior of plume parameters T, B/H_o, and Y/H_o against s/H_o is shown in Figures 3.2 and 3.3. Absolute values of the correlations are unimportant. It is the trends, or slopes of the functions that should be compared. The trend of temperature vs. distance compares well with the phenomenological model. The simplified form for initial mixing zone in the numerical model presents a somewhat unrealistic situation at the end of the zone, which is typical of numerical model output. Behavior of plume width is not as good. It is known intuitively that numerical model plume spreading is too rapid, and Figure 3.2 shows it more clearly, especially near the outlet. Farther downstream the spreading rate better compares with the data, but the data may be complicated by plume asymmetry. Numerical model axis location vs. downstream distance correlates well with laboratory data, but not so well with field data, except far downstream. Perhaps this is due to coastal effects. Behavior of layer depth H/H_o is not shown, but it varies little, steadily decreasing from H/H_o = 0.65 to 0.28 as s/H_o increases from 16 to 700. In all, numerical model behavior with respect to downstream distance is good. Plume widths tend to increase too quickly, but axis temperatures are not strongly affected by plume width.

Results for SMHIverket input variable sensitivities are shown in Figures 3.4 to 3.12. The figures are cross plots of a dependent variable, an independent variable, and downstream distance (s/H_o or x/H_o). Power law coefficients are calculated from the average slopes of the graphs in realistic ranges. Often values of dimensional quantities must be outside normal prototype ranges in order to test a non-dimensional variable. For example, testing of Froude number F_o = 10 requires a flow of 471 m^3/s, which is greater than values used for prototype correlation. Where possible the Shirazi (1973) power law coefficients are shown on the figures.

The effects of current ratio R on temperature T and plume width B/H_o are shown in Figure 3.4, and on trajectory location Y/H_o and layer depth H/H_o in Figure 3.5. Looking at the first graph, increased ambient current reduces the distance to a given isotherm. One can as well read the graph as saying that at any downstream distance, increased current reduces the temperature. Near the source (T = 0.5 and 0.4) the current has little effect on T until $R \geq 0.2$. Comparison with the phenomenological model is good, especially in the far field. The effect of current strength on plume width is not well described by a single power law. In the real world most ambient currents are less than 20 % of discharge velocity, and Shirazi's (1973) value is not so bad. Note that slope of distance vs. R changes significantly along the jet axis. Overall, behavior of plume width is not reliably correlated with field data. Behavior of trajectory with respect to R correlates well with laboratory data, but not so well with field data. Because the lines on the graph are straight and nearly parallel, description of the effect fits well to a power law model. The effect of R on layer depth H/H_o is variable, but not significant except far from the source. No data are available.

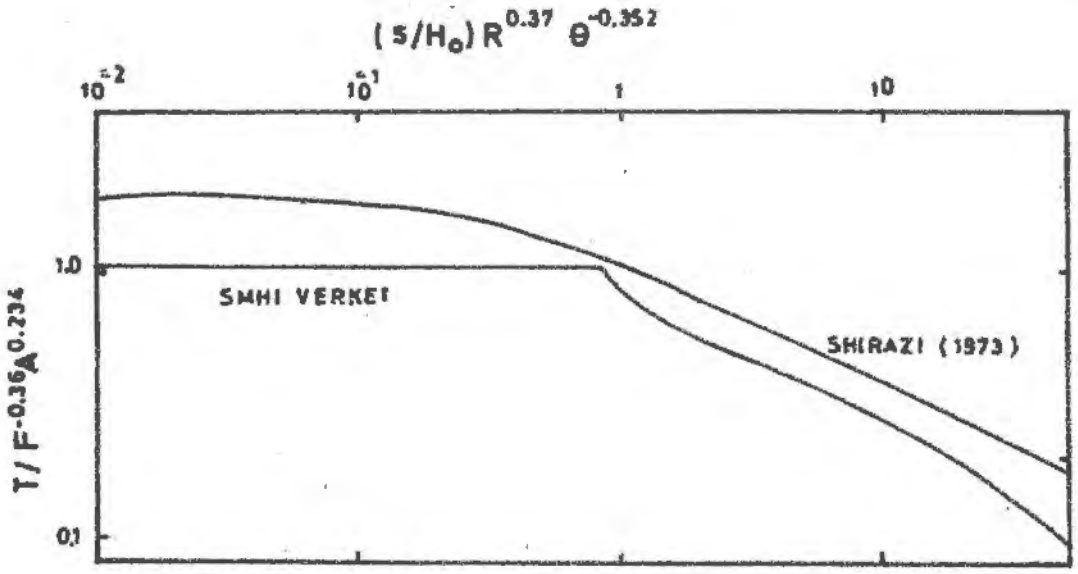

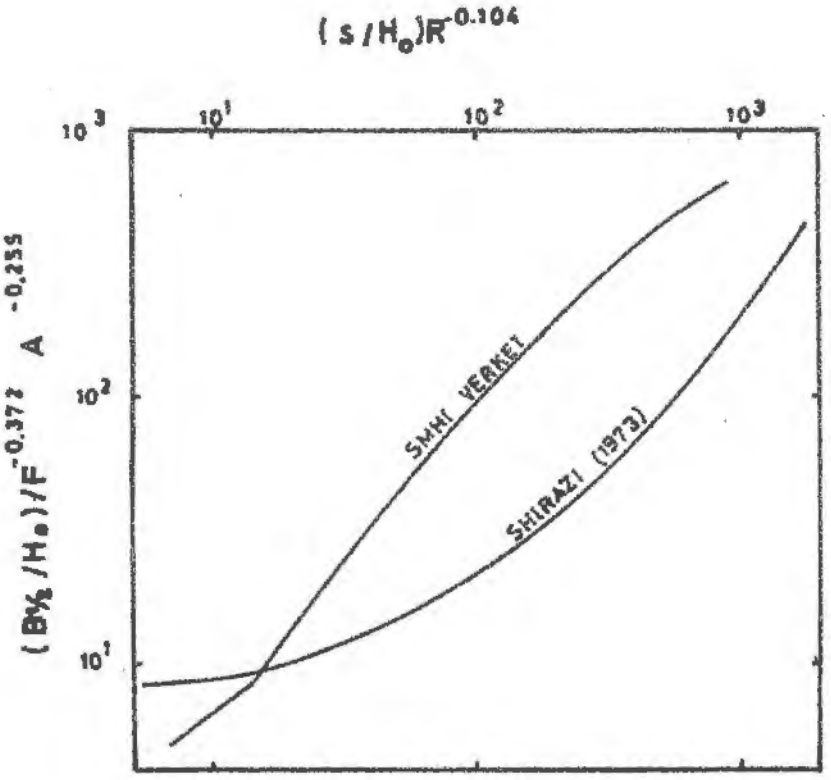

Figure 3.2 Temperature and plume width vs. distance, SMHIverket and laboratory and field data

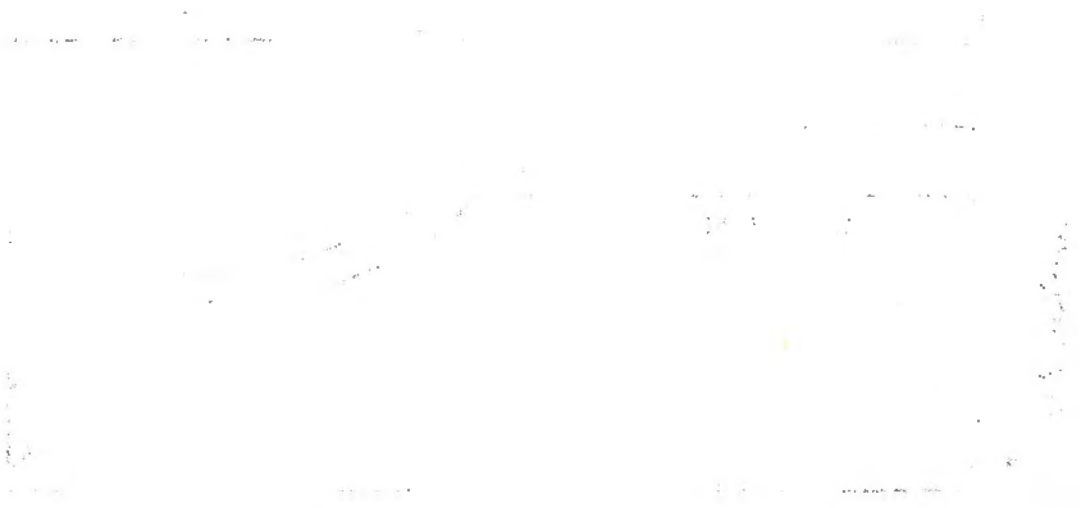

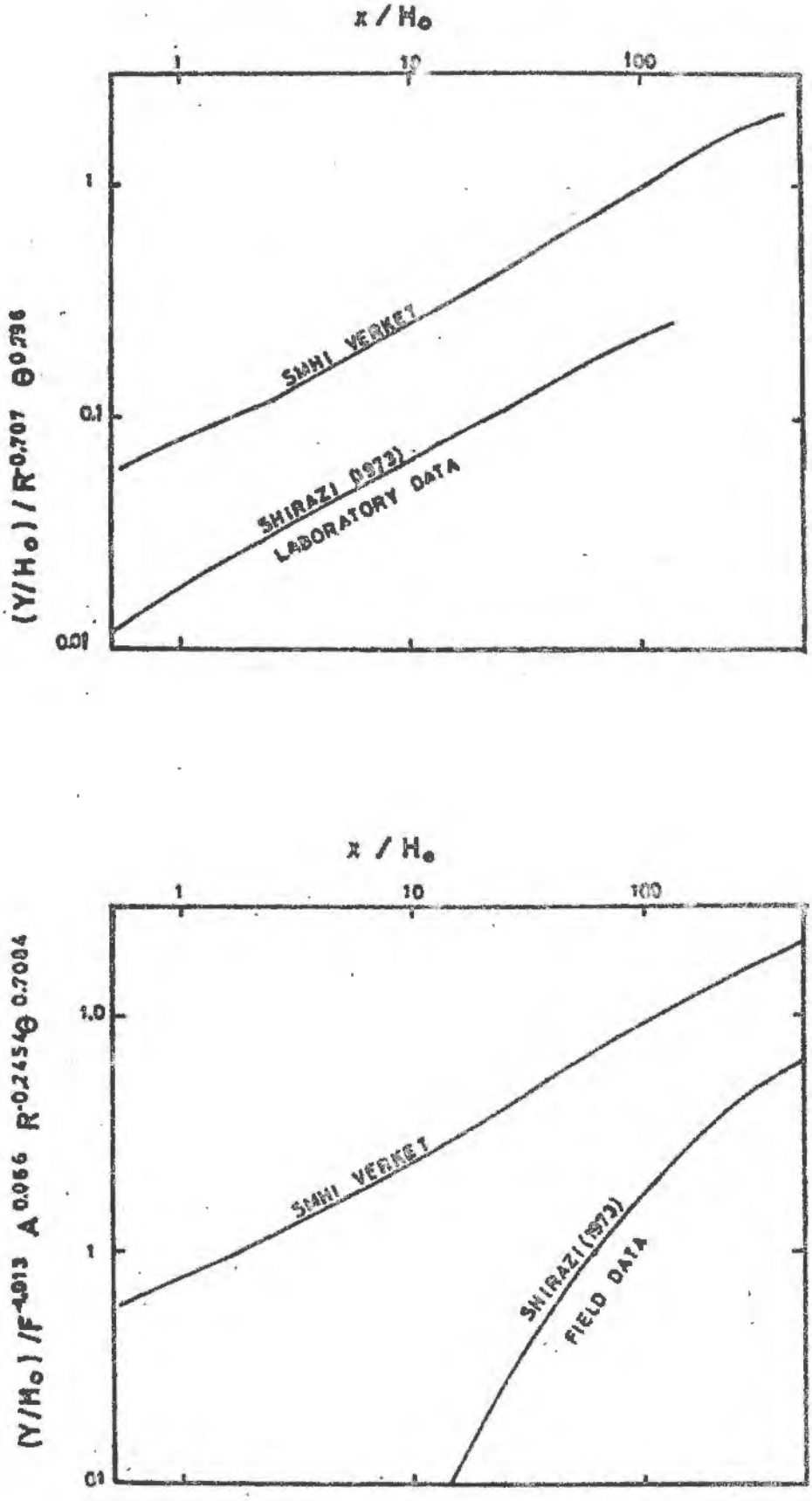

Figure 3.3 Trajectory vs. distance, SMHIverket and laboratory and field data

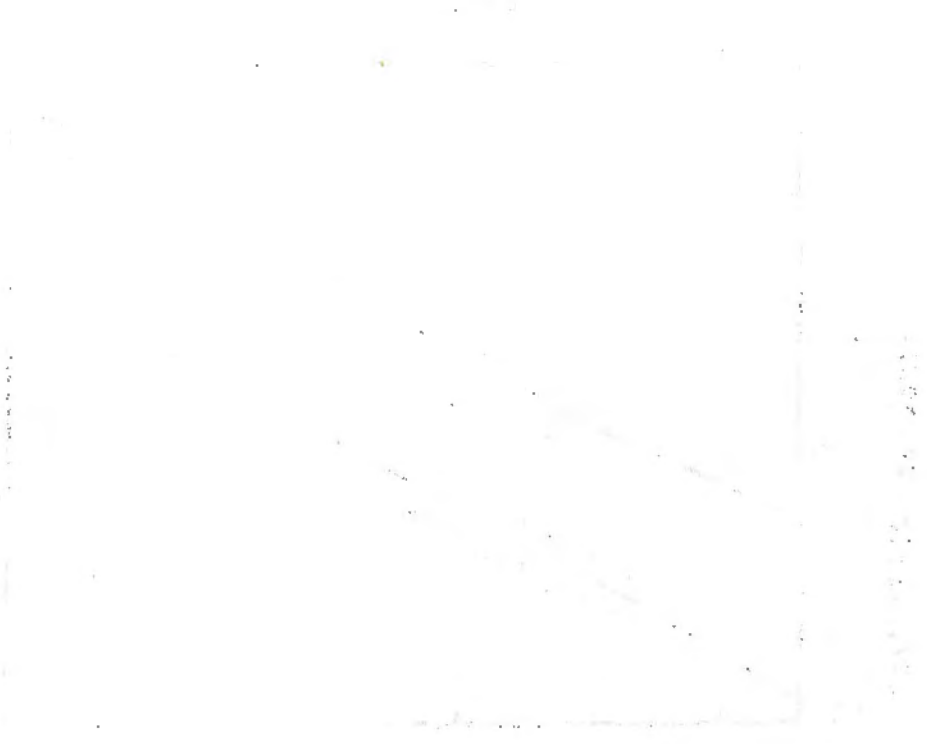

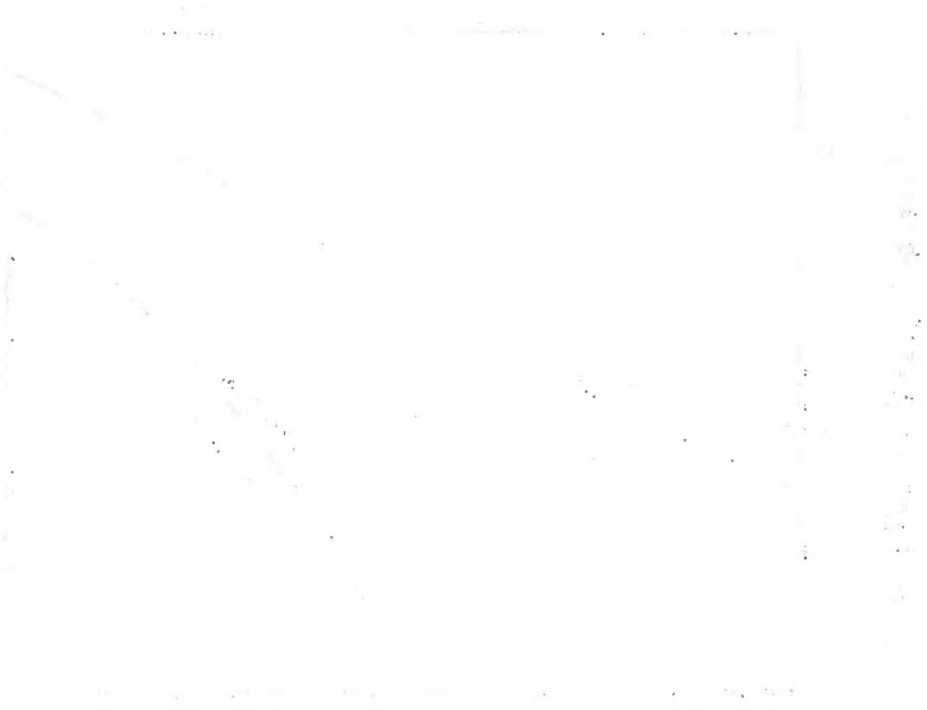

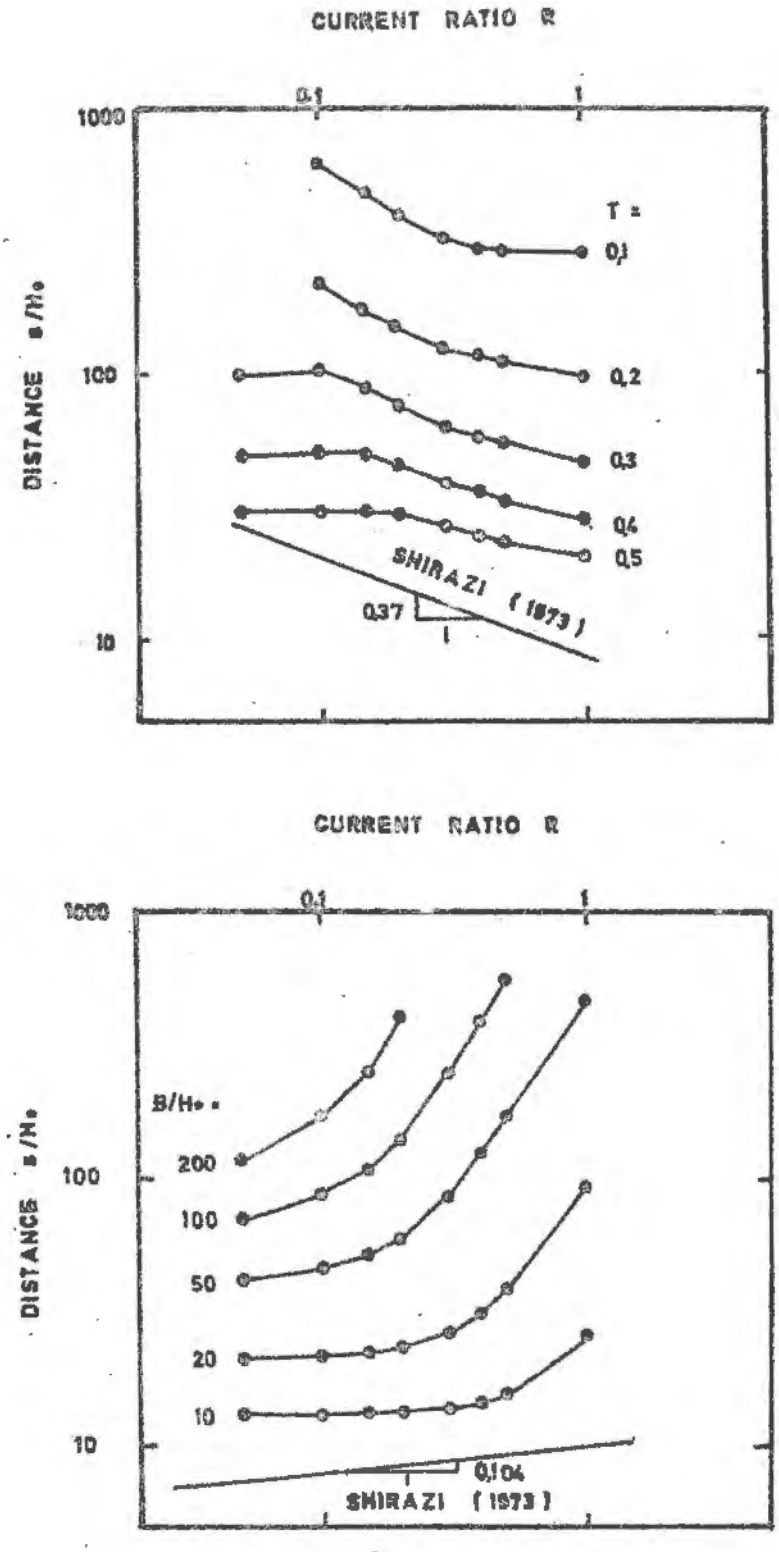

Figure 3.4 Effects of current strength on temperature and plume width, SMHIverket

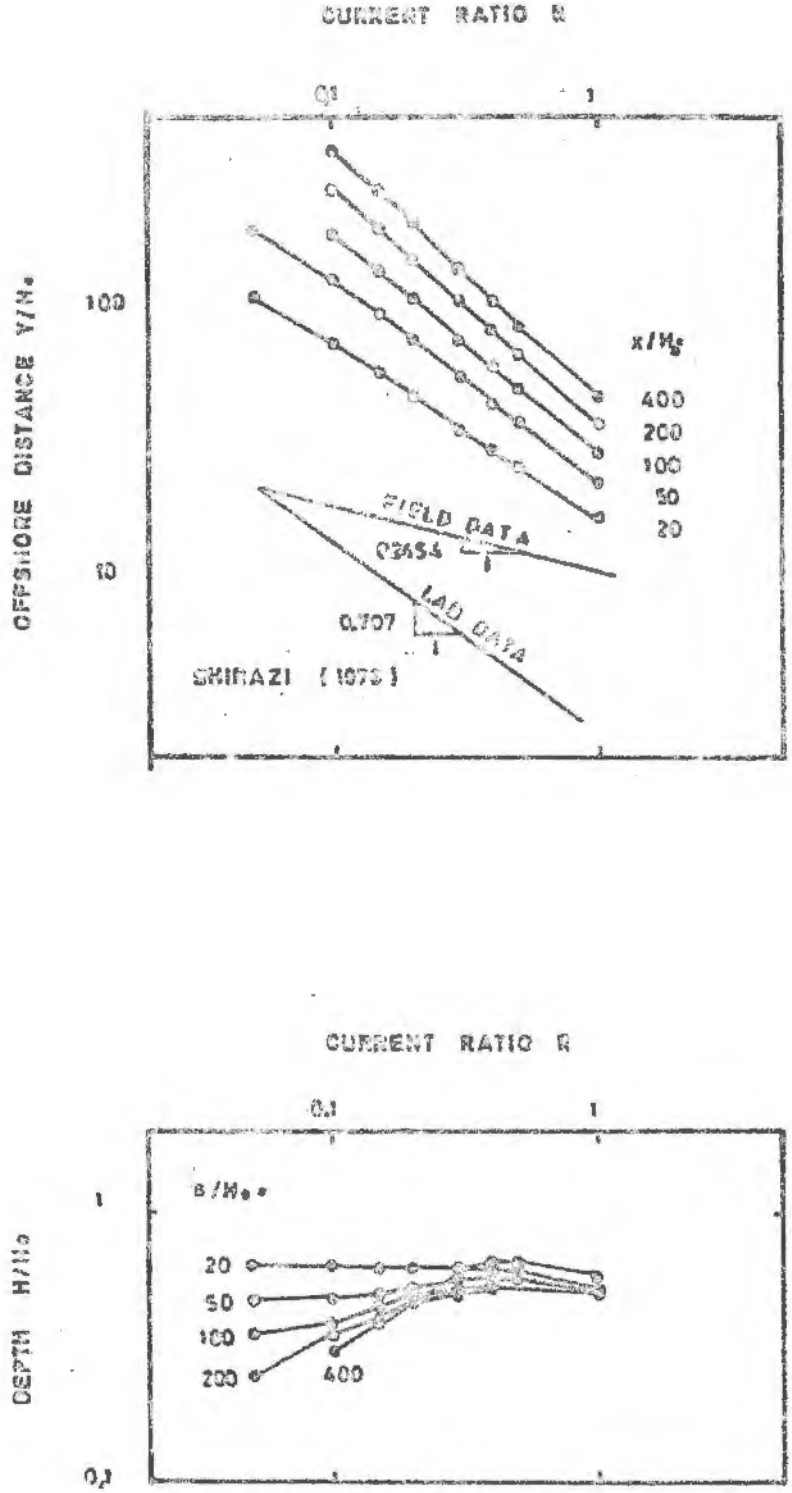

Figure 3.5 Effects of current strength on trajectory and layer depth, SMHIverket

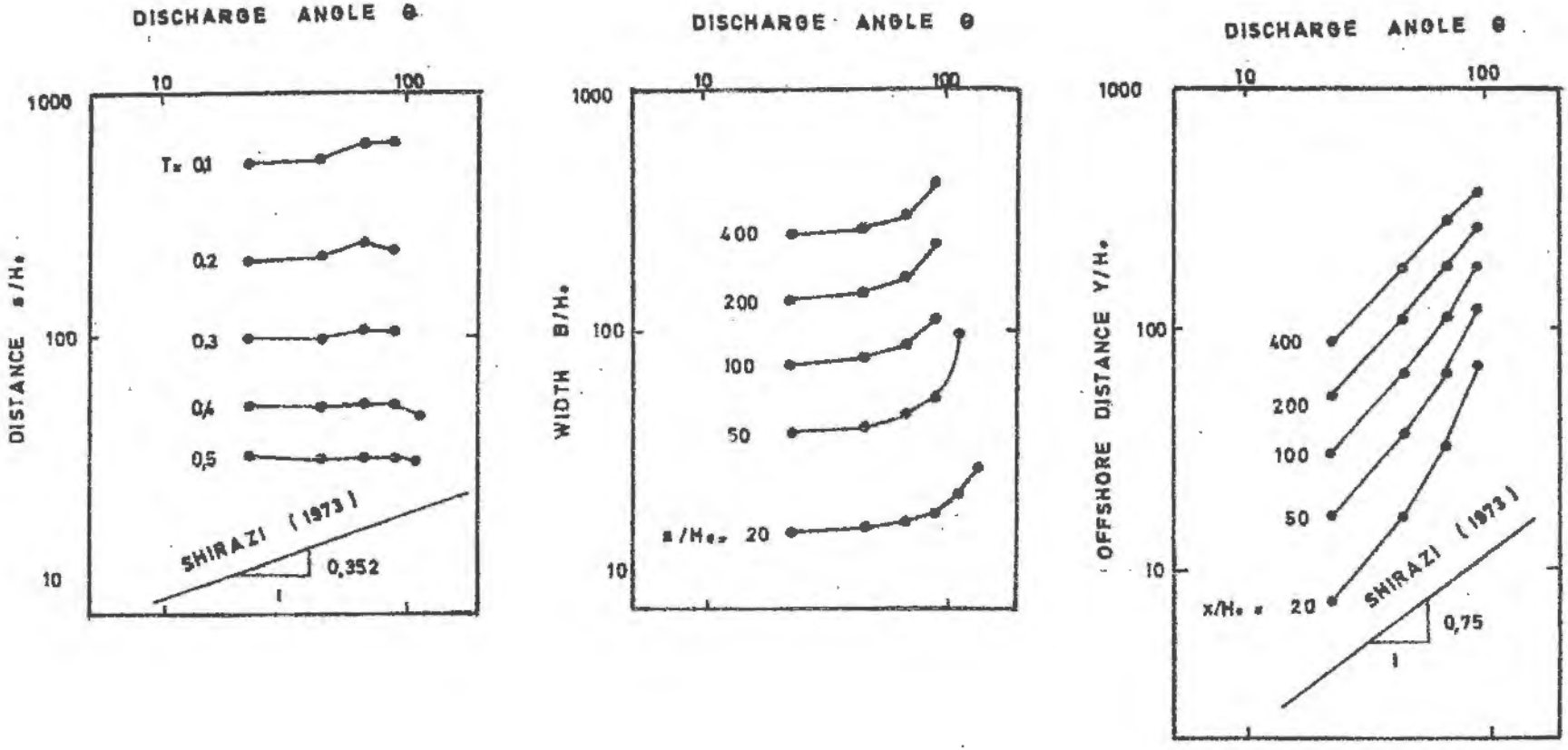

Figure 3.6 Effects of discharge angle on temperature, plume width, and trajectory; SMHIverket

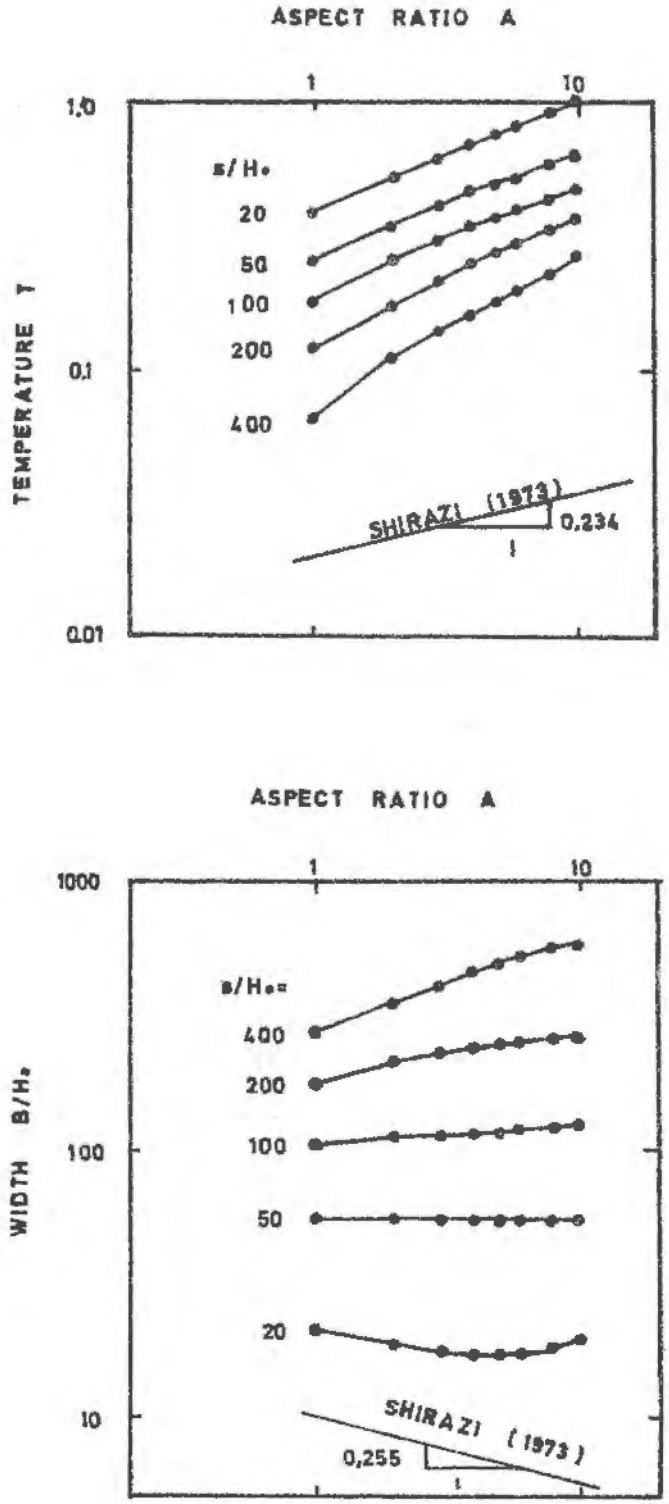

Figure 3.7 Effects of aspect ratio on temperature and plume width, SMHIverket

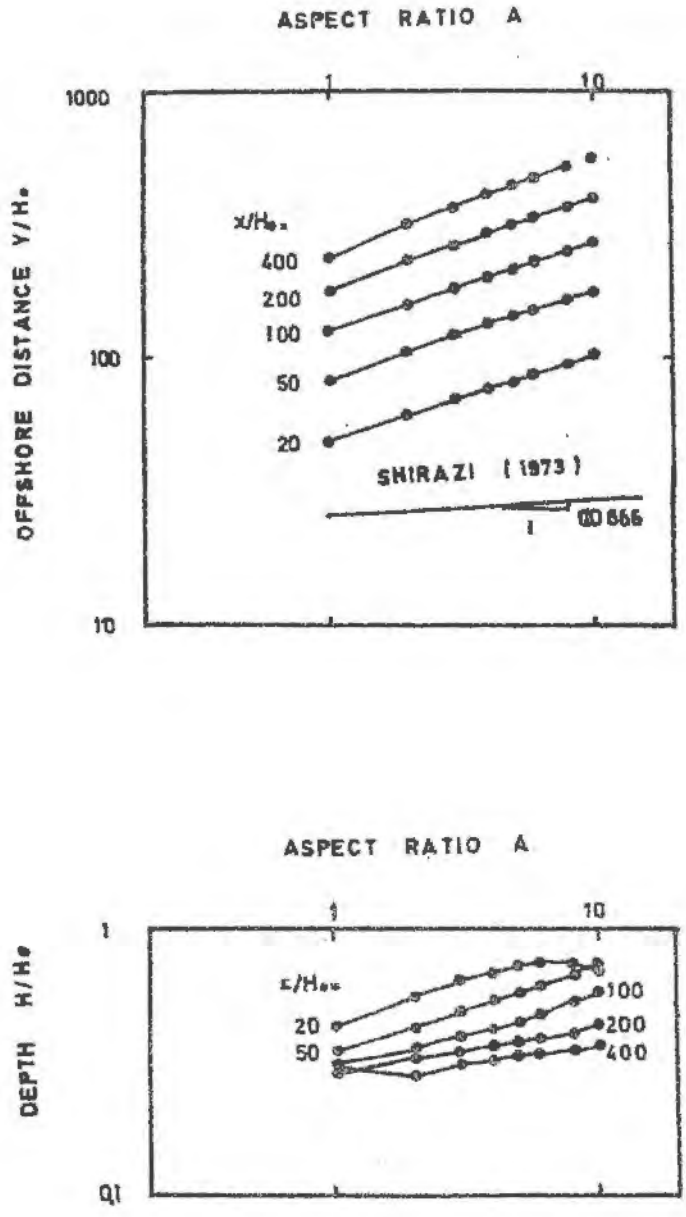

Figure 3.8 Effects of aspect ratio on trajectory and layer depth, SMHIverket

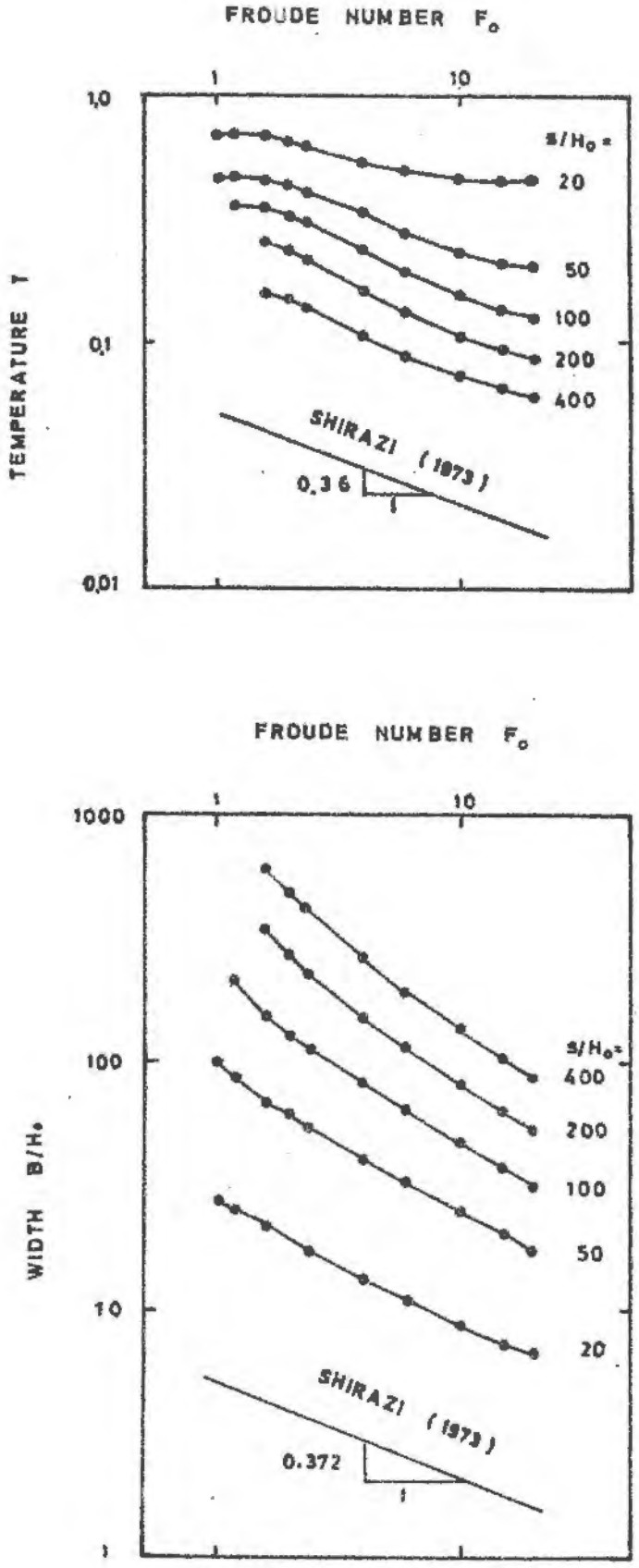

Figure 3.9 Effects of Froude number on temperature and plume width, SMHIverket

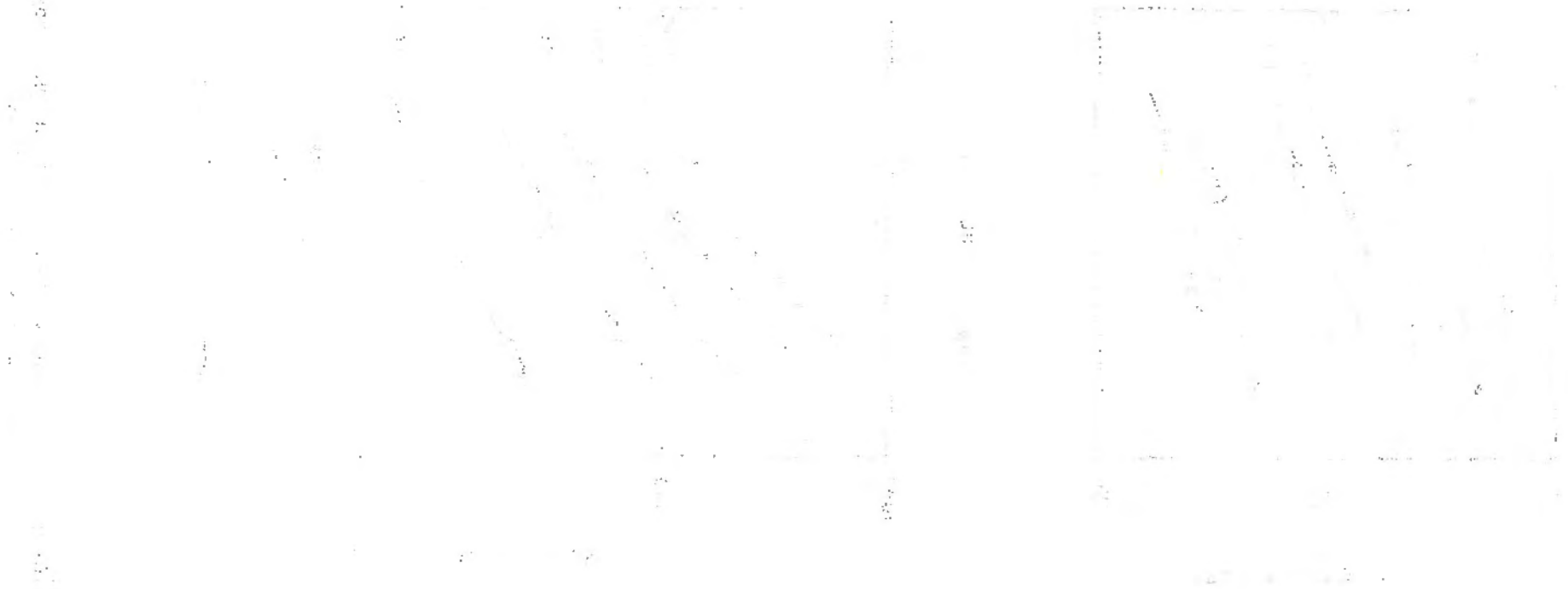

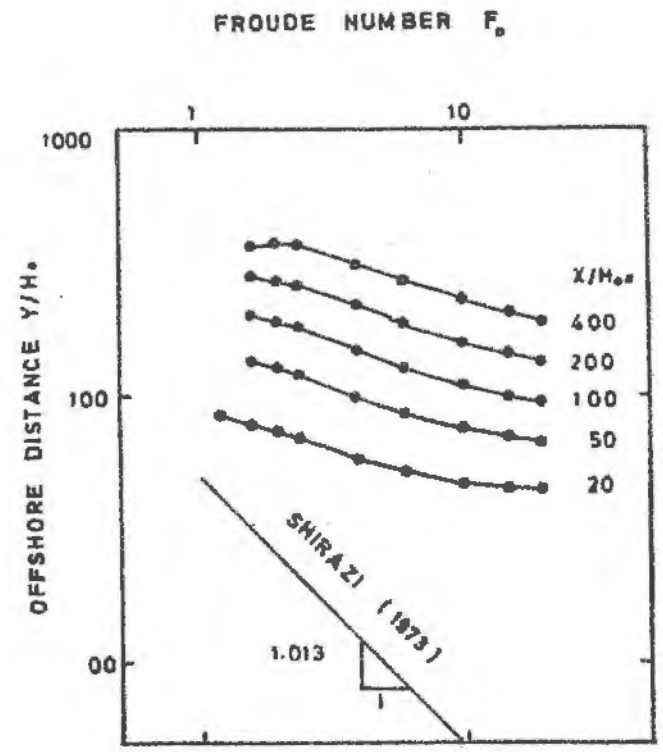

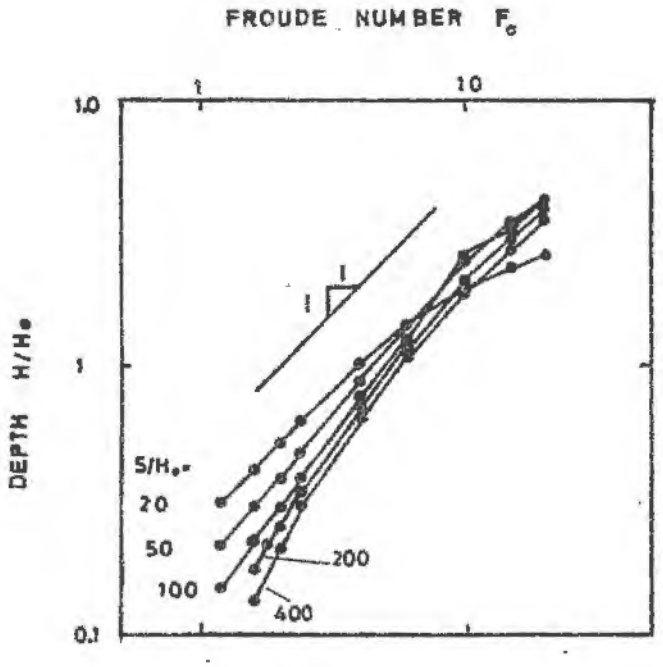

Figure 3.10 Effects of Froude number on trajectory and layer depth, SMHIverket

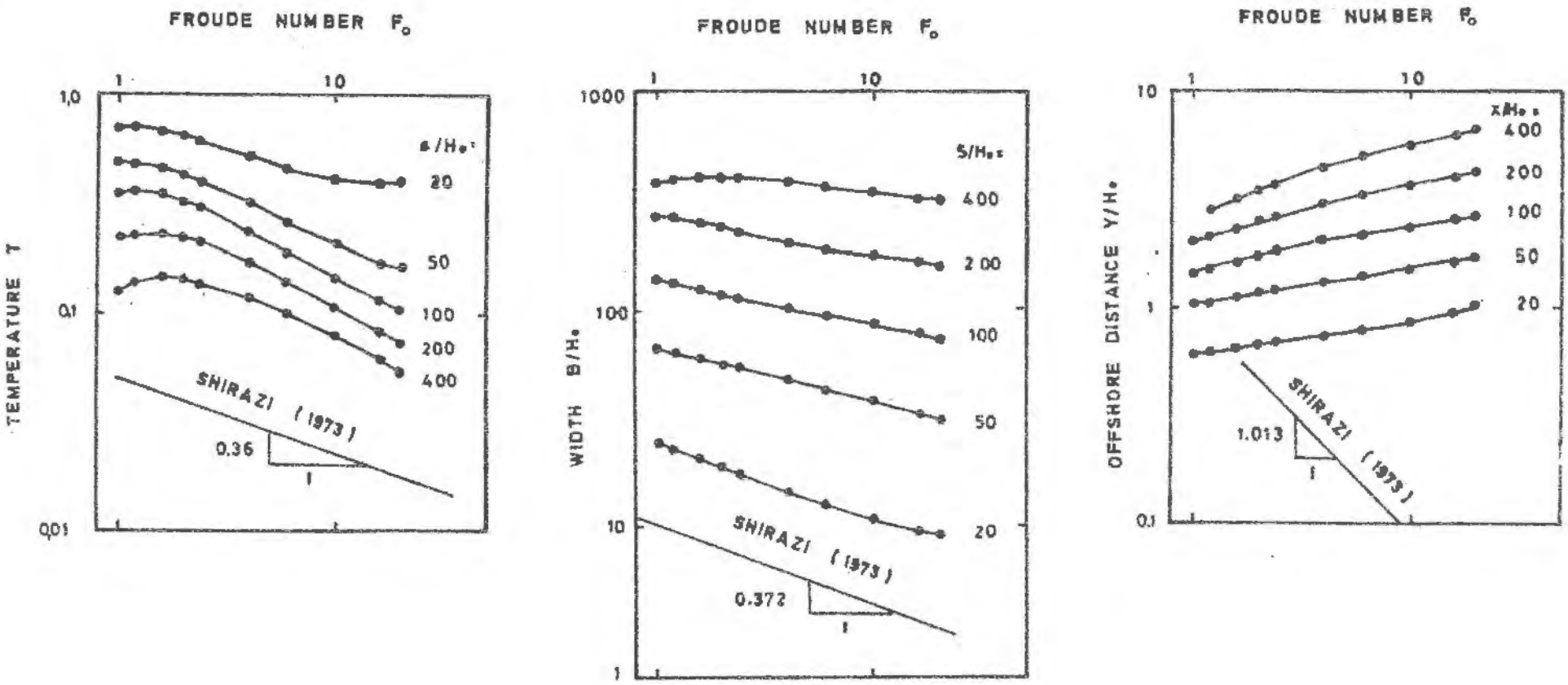

Figure 3.11 Effects of a design alternative on temperature, plume width, and trajectory; SMHIverket. Simultaneous variation of F_o, R, and E

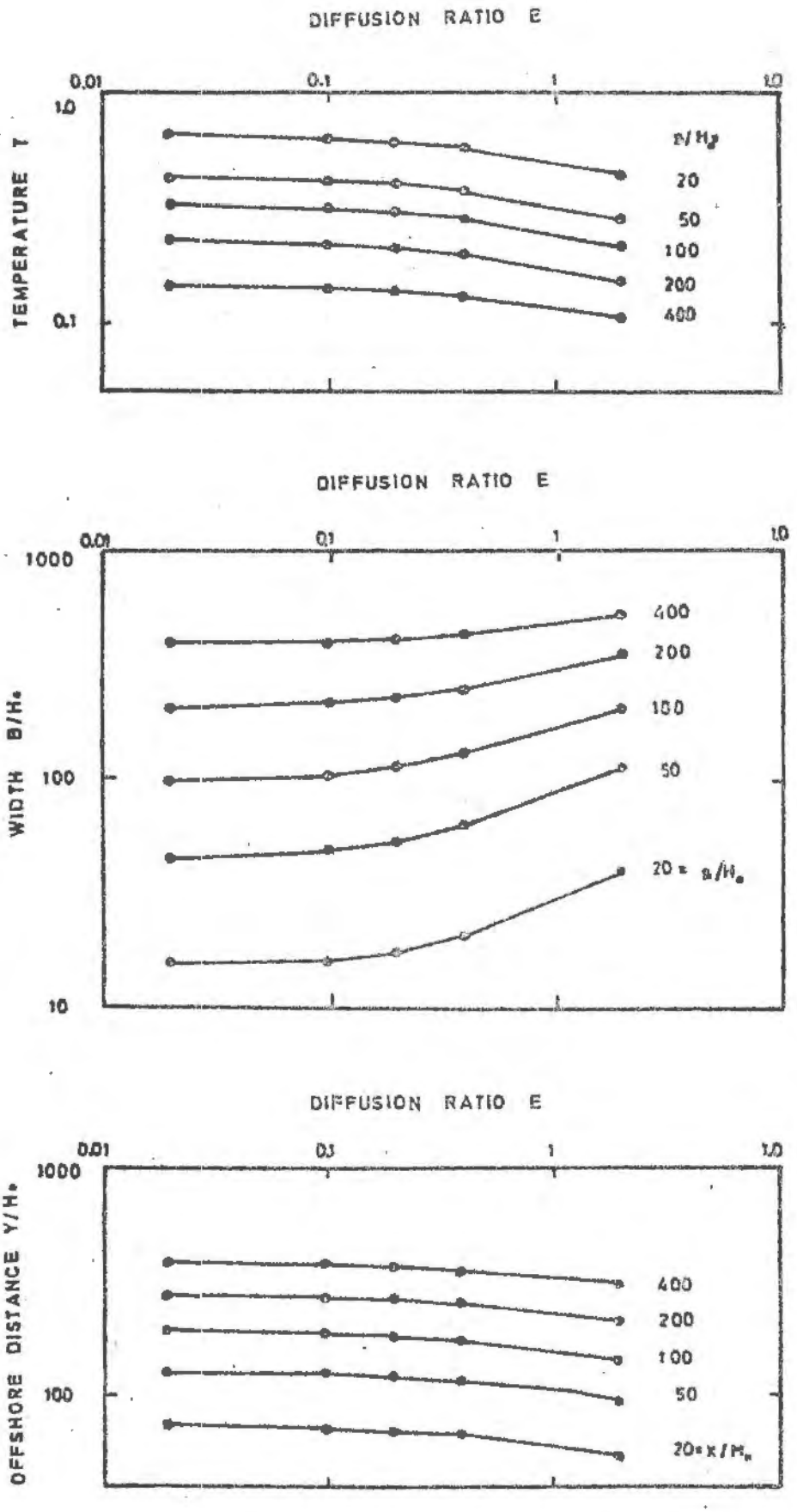

Figure 3.12 Effects of diffusion ratio on temperature, plume width, and trajectory; SMHIverket

Effects of discharge angle θ are shown in Figure 3.6. The numerical model shows little effect of θ on temperature, as mixing operates independent of axis curvature. This contradicts the power law model. The numerical model sensitivity of plume width to θ is shown, but no power law results are available. Effects of θ on trajectory are also shown, correlating well with the power law model except near the source. This may be an effect of initial zone definition.

It is not generally possible to vary outlet aspect ratio A as easily as R and θ, because the dimensional quantities within A occur in so many other non-dimensional parameters. Testing for aspect ratio is done in three ways, but only one is reported here. Setting H_o, $\Delta\rho$, and u_o constant at the outlet, A is increased by increasing $2B_o$, the outlet width. To maintain constant u_o, flow Q_o is made proportional to $2B_o$. By the present definition, Froude number is unchanged. This variation of A encompasses a method suggested by Prych (private communication) for including the effect of a nearby coastline. Prych suggests doubling the outlet width and flow to reduce effective horizontal entrainment on the side nearest the coast. Results for changing aspect ratio are shown in Figures 3.7 and 3.8. Relative temperature T is more sensitive to A in the model than in the published data, but the trend is the same and is describable by a power law coefficient. This is not true for the effect of A on plume width. The second graph in Figure 3.7 shows inconsistent behavior of B/H_o. Notice that most values of B/H_o are nearly equal to or greater than values of s/H_o. The plume is exceptionally wide, spreading laterally even faster than it is moving along the axis. This is also true for many other tests. Trajectory location responds to A more strongly in the numerical model than expected, but the effect can be described by a power law. The log-log plots are linear. The effects of A on layer depth H/H_o are irregular and not pronounced.

Two other tests for aspect ratio have been made. In one test, A is adjusted by distorting the outlet shape but maintaining constant flow and outlet area. This involves slight changes in Froude number as H_o is changed. In the other test the outlet area and Froude number are kept constant, adjusting flow Q_o and outlet depth H_o. In this test the value of current ratio R is slightly changed. For both alternate tests, the results are almost identical to those reported.

The effects of Froude number are tested five different ways, but only two are shown in the figures. The most representative results are shown in Figures 3.9 and 3.10. In the test the outlet dimensions and $\Delta\rho$ are constant, but flow is increased. This is equivalent to adding power plant units to an existing discharge structure. To maintain constant values of other dimensionless quantitities, the ambient current is increased such that R = constant. (Inadvertently, diffusion coefficients ε_H and ε_V were not adjusted for constant diffusion ratio E, but it is felt that this is not significant, because results are duplicated in other Froude number tests for which E = constant.) The effect of F_o on temperature closely matches the results of Shirazi (1973) for $F_o \geq 2$ and away from very near the source. Between $F_o = 1$ and 2 one cannot say whether the numerical model is imperfect or the power law description is oversimplified. The effect of F_o on

plume width is also adequately described by the power law model. This does not mean that plume widths are accurately predicted, only that the relative effects of Froude number are comparable. The numerical plumes are still too wide. The dependence of trajectory on F_o is shown in Figure 3.10. The effect as seen in the numerical model is much less pronounced than in the power law model. Increasing Froude number increases mixing, and thus limits penetration of the plume into the ambient current. This does not imply that increasing discharge velocity keeps a given plume near the coast. Intuitively we know otherwise. Increased velocity at a particular outlet pushes the plume away from the coast, but the effect is due to changing current ratio, not Froude number. The Froude number test was repeated for constant V (R not constant), and results for T, B/H_o, and H/H_o are unchanged, but the trajectory Y/H_o increases with F_o as expected. The power law model does not include layer depth, but the numerical model shows that H/H_o is approximately proportional to Froude number.

Other Froude number tests were also made. When discharge density deficit $\Delta\rho$ is changed, leaving all else constant, the results are almost identical to those of Figures 3.9 and 3.10. A test was made by expanding or contracting the outlet at constant aspect ratio, maintaining constant $\Delta\rho$ and velocity u_o. Results are somewhat irregular, but in normal ranges of Q_o reproduce the above results. Many of the situations involve unrealistically large or small values of Q_o. A special test was made to simulate a common design alternative, and results are shown in Figure 3.11. Constant values are chosen for discharge flow Q_o and density deficit $\Delta\rho$, aspect ratio, and ambient current V. These parameters are often fixed for the design engineer. The size of the outlet is then varied, changing velocity u_o and Froude number F_o. Simultaneous changes are made in current ratio R and diffusion ratio E, but only through u_o, not V or ε. The results for temperature and plume width are adequately described by the F_o dependence, but trajectory Y/H_o is significantly affected by the other variables, of which R surely dominates. This suggests that R has little effect on mixing for $R < 0.1$, although it retains its effect on plume width in that range, especially far downstream.

The last variable considered for the numerical model is diffusion ratio $E = \varepsilon_H/u_oH_o$, although it is not included in the power law model. Results are shown in Figure 3.12. For $E < 0.1$ almost no effects are seen. In the neighborhood of $E = 1.0$ (ε_H = 1-10 m^2/s) weak but predictable effects are seen. Mixing increases with E, but the effect is not more pronounced in the far field. Far field mixing may be dominated by diffusion, but only by the departure of other mechanisms. The effect of E on layer depth H/H_o is very small, and results are not shown.

The variable k/u_o is not considered herein.

With the above results at hand, a numerical model version of power law scaling can be constructed, including appropriate caution about variable ranges. Because the power law coefficients are calculated around only one standard situation, they should not be used in place of routine computer operation for design predictions. The numerical model's best fit values for universal mixing relationships are:

$T/F_o^{-0.53} A^{0.39} E^{-0.08}$ vs. $(s/H_o) R^{0.45} \theta^{-0.07}$,

$(B/H_o)/F_o^{-0.52} E^{0.15}$ vs. s/H_o, dependence on R, θ, and A not well defined,

$(Y/H_o)/F_o^{-0.48} A^{0.29} R^{-0.83} \theta^{1.22} E^{-0.06}$ vs. x/H_o,

$(H/H_o)/F_o^{1.35} A^{0.24}$ vs. s/H_o.

Limits to the relationships are $0.1 \leq R \leq 1.0$ for temperature, $0.05 \leq R \leq 1.0$ elsewhere; $45^\circ \leq \theta \leq 90^\circ$ for temperature, $20^\circ \leq \theta \leq 90^\circ$ for trajectory; $1 \leq A \leq 10$; $2 \leq F_o \leq 20$ for temperature and width, $1 < F_o \leq 20$ elsewhere; and $0.1 \leq E \leq 1.5$. The forms of the functions are not the same as the Shirazi (1973) functions, but more closely resemble the curves for SMHIverket in Figures 3.2 and 3.3.

Overall, the numerical model reproduces power law model results for temperature rather well. Numerical model plume width results compare favorably for Froude number dependence, but effects of most other variables do not fit a power law description. Trajectory results can be well described by power laws, but comparison with data is difficult because results for laboratory and field situations differ. Layer depth results can be correlated with Froude number and aspect ratio. In addition to the power law model parameters, the numerical model includes scaling effects for diffusion coefficient.

Limited results are available to compare the power law model with the distorted hydraulic model of Oskarshamnsverket. Results are very inconsistent. The effects of current ratio R on relative temperature T depend on the current direction. For south flowing currents, T decreases with R as the power law predicts, but T increases with R for north flowing currents. The dependence of temperature on Froude number is contradictory, with highest temperatures measured at intermediate values of F_o, and lower temperatures measured at high and low values of F_o. Even this behavior depends on distance from the outlet and method of Froude number variation. The hydraulic model predictions for trajectory Y/H_o as a function of current ratio compare well with the power law model (laboratory data), but dependence of trajectory on Froude number is unpredictable, as for temperature. All these results are entirely incompatible with the power law and numerical models. The data for the Oskarshamnsverket situation are limited, but that can only partly explain the inconsistencies.

3.3 Surface area model

A simple phenomenological model for surface areas enclosed within isotherms has been presented by Asbury and Frigo (1971). Surface area data are collected for 23 situations at six power plants on large lakes in the United States. All the plants have channel discharge structures, with flows of 3.2 to 53.1 m^3/s. The data are plotted as relative temperature T against A_T/Q_o^a, where A_T = surface area within the T isotherm, and a = a coefficient. Most

consistent grouping of the data occurs at a = 1. A best fit line is drawn by eye through the data. For Q_o = 33.4 m^3/s the model curve is shown in Figure 3.13. The solid line is the best fit for the data, and the dashed lines are upper and lower bounds to all the data for the 23 situations. It is remarkable that so simple a description covers many field situations. The data include many different flows, ambient currents, and nearshore topographies.

The Asbury and Frigo (1971) model is easily applied to data from Oskarshamnsverket. Field data for Cases A to H are shown in the first graph of Figure 3.13. Cases I and J are excluded because other data from the same power plants are used to construct the model. Correlation of the Oskarshamnsverket field data with the phenomenological model is excellent. Numerical model results for the same eight cases are shown in the second plot of the figure. Numerical model results cluster around the best fit line more closely than the field data, but this does not necessarily indicate better correlation. To check which model (numerical or Asbury and Frigo) fits the field data better, predictions should be compared individually for the eight cases. In seven of eight situations the numerical model better fits the near field data ($T > 0.6$), but in five of seven cases the phenomenological model better fits the far field data (in one case the numerical model does not reach the far field). Viewed on a log-log plot, for the same five of seven cases the phenomenological model gives a better overall fit to the field data. Phenomenological model errors in the near field are always smaller than numerical model errors in the far field. The numerical model shows a slight tendency toward too low mixing rate in the far field. In summary, the phenomenological model gives better surface area predictions than does the numerical model at Oskarshamnsverket, but the differences are not large. One cannot extend the generalization to all situations, but in the range of flows used to construct the phenomenological model it surely gives reasonable predictions. In some way the Oskarshamnsverket data better verifies the Asbury and Frigo model than the numerical model.

The phenomenological model scales surface area with flow Q_o. We have no information about the range of Froude numbers among the data used to construct the model, but we can test the flow scaling with the numerical model in two ways. Using the same technique as in Section 3.2, the trends of surface area A_T vs. Q_o are shown in Figure 3.14. The left graph in the figure shows surface area results for changing Froude number by increasing flow through the same outlet (using the same data as for the Froude number tests of Figures 3.9 and 3.10). If power plants are designed in this way, which is not generally so, the Asbury and Frigo (1971) model predicts areas proportional to flow. The reverse trend is seen, as expected. The right graph of Figure 3.14 shows surface area results for constant Froude number, increasing flow along with outlet aspect ratio (using the same data as for Figures 3.7 and 3.8). If power plants are all constructed with constant Froude number, which is also not true, the numerical model predicts a plot of relative temperature vs. $A_T/Q_o^{1.9}$, compared to Asbury and Frigo's A_T/Q_o. The numerical model cannot confirm the phenomenological flow scaling, but the correlation is not unreasonable. This is especially true if larger power plants have increased Froude number, but there is no evidence to support this.

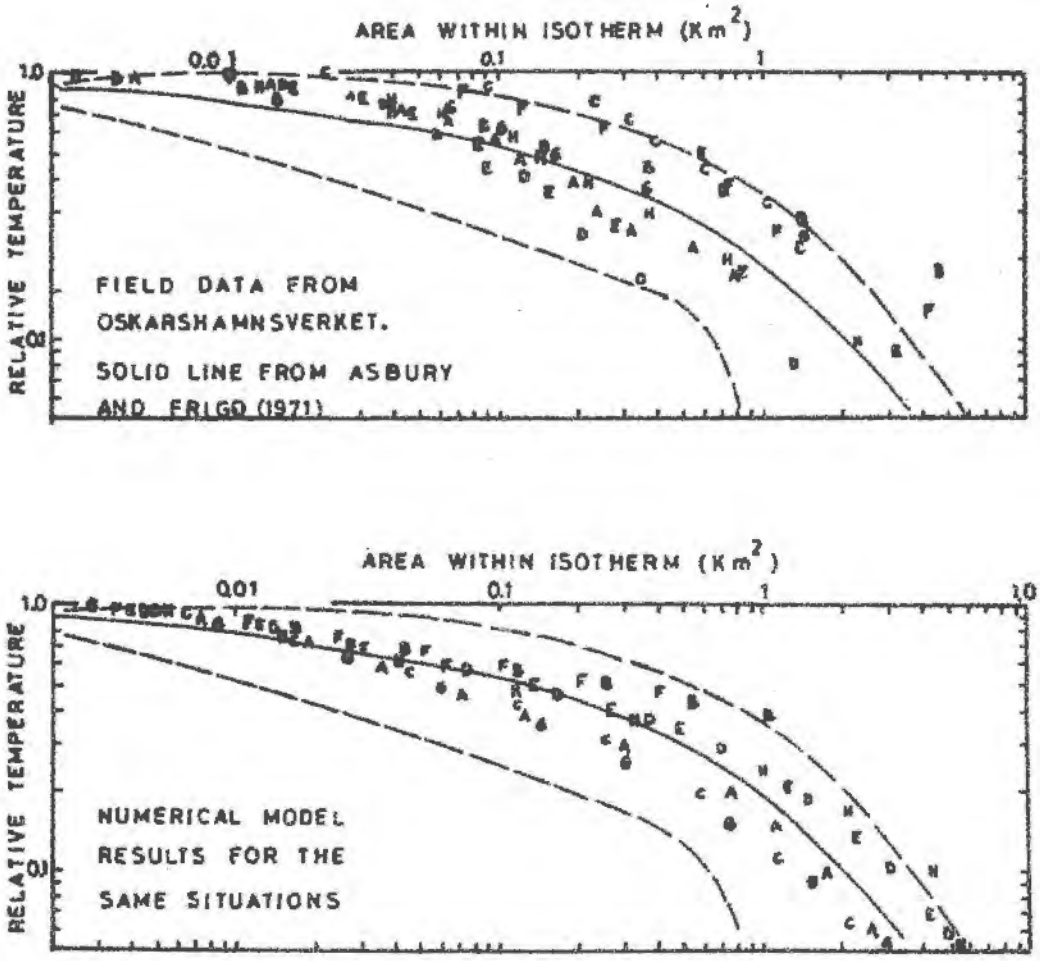

Figure 3.13 Comparison of Oskarshamnsverket data with phenomenological surface area model

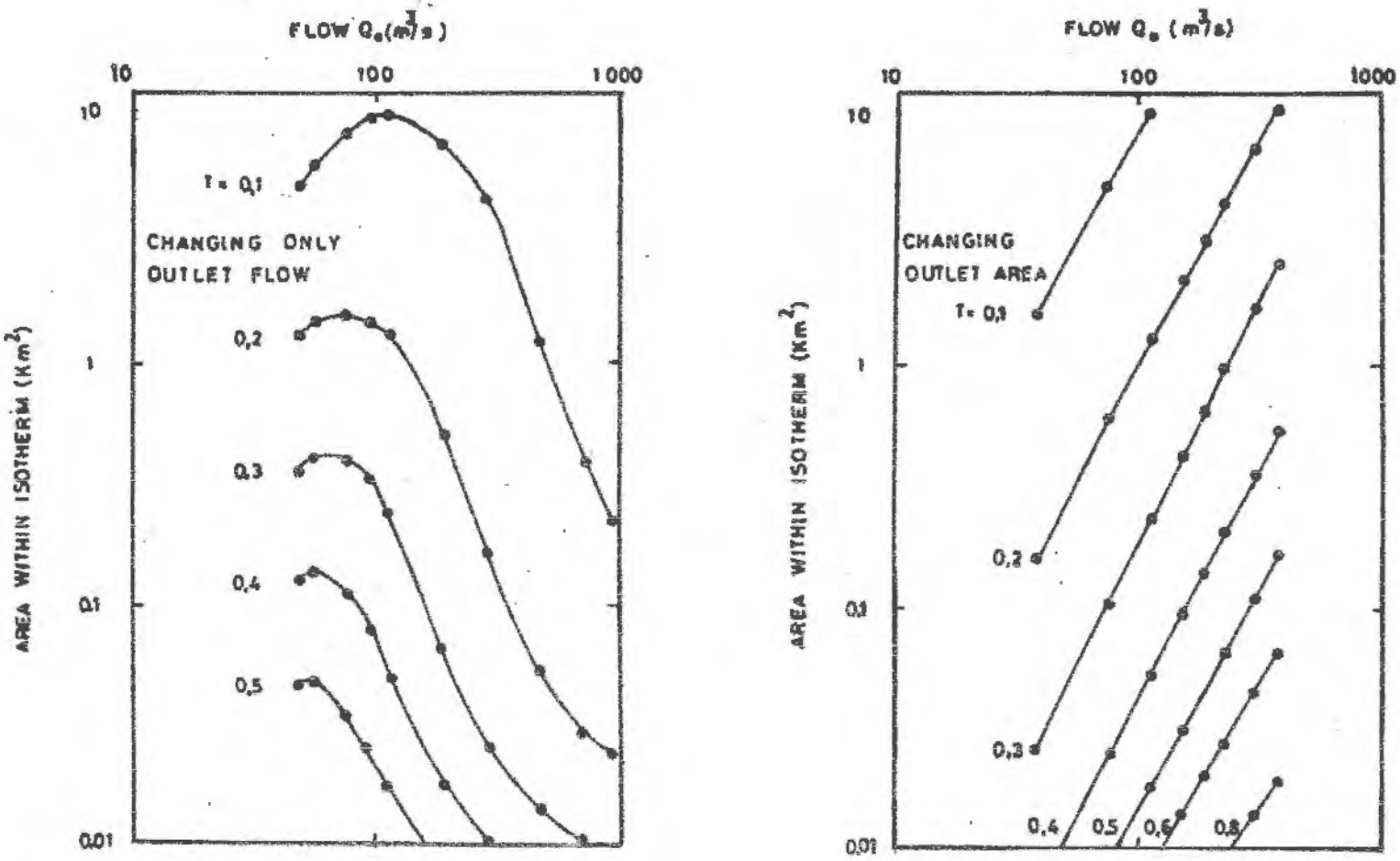

Figure 3.14 Numerical model scaling for enclosed area and flow, SMHIverket. Tests for changing Froude number and aspect ratio

3.4 Analytical models

There exist many analytical models for thermal discharge predictions in special and general situations. For a review of some of them, see Policastro and Tokar (1972). It is not intended herein to correlate the numerical model with all such analyses, but a few are simple enough that an easy comparison can be made.

Among the Oskarshamnsverket data, Cases D, E, and G are chosen as having similar discharge and ambient current conditions. They are now compared to two simple analytical models. The first is really a set of laboratory experimental results, not a discharge model per se. Jen, Wiegel, and Mobarek (1966) present results for axis temperature vs. distance for a round, buoyant, surface jet in stagnant receiving water. Values of Froude number are rather high, but the results have since been confirmed for lower Froude numbers. It is found that relative temperature is inversely proportional to distance, as is the case for submerged non-buoyant jets. The Oskarshamnsverket discharge is not round, but if an equivalent diameter is calculated the laboratory results can be applied. For Cases D, E, and G the Jen, Wiegel, and Mobarek results are shown in Figure 3.15. The jet model overestimates mixing, although the trend of temperature data with distance follows closely. The overestimation is because of high aspect ratio (A = 21, compared to A = 1 for the jet), but the effect is partly counteracted by increased mixing due to ambient currents. The definition of jet core length is important, and the core length for a high aspect ratio discharge is unknown.

Another semi-analytical model has been developed by Carter and applied by Pritchard (in Policastro and Tokar; 1972, p. 64). In the Carter-Pritchard model the flow field is divided into a core zone of no mixing; an early mixing zone, where temperature is proportional to distance to the minus one fourth power; a two-dimensional jet zone, where temperature is proportional to distance to the minus one half power; and a far field zone for relative temperature less than 0.2 and proportional to distance to the minus one power. Application of the model is also shown in Figure 3.15. The model core zone is scaled only with discharge width, making it too long for a high aspect ratio outlet. The early mixing zone is confined to the region where the plume turns to become parallel to the ambient current. Dilution is underestimated when compared to field data, but mixing rate compares well with the numerical model. From T = 0.6 to 0.2 the mixing is badly underestimated, probably due to the assumption of a two-dimensional jet, for which there is no vertical entrainment. Far field mixing rate is the same as for many jet and diffusion models.

It is not claimed that the numerical model compares well with or is better than all analytical models, but it does give improvement over the simplest of such models. The numerical model includes effects of aspect ratio and ambient current, giving more accurate predictions than a simple jet model, and includes both horizontal and vertical mixing, giving better predictions than a two-dimensional jet model in a moving current.

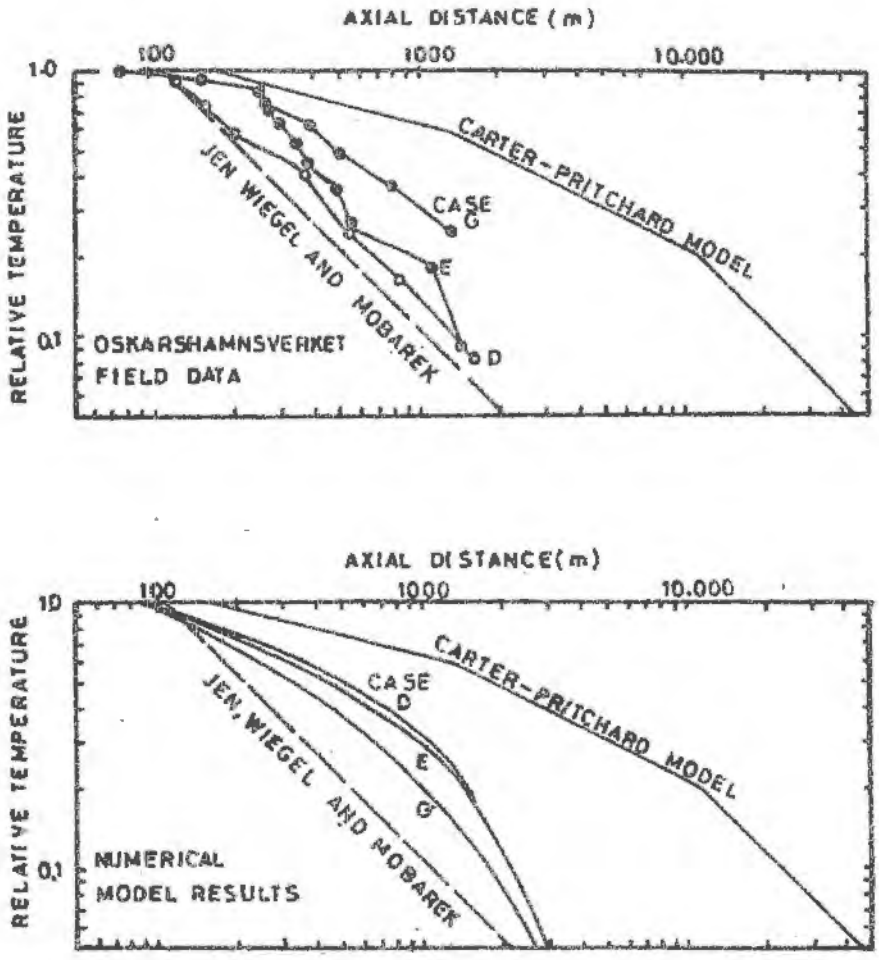

Figure 3.15 Comparison of Oskarshamnsverket data and two simple analytical models

CHAPTER 4. FIELD MEASUREMENT TECHNIQUES

4.1 Initial mixing at Oskarshamnsverket

In Section 2.2 a constant value is assumed for overall dilution due to mixing in Hamnefjärden at Oskarshamnsverket. The calculation is now explained. At the end of the field data collection period for Case A, 3 May 1972, vertical profiles of temperature and velocity were measured at the center of the channel where Hamnefjärden opens onto the Baltic Sea. The location is the origin for numerical model calculations. Volume and heat flux calculations are made from the profiles, determining overall mixing at that point.

The vertical profiles of temperature and velocity are shown in Figure 4.1. There exists a substantial return flow below the heated discharge layer, and the profiles are not similar in form, which complicates calculation of Froude number. The first estimate of dilution is made by volume flux calculation. The velocity profile is integrated to determine average velocity over the total depth of 7 m, which is 0.05 m/s. The effective outlet width is the width needed to produce the plant discharge at that velocity. Thus $2B_o$ = (plant flow)/u_oH_o = (22.0)/(0.05)(7.0) = 69 m. A similar calculation is made for heat flux through the section, yielding $2B_o$ = 57 m. Using an average value for outlet width of $2B_o$ = 63 m, the velocity profile is again integrated to the zero velocity depth (H_o = 3.0 m) to determine the discharge flow in the upper layer only. The discharge for modeling purposes is Q_o = 33.4 m^3/s. This represents a gross dilution of 22/33.4 = 0.66. In all cases at Oskarshamnsverket the outlet density decrease $\Delta\rho$ is calculated as 0.66 times the density difference between the plant discharge and the ambient water. The effects of fixing the effective outlet dimensions at 63 m x 3 m have been shown in Figure 2.21. Because plant flow and outlet dimensions are constant, the numerical model initial Froude number depends only on $\Delta\rho$. For Case A, F_o = 1.18. Model initial temperatures are measured values, not 0.66 times the plant temperature rise, because the temperature profiles are less consistent than total mixing.

Overall dilution was not measured for every case, but details of temperatures and velocities were measured on another occasion by personnel from Chalmers Tekniska Högskola. Data were taken between the sill in Hamnefjärden and the Baltic on 27 and 28 September 1972. Instrument buoy locations are shown in Figure 4.2. The sill location is also shown on a larger scale map in Figure 2.1.

Unfortunately the data are inadequate to check flow continuity. Referring to Figure 4.2, the measured flow through section one is 30.2 m^3/s by integration of the three velocity profiles (assuming triangular sections between the outer bucys and the shorelines). No evidence is found of a return flow at the bottom. Neither is a return flow found at any station in section two, but there the integrated flow is only 23.8 m^3/s. One suspects that the flow is time-varying over the two day period or that the measured velocities are not normal to the section due to geographic constraints. Also, flow conditions near the shoreline are not well known. Calculations of heat flux show the same

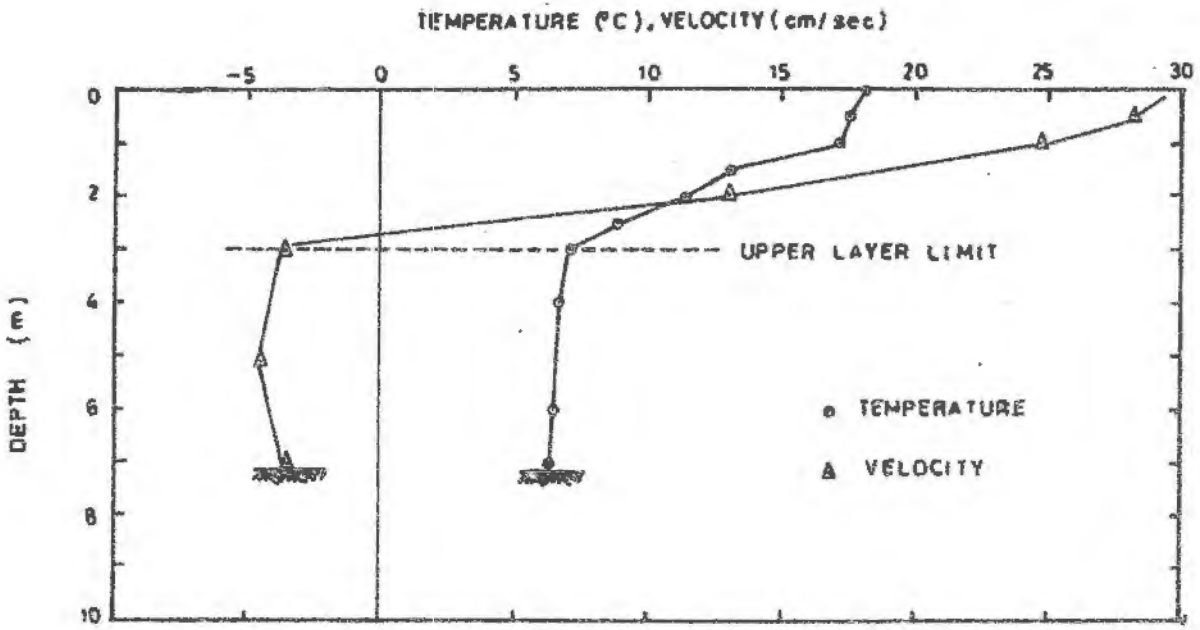

Figure 4.1 Temperature and velocity profiles at mouth of Hamnefjärden, Case A

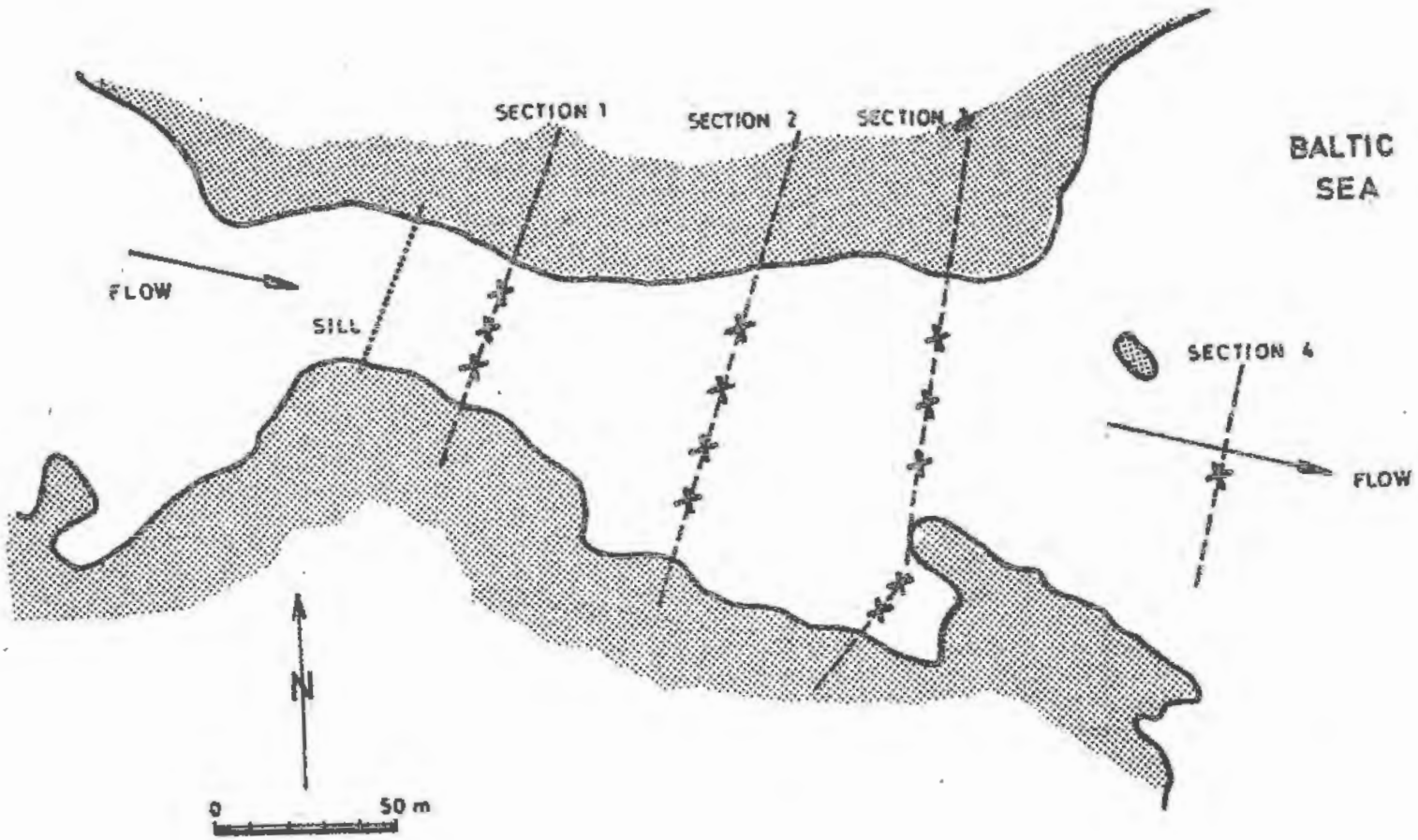

Figure 4.2 Buoy stations in outer part of Hamnefjärden, Oskarshamnsverket, September 1972

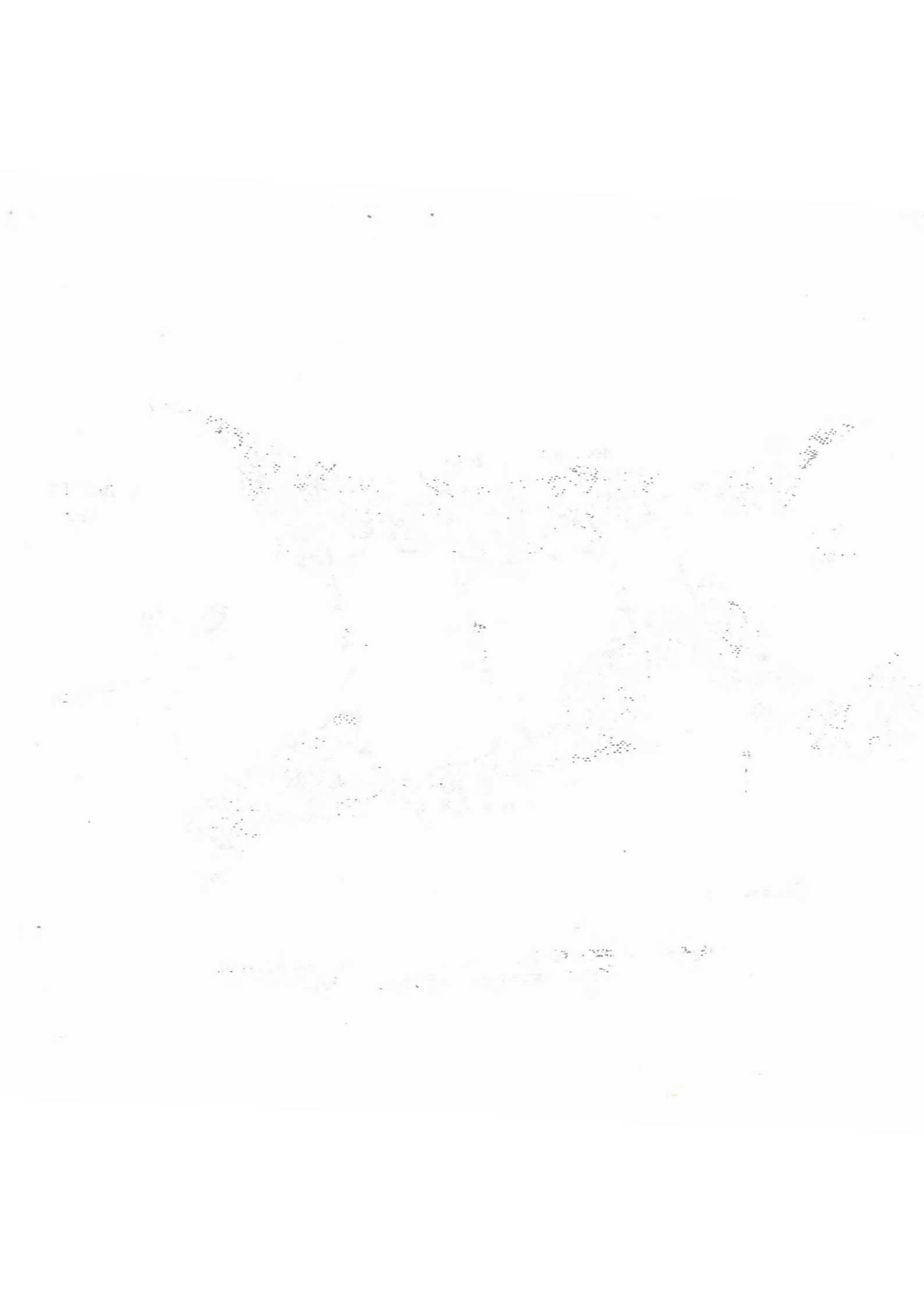

pattern. At section three the integrated upper layer flow from the three northern buoys is 39.4 m^3/s. Return flow data are insufficient for flow integration over the entire depth.

It is suspected that little mixing occurs inside the 3 m sill, but the data do not confirm that. No return velocities are measured, but the flow at section one is larger than the plant flow. If the integrated flow values are correct at section three then dilution at that point is 22/39.4 = 0.56. If the integrated flow values are incorrect, but the flow at section one properly represents the undiluted plant flow, then dilution at section three is 30.2/39.4 = 0.77. Unable to resolve this, one assumes that the first calculated value of 0.66 is reasonable for overall mixing inside Hamnefjärden.

The channel width at section three is 67 m, close to the calculated value of 63 m. If the chosen value of outlet area (63 m x 3 m) is correct then the velocity profile at the middle buoy of section three yields a discharge flow of 33.1 m^3/s. Similarity of this velocity profile to the profile measured for Case A leads one to conclude that mixing in Hamnefjärden is constant, more so than temperature difference. Compare the above dilution calculations with values of ΔT for Cases A to H in Table 2.2. The poor correlation of continuity between sections one and two opposes this reasoning, but may be due to other factors. For numerical model calculations, mixing in Hamnefjärden is assumed to be constant in every case.

As an aside to temperature investigations, it is noted that inlet depths at the Chalmers buoy locations are larger than those measured during a 1959 topographical survey. Between the sill and the mouth of Hamnefjärden the plant flow has scoured material away from the bottom by an average of about one meter. The greatest scour is on the north side of the inlet. The depth at the northernmost buoy of section two has increased by more than two meters.

4.2 Choice of ambient temperature

In many field situations ambient temperature varies spatially. When ambient currents are small the ambient temperature can be confused with far edges of the heated plume. Offshore winds can cause horizontal gradients due to upwelling, and changing current direction can cause previously heated water to be returned to the discharge area (especially tidal flow). Where horizontal temperature gradients exist, few plume models account for entrainment of ambient water at different temperatures along the plume axis. A constant value of ambient temperature must be chosen.

For Case B at Oskarshamnsverket, field data have been reduced for different values of ambient temperature T_a. Results are shown in Figure 4.3. The nominal value of T_a is 11.5°C. Lines on the graphs labeled "change in T_a = +1" correspond to reduction of the data using a value of T_a = 12.5°C, and so on. When the ambient temperature used for calculations is too high, mixing rate is exaggerated. This does not mean that increasing ambient temperature increases mixing, only that incorrect choice of T_a for calculation purposes can produce apparent errors in dilution. Figure 4.3 shows that the

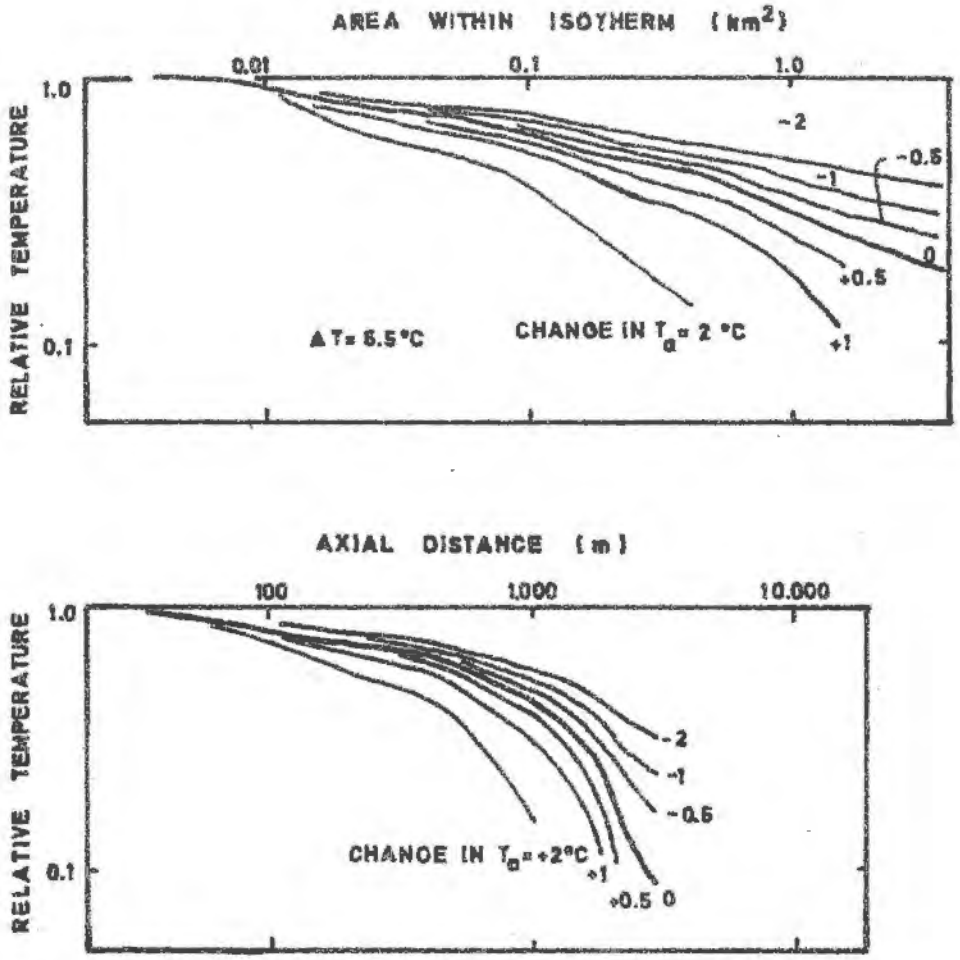

CASE B

OSKARSHAMNSVERKET 3 OCT 1972 A.M.

Figure 4.3 Effect of choice of ambient temperature on field data, Case B

degree of error increases far from the source, as plume temperatures approach ambient temperatures. Errors also increase in regions of rapid dilution.

In most situations T_a can be accurately selected within $\pm 0.5^{\circ}C$. That amount of error for Case B produces errors in relative temperature of 10 % of local value at T = 0.5 and 45 % at T = 0.2. For the case given, the initial temperature change is $\Delta T = 5.5^{\circ}C$, which is rather low compared to many discharge situations. More typical would be $\Delta T = 10^{\circ}C$, with corresponding errors about half of those above. Thus one can expect uncertainty in choice of ambient temperature to produce uncertainty in relative temperature of up to 5 % of the local value at T = 0.5 and up to 20 % at T = 0.2. For conservative temperature predictions the ambient temperature should be chosen on the low side where measurement is uncertain.

4.3 Subsurface temperature measurement

Mechanical difficulties often prevent collection of field temperature data at the water surface, and this can lead to errors in data presentation. Data collected at Oskarshamnsverket and reported in Chapter 2 are labeled as surface temperatures, but actually are measurements at a depth of 0.5 m. The surface temperatures are not available, either by thermistor or infrared measurement. In this section estimates are made of the errors induced and their consequences.

Estimates of true surface temperature are herein made by linear or hand-drawn extrapolations of data at depths of 0.5 m and 1.0 m or 1.5 m. The effects of subsurface data collection for Case B at Oskarshamnsverket are shown in Figure 4.4. Surface and subsurface relative temperatures coincide at the outlet and in the far field, but surface temperatures are higher in the intermediate region. The reduction of error with distance is seen in plots of vertical temperature distribution. For all cases at Oskarshamnsverket the temperatures far from the outlet are uniform over the top meter or two of water.

Subsurface temperature measurement causes errors in relative temperature in four ways, in the near and far fields and depending on initial temperature distribution. Recall the definition of relative temperature $T = (T_s - T_a)/(T_h - T_a)$. First, if the outlet temperature distribution is uniform, then only T_s is affected by subsurface measurement. In the near field measured temperatures are too small due to gradients near the surface, and reported values of T are too small. For example, if T_s is $1^{\circ}C$ too low at the $7^{\circ}C$ isotherm and the plant temperature rise is $10^{\circ}C$, then T is measured as 0.6 instead of the correct 0.7. In the far field the gradients in the top meter vanish, and T is correctly measured. A second case is for non-uniform outlet temperature distribution, such as at Oskarshamnsverket or deep channel discharges. Temperatures T_s and T_h are both measured incorrectly, and errors in T can be in either direction. Very near the source errors are small because T approaches 1.0 as it should. In some intermediate range errors of one type are seen. For example, if both T_s and T_h are too low by $1^{\circ}C$ ($\Delta T = 10^{\circ}C$), then the T = 0.7 isotherm would be

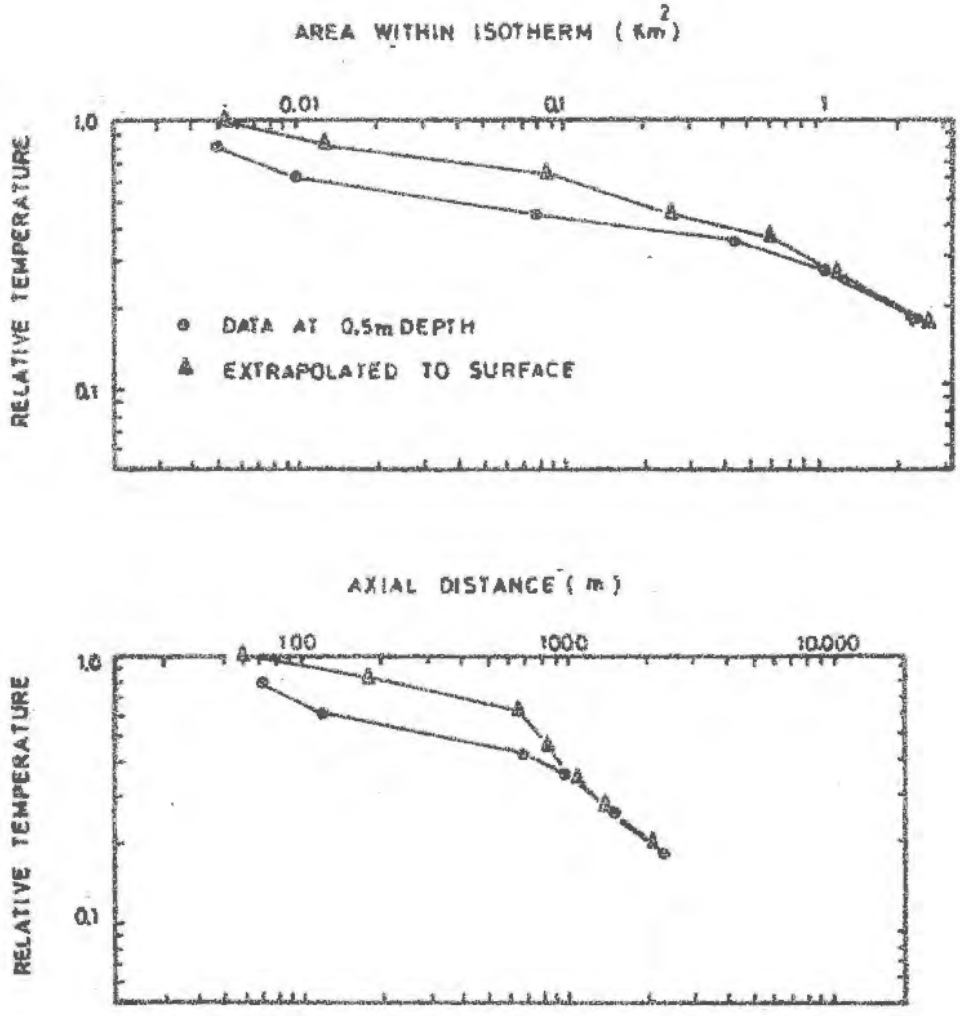

CASE B

OSKARSHAMNSVERKET 3 OCT 1972 A.M.

Figure 4.4 Effects of subsurface data collection, Case B

measured as T = 0.67. But nearer the far field only the source temperature would be in error. If T_h for the 2°C isotherm is 1°C too low but T_s is correct, then the measured value of relative temperature is T = 0.22, an error of opposite sign. As we go from the source to the far field, relative temperature is correct, then too low, then too high. Whether initial temperature is uniform or with vertical gradients, calculations of relative temperature must be presented with caution.

The trend of subsurface measurement errors is shown, but not their magnitude. The size of error depends very much on plume layer thickness, which in turn depends strongly on outlet Froude number. The best data available are from Oskarshamnsverket, which operates in a limited range of Froude number. Data have been collected at Oskarshamnsverket by personnel from S.M.H.I. and Chalmers Tekniska Högskola. The S.M.H.I. data selected for this purpose were taken on nine occasions in 1972, approximately corresponding to Cases A to H. The Chalmers data were taken during five days in the first week of October 1972.

Again using linear or hand-drawn extrapolations, results for induced error are shown in Figure 4.5. Absolute and fractional excess temperature errors are plotted against distance from the source (radial distance, because most data points are not on plume centerlines). In every case the surface temperatures are higher than or equal to the temperatures at 0.5 m depth. It is seen that at Oskarshamnsverket absolute errors are generally limited to 1.5°C, and to 0.6°C for distances greater than 400 m from the source. The median error is only 0.3°C, but that calculation includes much data of zero error in the far field. Approximate limits to fractional error are 45 % up to 500 m and 16 % beyond that. The results shown are for errors in the numerator of the expression for relative temperature, and errors in T depend further on errors of source temperature.

For Case B at Oskarshamnsverket the numerical model estimates of subsurface data collection error are also shown in Figure 4.5. The order of magnitude of numerical model estimates is the same as for the field data, but the trend is significantly different. In the far field the numerical model predicts larger errors because of reduced layer thickness and temperature level. The prototype data show a more uniform layer far from the source. Thus it is recommended that numerical model results always be presented for surface temperatures. If adjustment for subsurface measurement must be made, let the field data be adjusted upward to the surface, not the numerical model results downward to the 0.5 m level.

The numerical model also shows that errors are reduced by increasing Froude number. This is expected, and is verified by one set of data for a nearly neutrally buoyant plume, for which almost no error is found (Oskarshamnsverket, 18 January 1973, $\Delta\rho/\rho = 0.3 \times 10^{-3}$).

Limited data are available for the hydraulic model of Oskarshamnsverket. The hydraulic model generally exhibits plumes that are relatively too thin, and errors are larger than are seen in field data. The hydraulic model also verifies that errors are reduced by increasing Froude number.

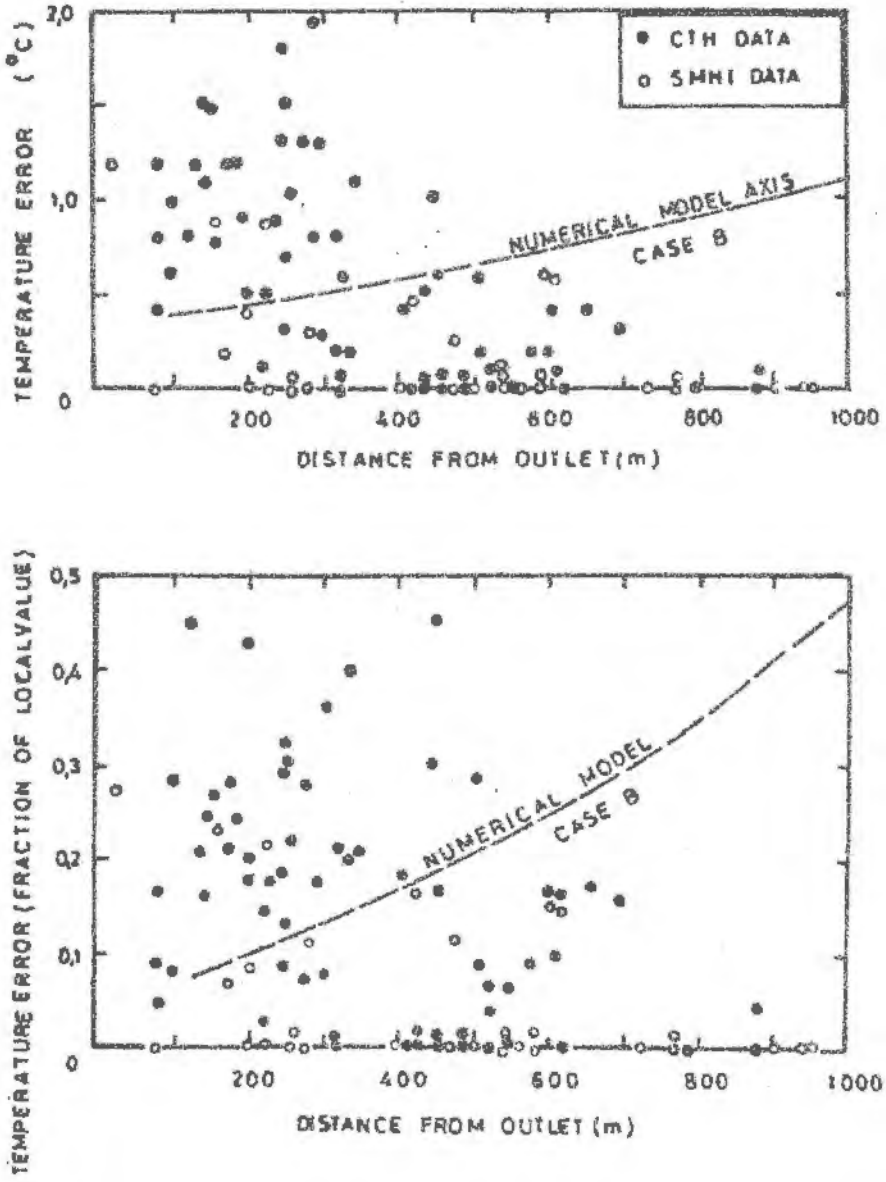

Figure 4.5 Temperature errors due to subsurface measurement, Oskarshamnsverket

CHAPTER 5. CONCLUSIONS

5.1 Direct model application

Subject to the conditions explained below, the Prych (1972) numerical model for surface discharge of heated water is verified for prediction of temperatures near proposed power plants. That this conclusion not be presented by edict, recall the definition of verification as a check or test of accuracy, not necessarily a substantiation of absolute precision.

An advantage of the numerical model is presentation of much more temperature information than other phenomenological, analytical, or laboratory models. Separation of the effects of various dilution mechanisms is not always distinct, due to numerical complexity, but output is given for full-field temperatures and for many internal parameters such as heat content, local Richardson number, etc.

The model can be directly applied to discharge situations with low outlet Froude number, limited coastal constraint, and deep receiving water. Prediction errors may be significant, but no systematic bias is introduced by low Froude number. For the field data considered, predicted temperatures are both too high and too low. It is suspected that the model performs better at high Froude numbers, but this is not yet verified with field data. As outlet Froude number is increased the layer thickness is increased, and finding situations not restricted by shallow receiving water is more difficult. Applicable ranges of other dimensionless input parameters are larger. Although numerical difficulties are sometimes encountered for zero ambient current the model is verified for ambient currents up to 60 % of outlet velocity. Data for varying discharge angle is sparse, but the model has been applied to field situations with angles of 39° to 90°, and to a laboratory situation of 0° angle. Aspect ratios of 2 to 21 are correctly modeled. Inclusion of receiving water diffusion is a feature not found in most other discharge models. Diffusion is not verified with field data because such data are not generally available, but the effects of diffusion are verified for a laboratory situation.

The overall accuracy of the numerical model is only fair, but for the data considered it is better than for other models. Comparison of accuracy with the model's precursor by Stolzenbach and Harleman (1971) has not been made. Fit with ten sets of field data ranges from very good to poor. Prediction of plume axis temperatures is better than for characteristic widths. Absolute plume width predictions are usually too large, sometimes larger than centerline length, which is a theoretical limit for low Froude number. Predictions of layer depth and trajectory are reasonably good. Layer depth does not vary much over the length of the plume, and field data correlation is complicated by non-preserving vertical temperature distributions. Surface areas within isotherms are modeled no better than with a simple phenomenological model, although differences between the two are not large.

Sources of prediction errors are not confidently known. Predictive uncertainty is larger than the uncertainty expected from incorrect choice of ambient temperature, subsurface measurement, or incorrect

specification of input parameters. No correlation is found between sign or magnitude of prediction error and any available discharge or hydrological parameter. Prych (1972) concludes that the principle model limitation is exclusion of coastal effects. Coastal effects probably do not account for prediction errors measured for several situations at Oskarshamnsverket, a Swedish coastal power plant. Additional uncertainty may be due to inconsistency of vertical and horizontal temperature profiles, and to time-varying ambient conditions.

Away from the natural coastline the numerical model gives better temperature predictions than hydraulic models. In order to preserve the topographical advantages of hydraulic models and the far field superiority of the numerical model, a scheme for interfacing these two predictive methods has been presented. The scheme also circumvents problems of oversimplification of the initial mixing zone, an admitted shortcoming of the numerical model. Limited verification is very encouraging.

5.2 Comparative model application

The numerical model can be used more confidently for relative or comparative predictions than for direct application. This conclusion is not unique to the model, but is a consequence of the sources of predictive errors. Receiving water limitations of coastal constraint, non-uniform temperature distributions, and time-varying conditions act equally on the plume for different values of input parameters. As for direct application, the model provides more output information than most other models.

The general discharge situation is described by the dimensionless independent variables of ambient current ratio R, discharge angle θ, outlet aspect ratio A, outlet Froude number F_o, diffusion ratio E, and axial distance s/H_o. The response of the numerical model to changes of these variables compares very well to a power law model determined from field and laboratory data. Quantitative results for such changes have been presented for an idealized power plant.

The response of dimensionless plume axis temperature T to distance s/H_o compares well with data except at the end of the jet core, or initial mixing zone. Responses of T to A, F_o, and E are suitable for power law description and fit available data. Responses of T to R and θ are less regular. Temperature T does not depend strongly on R for $R < 0.1$. The behavior of plume width B/H_o with respect to Froude number F_o follows data very well, but the effects of all other variables on B/H_o are inconsistent. This does not mean that the relative predictions are wrong, but that they do not fit a power law description and thus are not verified with field data. The comparative behavior of layer depth H/H_o with respect to F_o and A is predictable, but data are not available for verification. Response of axis trajectory location Y/H_o to R matches laboratory data, but not field data. Dependence of Y/H_o on s/H_o and θ coincides with both data sources. Dependencies on A and F_o are inconsistent. Reported power law scaling should not be substituted for program operation at particular sites.

With special exclusions explained earlier in the report, the model is generally verified for comparative application for $0.05 \leq R \leq 1.0$, $20^{\circ} \leq \theta \leq 100^{\circ}$, $1 \leq A \leq 10$, $1 < F_o \leq 20$, $0.1 \leq E \leq 1.5$, and $0 \leq s/H_o$.

Based on data for a single situation the numerical model provides better comparative predictions than hydraulic models. The uniformity of numerical predictions eliminates inconsistencies in the laboratory model data considered.

REFERENCES

Asbury, J.G., and Frigo, A.A. (1971), "A Phenomenological Relationship for Predicting Surface Areas of Thermal Plumes in Lakes," Report ANL/ES-5, Argonne National Laboratory, Argonne, Illinois.

Doret, S.C., Harleman, D.R.F., Ippen, A.T., and Pearce, B.R. (1973), "Characteristics of Condenser Water Discharge on the Sea Surface (Correlation of Field Observations with Theory)," Parsons Laboratory Report No. 170, Department of Civil Engineering, Massachusetts Institute of Technology, Cambridge, Massachusetts.

Frigo, A.A., and Frye, D.E. (1972), "Physical Measurements of Thermal Discharges into Lake Michigan: 1971," Report ANL/ES-16, Argonne National Laboratory, Argonne, Illinois.

Hindley, P.D., Miner, R.M., and Cayot, R.F. (1971), "Thermal Discharge: A Model-Prototype Comparison," ASCE, Journal of the Power Division, vol. 97, no. PO4, pp. 783-798.

Jen, Y., Wiegel, R.L., and Mobarek, I. (1966), "Surface Discharge of Horizontal Warm-Water Jet," ASCE, Journal of the Power Division, vol. 92, no. PC2, pp. 1-30.

Policastro, A.J., and Tokar, J.V. (1972), "Heated-Effluent Dispersion in Large Lakes: State-of-the-Art in Analytical Modeling," Report ANL/ES-11, Argonne National Laboratory, Argonne, Illinois.

Prych, E.A. (1972), "/ Warm Water Effluent Analyzed as a Buoyant Surface Jet," Serie Hydrologi Report Nr 21, Swedish Meteorological and Hydrological Institute, Stockholm.

Prych, E.A. (1973), "An Analysis of a Jet into a Turbulent Ambient Fluid," Water Research, vol. 7, pp. 647-657.

Shirazi, M. (1973), "A Critical Review of Laboratory and Some Field Experimental Data on Surface Jet Discharge of Heated Water," PNERL Working Paper No. 4, U.S. Environmental Protection Agency, Corvallis, Oregon.

Statens Vattenfallsverk (1972), "Forsmarks Kraftstation, Kylvattnets Spridning i Utloppsområdet; Redogörelse för Modellförsök Februari-November 1972," Vattenbyggnadslaboratoriet, Älvkarleby.

Stolzenbach, K.D., and Harleman, D.R.F. (1971), "An Analytical and Experimental Investigation of Surface Discharges of Heated Water," Parsons Laboratory Report No. 135, Department of Civil Engineering, Massachusetts Institute of Technology, Cambridge, Massachusetts.

Tokar, J.V. (1971), "Thermal Plumes in Lakes: Compilations of Field Experience," Report ANL/ES-3, Argonne National Laboratory, Argonne, Illinois.

Weil, J.G. (1972), "Mixing of a Heated Surface Jet in Turbulent Channel Flow," Report No. WHM-1, Hydraulic Engineering Laboratory, University of California, Berkeley, California.

LIST OF SYMBOLS

A	aspect ratio = $2B_o/H_o$
A_T	surface area enclosed within isotherm
B	characteristic plume half width
$2B_o$	outlet width
C_D	drag coefficient
C_F	shear coefficient
d	channel flow depth
E	diffusion ratio = ε_H/u_oH_o
E_o	entrainment coefficient
F_o	outlet Froude number = $u_o/(\frac{\Delta\rho}{\rho}\ g\ H_o)^{1/2}$
g	acceleration of gravity
H	characteristic layer thickness
H_o	outlet depth
k	atmospheric heat transfer coefficient
Q	mass flow within plume region
Q_o	outlet flow
R	current ratio = V/u_o
s	distance along jet axis
s_o	initial zone length
Δs	maximum integration step size
T	relative temperature = $(T_s-T_a)/(T_h-T_a)$
T_a	ambient temperature
T_h	outlet temperature
T_s	temperature on jet axis
ΔT	plant temperature rise = T_h-T_a
u_o	outlet velocity
u_*	channel shear velocity
V	ambient velocity
W	wind speed
x	coordinate in ambient current direction
y, Y	offshore coordinate, perpendicular to x
z	vertical coordinate
ε_H	horizontal diffusion coefficient
ε_V	vertical diffusion coefficient
θ	angle between outlet and ambient velocities
ν	kinematic viscosity of water
ρ	density of water
$\Delta\rho$	outlet density difference

Notiser och preliminära rapporter

Serie HYDROLOGI

Nr 1 Sundberg-Falkenmark, M
Om isbärighet. Stockholm 1963

Nr 2 Forsman, A
Snösmältning och avrinning. Stockholm 1963

Nr 3 Karström, U
Infrarödteknik i hydrologisk tillämpning: Värmebilder som hjälpmedel i recipientundersökningar. Stockholm 1966

Nr 4 Moberg, A
Svenska sjöars isläggnings- och islossningstidpunkter 1911/12-1960/61. Del 1. Redovisning av observationsmaterial. Stockholm 1967

Nr 5 Ehlin, U & Nyberg, L
Hydrografiska undersökningar i Nordmalingsfjärden. Stockholm 1968

Nr 6 Milanov, T
Avkylningsproblem i recipienter vid utsläpp av kylvatten. Stockholm 1969

Nr 7 Ehlin, U & Zachrisson, G
Spridningen i Vänerns nordvästra del av suspenderat materiel från skredet i Norsälven i april 1969. Stockholm 1969

Nr 8 Ehlert, K
Mälarens hydrologi och inverkan på denna av alternativa vattenavledningar från Mälaren. Stockholm 1970

Nr 9 Ehlin, U & Carlsson, B
Hydrologiska observationer i Vänern 1959-1968 jämte sammanfattande synpunkter. Stockholm 1970

Nr 10 Ehlin, U & Carlsson, B
Hydrologiska observationer i Vänern 17-21 mars 1969. Stockholm 1970

Nr 11 Milanov, T
Termisk spridning av kylvattenutsläpp från Karlshamnsverket. Stockholm 1971

Nr 12 Persson, M
Hydrologiska undersökningar i Lappträskets representativa område. Rapport I. Stockholm 1971

Nr 13 Persson, M
Hydrologiska undersökningar i Lappträskets representativa område. Rapport II: Snömätningar med snörör och snökuddar. Stockholm 1971

Nr 14 Hedin, L
Hydrologiska undersökningar i Velens representativa område. Beskrivning av området, utförda mätningar samt preliminära resultat. Rapport I. Stockholm 1971

Nr 15 Foraman, A & Milanov, T
Hydrologiska undersökningar i Velens representativa område. Markvattenstudier i Velenområdet. Rapport II. Stockholm 1971

Nr 16 Hedin, L
Hydrologiska undersökningar i Kassjöåns representativa område. Nederbördens höjdberoende samt kortfattad beskrivning av området. Rapport I. Stockholm 1971

Nr 17 Bergström, S & Ehlert, K
Stochastic Streamflow Synthesis at the Velen representative Basin. Stockholm 1971

Nr 18 Bergström, S
Snösmältningen i Lappträskets representativa område som funktion av lufttemperaturen. Stockholm 1972

Nr 19 Holmström, H
Test of two automatic water quality monitors under field conditions. Stockholm 1972

Nr 20 Wennerberg, G
Yttertemperaturkartering med strålningstermometer från flygplan över Vänern under 1971. Stockholm 1972

Nr 21 Prych, A
A warm water effluent analyzed as a buoyant surface jet. Stockholm 1972

Nr 22 Bergström, S
Utveckling och tillämpning av en digital avrinningsmodell. Stockholm 1972

Nr 23 Malander, O
Beskrivning till jordartskarta över Lappträskets representativa område. Stockholm 1972

Nr 24 Persson, M
Hydrologiska undersökningar i Lappträskets representativa område. Rapport III: Avdunstning och vattenomsättning. Stockholm 1972

Nr 25 Häggström, M
Hydrologiska undersökningar i Velens representativa område. Rapport III: Undersökning av torrperioderna under IHD-åren fram t o m 1971. Stockholm 1972

Nr 26 Bergström, S
The application of a simple rainfall-runoff model to a catchment with incomplete data coverage. Stockholm 1972

Nr 27 Wändahl, T & Bergstrand, E
Oceanografiska förhållanden i svenska kustvatten. Stockholm 1973

Nr 28 Ehlin, U
Kylvattenutsläpp i sjöar och hav. Stockholm 1973

Nr 29 Andersson, U-M & Waldenström, A
Mark- och grundvattenstudier i Kassjöåns representativa område. Stockholm 1973

Nr 30 Milanov, T
Hydrologiska undersökningar i Kasajöåns representativa område. Markvattenstudier i Kasajöåns område. Rapport II. Stockholm 1973

SMHI Rapporter
HYDROLOGI OCH OCEANOGRAFI

Nr RHO 1

Weil, J G
Verification of heated water jet numerical model.
Stockholm 1974